

**ALMA MATER STUDIORUM
Università di Bologna**

DOTTORATO DI RICERCA IN BIOLOGIA CELLULARE E MOLECOLARE

Ciclo XXXV

Settore concorsuale: 05/E2 – Biologia Molecolare
Settore scientifico disciplinare: BIO/11 – Biologia molecolare

*R-loops and G4-structures:
from DNA damage to innate immune response gene
activation*

Candidato: Andrea Arleo

**Supervisore:
Chiar.mo Prof. Giovanni Capranico**

**Coordinatore Dottorato:
Chiar.mo Prof. Vincenzo Scarlato**

**Co-supervisore:
Prof.ssa Jessica Marinello**

Esame finale anno 2023

Abstract

Non-B DNA structures like R-loops and G-quadruplexes play a pivotal role in several cellular vital processes like DNA transcription regulation. Misregulation of said non-canonical DNA structures can often lead to genome instability, DNA damage, and, eventually, to the activation of an innate immune response. For such reasons they have been studied as adjuvants in anticancer therapies. Here we studied drugs targeting R-loops (Top1 poisons) and G4s (hydrazone derivatives) in order to observe their effects in terms of DNA damage induction and, subsequently, activation of innate immune response.

DNA topoisomerase I (Top1) acts on DNA supercoilings, showing an uttermost importance in regulating non-B DNA structures as R-loops. The targeting of Top1 is a milestone in cancer therapy, especially for small cell lung cancers (SCLC); unfortunately, these types of cancer often relapse and the effectiveness of these therapies varies among cancer cell lines. Top1 poisons are able to selectively bind Topoisomerase 1 and, by blocking it on DNA, they promote the formation of unscheduled R-loops which, if not resolved, can lead to DNA damage, genome instability and DNA single/double-strand breaks. We studied how non-cytotoxic doses of Camptothecin and LMP-776 impact on genome instability, are capable to induce DNA damage and micronuclei, and, eventually lead to an innate immune gene response via the cGAS/STING pathway. We conducted experiments on both HeLa and 3 Small Cell Lung Cancer cell lines (H209, H889, and DMS114) because Top1 poisons are widely adopted as coadjuvant in lung cancer treatment. We observed that both Camptothecin and LMP-776 were able to induce high levels of micronuclei in all tested cell lines, thus demonstrating a high degree of genome instability and DNA breaks. These micronuclei levels decreased as a result of RNaseH1 overexpression in a dose-dependent manner, hence showing the importance of R-loops in micronuclei formation. However, the analysis of a wide panel of cytokines revealed variable levels of innate immune response which are reflected by variable levels of the cGAS/STING pathway completeness. Therefore, the presence of cytosolic DNA fragments

activates the cGAS/STING pathway, leading to an innate immune gene response activation that is much stronger in those cell lines that exhibit a more complete cGAS/STING pathway.

G-quadruplexes are another ubiquitous, non-canonical DNA structure, more abundant in telomeric regions, demonstrating a marked relation with the impairment of telomerase and the regulation of DNA replication and transcription. For these reasons, in recent years scientists tried to synthesize more and more effective G4-binders, which are able to strongly stabilize G4s with the ultimate goal of acting on the correct regulation of oncogenes and telomeres for cancer therapy. In this perspective, we studied the properties of new-synthesized molecules belonging to the highly promising class of hydrazone-derivatives, in terms of cytotoxicity, ability to stabilize G4 structures, induce DNA damage, and activate interferon- β production. Despite all tested compounds revealed a significant micronuclei production, micronuclei alone were not sufficient to trigger the production of IFN-B because they need to be balanced by other factors, including cytotoxicity. The findings obtained allow to infer that IFN-B gene activation can require on the one hand a good G4 binding affinity and stabilization capability, and on the other hand low cytotoxicity levels that allow the cell to function properly without compromising its vital functions. Therefore, the most desirable combination is likely found in those compounds which exhibit a high G4 structure stabilizing capacity together with low cytotoxicity.

Both Top1 poisons and G4-stabilizers possess several features that can be very useful in clinical applications, in light of their ability to stimulate innate immune response factors and exert a certain cell-killing power, plus they offer a broad and diverse range of treatment options in order to face a variety of patient treatment needs. It is for these very reasons that it is of uttermost importance that further studies are conducted on these compounds, in order to synthesize new and increasingly powerful and flexible ones, with fewer side effects to customize therapies on specific cancers' and patients' features.

CHAPTER I: Introduction	1
1.1	Non-canonical DNA structures 2
1.1.1	R-loops 2
1.1.1.1	R-loop formation process 4
1.1.1.2	R-loop's role and detection 5
1.1.2	G-quadruplexes structures 7
1.1.2.1	G4 formation and structure 7
1.1.2.2	G4 detection 8
1.1.2.3	G4 biological function and further applications 10
1.1.2.4	G4-binders 12
1.2	DNA topoisomerases 15
1.2.1	Topoisomerase 1 17
1.2.1.1	Topoisomerase and R-loops 18
1.2.2	TOP1 poisons 19
1.3	DNA damage and DNA damage response 21
1.3.1	Micronuclei 23
1.4	Innate immune response triggered by the cGAS/STING pathway 25
1.5	TOP1 poisons and Small Cell Lung Cancers 28
Aim of the project	30
CHAPTER II: Methods	31
2.1	Cell lines, cultures and treatments 31
2.2	Immunofluorescence 32
2.2.1	TOP1 poisons and S9.6 32
2.2.2	U2OS overexpressing RNaseH1 33
2.2.3	γ H2AX 34
2.2.4	STING and cGAS 34
2.2.5	Micronuclei Immunofluorescence 35
2.2.6	BG4 Immunofluorescence 36
2.3	RNA extraction, retrotranscription and qRT-PCR 37
2.4	RNaseH1 overexpression 39
2.5	Western blot 39
2.6	cGAMP ELISA 40
2.7	STING gene silencing 40
2.8	STING chemical inhibition 41

2.9	DNA demethylation by 5'-Azacytidine	41
2.10	Sting overexpression in DMS114	42
2.11	Viability assay (MTT assay)	42
2.12	IFN β ELISA	43
CHAPTER III: Results		44
3.1	TOP1 poisons induce micronuclei production mediated by R-loop stabilization	44
3.2	Micronuclei trigger innate immune gene activation	52
3.3	cGAS/STING pathway impairment and its effects	56
3.4	STING expression alteration affects the initiation of innate immune response	61
3.5	G4 stabilization and cytotoxicity properties of hydrazone derivatives impact IFN-B stimulation	72
3.5.1	Cytotoxicity correlates with chemical structure in hydrazone derivatives	74
3.5.2	G4 stabilization and DNA damage induction in U2OS cells	76
3.5.3	Micronuclei production and IFN-B stimulation induced by hydrazone derivatives	81
CHAPTER IV: Discussion		85
4.1	TOP1 poisons induce DNA damage and innate immune response activation	85
4.2	G4 stabilization/cytotoxicity balance affects IFN-B stimulation in hydrazone-based G-4 binders	89
Conclusions		93
References		94
Publications		114

CHAPTER I

Introduction

Tumors are the second most frequent cause of death in Europe and USA (Eurostat, 2020; Sherry et al., 2021), which explains why it is of uttermost importance to develop more powerful weapons against these diseases. In light of this urge, Camptothecin (CPT) and its derivatives, commonly known as TOP1 poisons, have been identified as effective tools for the treatment of various cancer types and are currently being used as standard therapy in ovarian, colorectal and lung cancers. However, the underlying mechanisms by which these compounds show their effectiveness are still to be fully unveiled, pushing researchers to investigate them in detail to gather a deep understanding of how to deploy them in clinical applications to develop new therapeutic approaches and tailor them on diverse tumor features. Considering the general ability of TOP1 poisons to induce DNA damage, they can be effectively used as a therapeutic strategy to target cancer cells, eventually leading them to death. Therefore, DNA damage constitutes a major area of investigation and involves different lines of research, including (among others) the study of the role of topoisomerases in DNA topology, TOP1 poisons and G4 binders, as described in the following paragraphs. Specifically, TOP1 poisons are molecules that are able to bind specifically to DNA/Top1 interface (Pommier et al., 2016) causing DNA damage and genome instability (Capranico et al., 2004; Pommier et al. 2016). However, another intriguing aspect of both TOP1 poisons and G4 binders is their potential ability to trigger innate immune response activation, which is one of the investigation goals of this work.

1.1 Non-canonical DNA structures

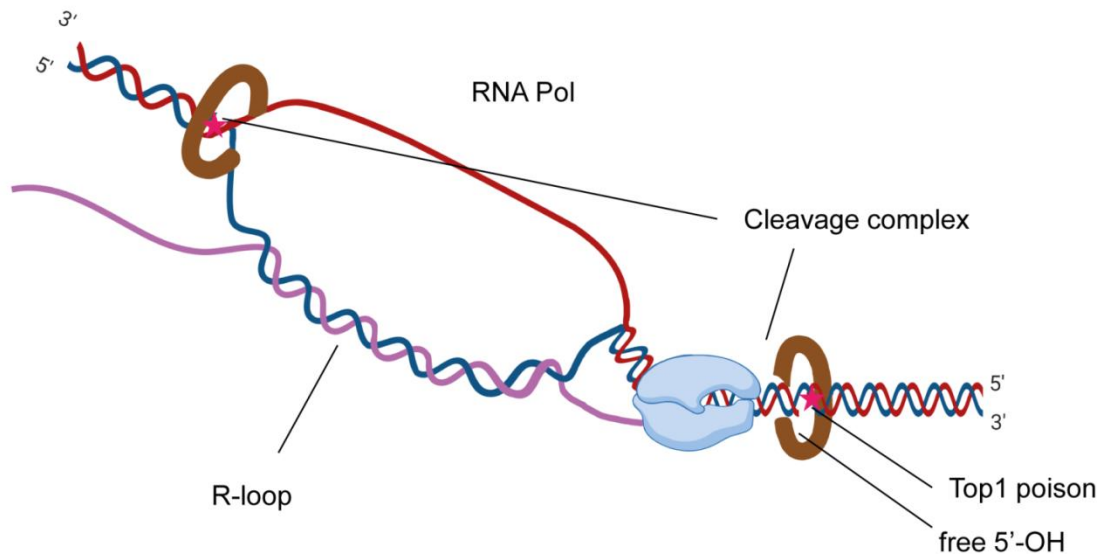
DNA B-shape was first described by Franklin, Watson and Crick in the 1950s, as a double stranded, naturally wrapped, right-handed 20 Å-wide helix (Watson and Crick, 1953), which is the most common form of DNA. Since then, many other DNA forms were observed over time, including the A-form (Franklin et al., 1953), which is essentially the shape that B-DNA takes in a dried condition, G-quadruplexes (Gellert et al., 1962), R-loops (Richardson, 1975), Z-form (Gessner et al., 1989), and hairpin/cruciform (Palecek, 1991). This great number of possible structures suggests that DNA is a fluidic, dynamic structure that adapts to the local environment and is able to fulfill various and diversified tasks. These different DNA geometries come into shape also due to Hoogsteen bonds and reversed Hoogsteen bonds, a particular type of hydrogen bond described for the first time by Karst Hoogsteen (Hoogsteen, 1962). These hydrogen bonds differ from “canonical” bonds occurring among deoxyribonucleotides, in that they bind atoms which are located in positions others than those predicted by Watson and Crick.

These non-canonical structures are involved in cancer progression, as they can alter the physiological transcription of a vast number of genes involved in key mechanisms for cell homeostasis and survival (Kim et al., 1998; Siddiqui-Jain et al., 2002). Among all of these structures, R-loops and G-quadruplexes, which are at the core of this work, have been extensively studied and seem to be the most promising ones in order to set up new strategies against cancer.

1.1.1 R-loops

R-loops are hybrid co-transcriptional structures that originate during DNA transcription events when, following DNA denaturation, the neo-synthesized RNA anneals with the DNA template, leaving the other DNA strand displaced out (Figure 1.1). R-loops can arise as a

result of a scheduled process involving a number of factors concurring to their formation or in an accidental manner as an unscheduled event, thus differentiating between physiological and pathological R-loops. R-loops are intermediates in several genome-regulation processes, including the class-switch recombination (CSR) of Ig (Reaban et al., 1994; Yu et al., 2003), bacterial plasmid and mitochondrial DNA replication (Aguilera and



Top1cc blocked by Top1 poison; transcription blocked by stalled Top1cc

Figure 1.1 R-loop schematic representation when a Top1 cc occurs close to RNAPol. Created with BioRender.com.

García-Muse, 2012), and CRISPR-Cas9 activity (Jinek et al., 2012). Overall, R-loops play a critical role in transcription regulation and gene expression, as proven by an increasing number of scientific evidence (Sun et al., 2013; Boque-Sastre et al., 2015; Arab et al., 2019), and the role in to transcription termination (Castel et al., 2014; Morales et al., 2016; Sanz et al., 2016). Also, R-loops easily form at CpG islands (which are known to be present at a wide range of gene promoters in mammals) and exercise some protection over these regions from DNA methylation (Ginno et al., 2012, Grunseich et al., 2018). The emergence of R-loops serving a physiological function has been investigated to assess whether these structures are the result of a spontaneous process or a scheduled

mechanism mediated by protein factors. The existence of such regulated processes has been proven by a number of data, including studies describing the function exercised by the mammalian capping enzyme (Kaneko et al., 2007), the virus-encoded ssDNA-binding protein ICP8 (Boehmer, 2004), and CRISPR-Cas9 (Jinek et al., 2012) to promote the formation of R-loops.

1.1.1.1 R-loop formation process

R-loop formation is strongly promoted by a series of favorable conditions. A high GC content in the DNA sequence (Roy and Lieber, 2009) is found to contribute to strengthen the bond between the newly formed RNA and its DNA template and previous studies have observed that DNA segments exhibiting an asymmetrical GC distribution due to a GC-skew of CpG islands, easily form R-loops (Ginno et al., 2012). Another factor stimulating R-loop formation is the presence of G-quadruplexes (Roberts and Crothers, 1992; De Magis et al., 2019) and a high number of negative supercoils behind the transcriptional fork (Drolet et al., 1994), since they enhance the stabilization of the two separated DNA strands, thus creating space for R-loop formation.

On the contrary, elements that can negatively affect the emergence of R-loops and can ultimately resolve these structures are enzymes like topoisomerases (Phoenix et al., 1997; Drolet et al., 1995), helicases (Chang, Novoa et al., 2017), and RNaseH (Wahba et al., 2011), due to their ability to specifically break down the hybrid duplex. Out of these enzymes, the endonuclease RNaseH is the one that exercises a direct action on the hybrid duplex. Two RNaseH enzymes are present in the human genome: the monomeric RNase H1 and the trimeric RNase H2 forms. Both enzymes exhibit a hybrid-binding domain, which is able to bind the R-loop, and an RNaseH domain, with the ability to perform the RNA hydrolytic cleavage. TOP1 is able to remove negative supercoils behind the transcriptional complex, thus eliminating one of the most favorable conditions to the

emergence of R-loops. In this regard, it was shown that inactive TOP1A in *E. coli* hampered cell growth but this negative effect could be fixed by RNaseH overexpression, hence restoring the physiological number of negative supercoils (Phoenix et al., 1997; Massé et al., 1997). Furthermore, structural problems in the TOP1 enzyme can result in enhanced stalled forks and DNA breaks (Tuduri et al., 2009; Manzo et al., 2018; Marinello et al., 2022); these two issues can be fixed, at least in part, by RNaseH1.

Helicases can separate the RNA strand from the annealed DNA strand of the hybrid duplex. In living cells, hybrid duplexes can be resolved by helicases such as Pif1, Senataxin, Rho, and DHX9, contributing to prevent genome instability (Chakraborty and Grosse, 2011). Interestingly, the inactivation of some helicases such as Senataxin or Aquarius, causes an accumulation of R-loops at highly transcribed loci and transcription termination regions (Sollier et al., 2014; Skourti et al., 2011).

1.1.1.2 R-loop's role and detection

R-loops were first discovered in bacterial DNA replication (Masukata and Tomizawa, 1984) and, since then, they were found in a plethora of very different organisms, from viruses (Wongsurawat et al., 2020) to humans, and in the mitochondrial genome (Xu and Clayton, 1996). This wide diffusion of R-loops clearly suggests that they play a critical role in DNA replication, even though their specific mechanisms of action are still to be fully unveiled, while it seems that they can be involved in keeping unmethylated CpG islands at promoter regions (Ginno et al., 2012).

These particular hybrid structures can be detected in a highly specific manner by the S9.6 antibody, a murine IgG (Boguslawski et al., 1986) that was validated and used in many studies (Ginno et al., 2012; De Magis et al., 2019). R-loops and S9.6 antibody were used to develop new techniques, such as the DNA-RNA Immunoprecipitation (DRIP), which allows

to immunoprecipitate R-loops, following gentle isolation of genomic DNA (Ginno et al., 2012), and then sequence the isolated genomic fragments (DRIP-seq).

Unscheduled R-loops are associated to uncontrolled recombination and impairment of transcription elongation (Huertas and Aguilera, 2003) and these can lead to enhanced mutation risk and genome instability, since the displaced single-stranded DNA is more likely to undergo mutations than the double-strand DNA (Gómez-González and Aguilera, 2007; Muers, 2011). Huertas and Aguilera propose two mechanisms in order to explain genome instability and hyper-recombination ascribed to R-loops. In the first scenario the replication fork stops and collides with the R-loop or with the RNA polymerase, creating a recombinant DSB. The second possibility suggests that displaced ssDNA segments might be more sensitive to a series of mutagens and DNA-damaging factors thus triggering mutagenesis and recombination events (Huertas and Aguilera, 2003).

GC-rich hybrid duplexes are structures characterized by a significant stability and were, in fact, identified as more thermodynamically stable than dsDNA bearing the same sequence (Ratmeyer et al., 1994; Roberts and Crothers, 1992). Another major feature displayed by R-loops is that they are diffusely distributed across the entire genome, although they tend to group in some strategic regions, such as: ribosomal DNA, tRNA genes, Ty transposons, telomerase regions and highly transcribed genes, encoded by Pol II (Santos-Pereira and Aguilera, 2015).

A work previously published by our research group demonstrated that the complex formed by TOP1, CPT, and DNA results in the enhancement of antisense transcripts at divergent CpG-island promoters (Marinello et al., 2013). The formation of TOP1cc sets off two main consequences: the blocking of RNA Pol II at the promoter level and R-loop formation.

1.1.2 G-quadruplex structures

A G-quadruplex (G4) is a structure firstly reported in 1962 (Gellert et al., 1962) and arranged in a columnar geometry characterized by distinctive features that bestow it with some specific properties. G-quadruplexes originate in the presence of G-rich sequences, on both DNA (telomeres, microsatellites, and CpG islands) and RNA (Varshney et al., 2020). Recently, they were also found at the replication origins of common fragile sites (CFSs), i.e., genomic regions that exhibit extensive chromosomal rearrangements in cancer cells (van Wietmarschen et al., 2018; Pladevall-Morera et al., 2019; Maffia et al., 2020).

1.1.2.1 G4 formation and structure

G4s arise as a consequence of the ability of guanylic acids to form four-stranded, right-handed helices: The structure is then stabilized by guanines held together by Hoogsteen hydrogen bonds, resulting in co-planar G-quartets (Gellert et al., 1962; Arnott et al., 1974), and by a monovalent cation located at the center of the stack (Figure 1.2).

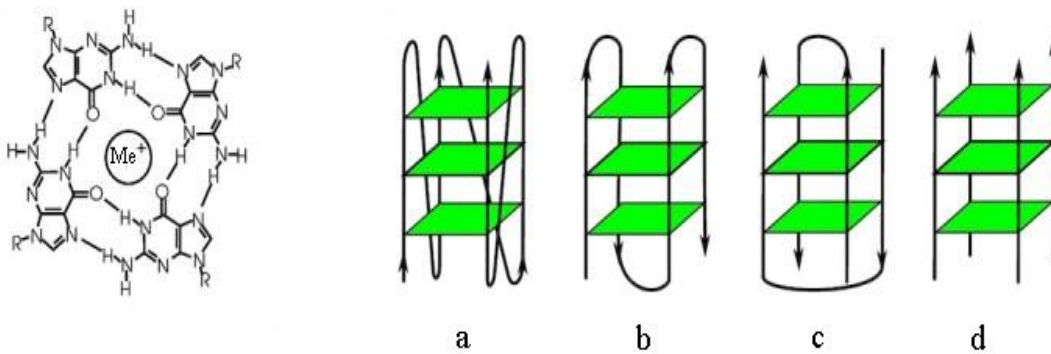


Figure 1.2 *Left:* An example of G-quadruplex seen from the top of the structure; the inner circle signals a general monovalent cation. *Right:* Different possible stacks: (a) intra-strand, parallel; (b) intra-strand, antiparallel; (c) inter-strand, antiparallel; (d) inter-strand, parallel. Adapted from Miglietta et al., 2020. Image licensed under the Creative Commons Attribution 4.0 International License. To view a copy of this license, visit <http://creativecommons.org/licenses/by/4.0/> or send a letter to Creative Commons, PO Box 1866, Mountain View, CA 94042, USA.

Different cations have a different G4-stabilizing power, depending on their charge-dimension ratio. This allows to place the most common cations on a continuum from the most stabilizing cation to the less powerful one, such as follows: K^+ at one end of the continuum, followed by Ca^{2+} , Na^+ , Mg^{2+} and Li^+ (Bhattacharyya et al., 2016).

G4s can occur in different shapes and layouts, depending on several variable factors. Depending on whether G-tracts are connected by a single strand or multiple DNA strands, the process can lead to the formation of unimolecular (intra-strand) or intermolecular (inter-strand) G4s (Miglietta et al., 2020). Also, other arrangements are characterized by different DNA strand directions and different lengths and loop compositions (Burge et al., 2006; Zhou et al., 2012). In the case of inter-strand guanines, when they belong to both RNA and DNA strands, they elicit the formation of a particular type of G-quadruplex, namely a hybrid inter-strand G4. This process occurs during DNA transcription and involves the nascent RNA strand and the non-template DNA strand of a G-rich sequence (Xiao et al., 2013).

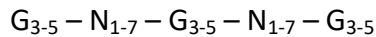
1.1.2.2 G4 detection

Extensive research has established that G4s are extremely numerous in regions commonly involved in genome regulation, such as promoters and telomeres (Huppert and Balasubramanian, 2005). On a first instance, antibodies have been used to detect and monitor G4-related dynamics in ciliates (Paeschke et al., 2008), human cells (Biffi et al., 2013; Henderson et al., 2014; Moye et al., 2015; Liu et al., 2016), and cancer tissues (Biffi et al., 2014). In 2013, a group of researchers managed to produce an engineered antibody that binds G4s with high specificity, while demonstrating an affinity level towards other structures like ssDNA, dsDNA and hairpins below detection levels (Biffi et al., 2013). This antibody, known as BG4, is the most commonly-used antibody to study G4 structures. In a very short time, BG4 has been exploited in many different techniques, like

immunofluorescence microscopy and ChIP-Seq experiments. The use of antibodies to detect G4s allowed researchers to identify a high number of G4 foci staining in cell nucleus after administering pyridostatin ligand treatment (Biffi et al., 2013). Also, colocalization of telomeric BG4 foci and human telomerase has been observed, thus pointing to the enzyme recruitment to G4 structures (Moye et al., 2015). Antibodies are not the only solution found to detect G4s in cells. Indeed, small molecules like radiolabeled ligands (Granotier et al., 2005) and intrinsically fluorescent molecules allowed to assess the presence of G4s, by checking for G4 specificity through the use of BG4 antibody (Zhang 2018).

Technological advancement has definitely contributed to a more specific mapping of G4s in genomes. As an example, next-generation sequencing has allowed to identify a significant number of G4 sites in human genome (Chambers et al., 2015) and a strong tendency of G4s to form in promoters which is typical of mammals but less frequent in other organisms (Marsico et al., 2019). In a study employing BG4 antibody, endogenous G4s were mapped in fixed chromatin of human epidermal keratinocytes (NHEKs) and immortalized HaCaT keratinocytes. A much higher number of G4s was detected in precancerous HaCaT, as compared to standard keratinocytes, thus signaling a key role played by the chromatin setting and other relevant proteins in promoting G4 formation. Moreover, most G4s were located in nucleosome-depleted regions (NDRs) and were particularly enriched at regulatory regions and promoters of highly transcribed genes (Hänsel-Hertsch, et al., 2016), although further studies on different cell lines proved that G4 mapping exhibits a high rate of cell-type specificity (Hänsel-Hertsch, et al., 2018).

The study of G4 formation and mapping is of utmost importance to predict the origination of G4s. In this regard, guanosines involved in the formation of G4s can even be located quite far from each other but the resulting G4-formation process can still be predicted thanks to a consensus sequence. This sequence was employed by Todd in the development of a bioinformatic tool called Quadparser (Todd et al., 2005), which uses the following consensus of G4-forming sequences:



where G=guanine and N=any base.

Over the years, efforts to produce new search engines that can predict G4 structures across all the genome have multiplied. Another famous example of this type of software, which is also commonly used in current research, is G4hunter, a tool which analyzes different parameters such as the content in guanines and G-skew levels (Bedrat et al., 2016). Analyses performed by means of this technology proved extremely fruitful, allowing to identify more than 700,000 putative G4 sequences (Tu et al., 2021).

1.1.2.3 G4 biological function and further applications

In light of the localization of G4s at genome regulating regions, research has been conducted to unveil the extent to which these structures are involved in a wide range of biological processes. As an example, telomeric repeats are characterized by a significant richness of G4-forming sequences and are likely to form G4 structures, suggesting a connection with the extension of telomeres mediated by telomerase. This knowledge has raised interests on possible uses of G4 stabilizing binders to impair telomere maintenance and inhibit cancer cell growth (Fouquerel et al., 2016). Indeed, it has been suggested that G4s might play a key role in hindering the functioning of telomerase (Zahler et al., 1991), although they might also be involved in its recruitment (Moye et al., 2015).

Another process in which G4 structures show their involvement is genomic and epigenetic instability. For example, Pif1 helicase has been found to be recruited to DNA DSBs, in order to promote homologous recombination at sequences that are known to form G4s. Pif1 can be hindered by administering G4 stabilizing treatment, although this effect can be reverted in case of Pif1 overexpression (Jimeno et al., 2018). Moreover, it has also been suggested that G4s can serve as “catching sites” of oxidative DNA damage, since 8-oxoG

incorporation can impact on the stability of promoter G4 structures and thus alter the expression of reporter gene assays (Fleming et al., 2017; Cogoi et al., 2018), and any modification of 8-oxoG can promote the activity of telomerase (Lee et al., 2017) and interfere with the formation of telomeric DNA G4s (Bielskutė et al., 2019).

G4s play an important biological role in DNA replication as they are able to block the progression of polymerase on the DNA template leading to genomic instability and DNA double strand breaks (Xu et al., 2017; Rodriguez et al., 2012). Recent studies report that the mechanism leading to DSBs can implicate R-loops (De Magis et al., 2019; Miglietta et al., 2020). Indeed, a replication arrest can arise when, moving along the DNA strand, DNA polymerase reaches a G-quadruplex; in such an occasion, the block can be resolved by a group of helicases, allowing the replication fork to move on. Examples of these helicases include Bloom (BLM), Werner-syndrome helicase (WRN), and FANCD1. Their mutations often lead to genome instability and eventually cancer (Crabbe et al., 2004; Brosh and Cantor, 2014). In general, G4s have been observed to act as an impediment blocking the transcription machinery progression, as a result of low mRNA levels found at genes containing G4 sequences in their promoters (Siddiqui-Jain et al., 2002; Cogoi and Xodo, 2006). Indeed, when G4 structures are stabilized by specific ligands, an enhanced production of DNA damage and an increased DNA damage responses can be observed (Rodriguez et al., 2012; Xu et al., 2017).

Due to their involvement in major processes governing the growth of cancer cells, like the regulation of cancer-related genes, genome instability, and replication, G4s represent an interesting object of study for their implication in cancer treatment and related applications, especially if taken as molecular targets. Interestingly, G4 foci tend to show higher levels in cancer tissues as compared to normal ones, as it has been observed for stomach and liver cancers (Biffi et al., 2014). Moreover, cancer cells are known to be sensitive to G4 binders, like pyridostatin, when their repair pathways have been impaired (Rodriguez et al., 2012), as shown in studies conducted on BRCA2-deficient (McLuckie et al., 2013; Zimmer et al., 2016) and PARP1-knockdown cells (Salvati et al., 2010), implying

that G4 binders might constitute an effective therapeutic approach in cancer types with deficient HR. As a matter of fact, the G4 binder CX-5461 is being currently used in clinical trials on human breast cancer, in patients with BRCA1/2 germline aberrations (Xu et al., 2017). G4 binders have been shown to be effective in glioma tumor models (Wang et al., 2019) and in combination with inhibitors of proteins involved in the DNA repair pathway in colon tumors (Salvati et al., 2010).

Considering that it has been observed that G4s are often deployed near telomeres and on promoters of cancer-related genes, in recent years scientists tried to synthesize hundreds of G4-binder molecules, which are able to stabilize G4s with the ultimate goal of acting on the correct regulation of oncogenes and telomeres for cancer therapy.

1.1.2.4 G4 binders

G4 binders are molecules that can recognize stacked guanines (G-quadruplex) and distinguish them from other non-secondary DNA structures. Once they bind to G-quadruplexes, these are not able to interact with other molecules, often preventing any G4 resolution mediated by helicases. G4 binders can also trigger the formation of micronuclei via R-loop stabilization (De Magis et al., 2019), thus promoting the transcription of type I interferon genes and IFN-stimulated genes (Miglietta et al., 2021).

First studies on G4 binders originally described them as telomerase inhibitors but, as research advanced, it became clear that they specifically target telomeres but not the enzyme, as they bind to G4s (Sun et al., 1997; Gowan et al. 2002).

Since G4 structures seem to be much more numerous in cancer cells than in healthy cells, they were investigated as potentially able to inflict cytotoxicity to cancer cells. Thus, they are considered an interesting target to be exploited for the development of new anticancer drugs. Although these promising premises, in spite of the great number of G4-binders synthesized in last decades, only two molecules have been entered into early

clinical trials: CX-3543, and CX-5461 and none of them has yet exhibited an effective activity against human cancers (Miglietta et al., 2022).

Nevertheless, some G4-binders, like Pyridostatin (PDS), BRACO19, and Phen-DC3 (Figure 1.3) demonstrated a strong efficacy in inducing DNA double strand breaks, raising considerable interests and leading to a large number of studies investigating these molecules. Despite the differences among all these structures, there are some recurring common features that confer these molecules their binding properties. First of all, a structure that enables them to insert themselves in the columnar motifs of G-quadruplexes and then the presence of hydrophobic rings that make the G4-binders capable of establishing Hoogsteen bonds with guanines.

PDS was designed by Rodriguez in 2008 (Rodriguez et al., 2008) and acts both as a G4-stabilizer and as an inducer. Its affinity for G4 structures is so strong that it displaces transcription factor proteins, which are able to bind G4 structures. Furthermore, PDS can

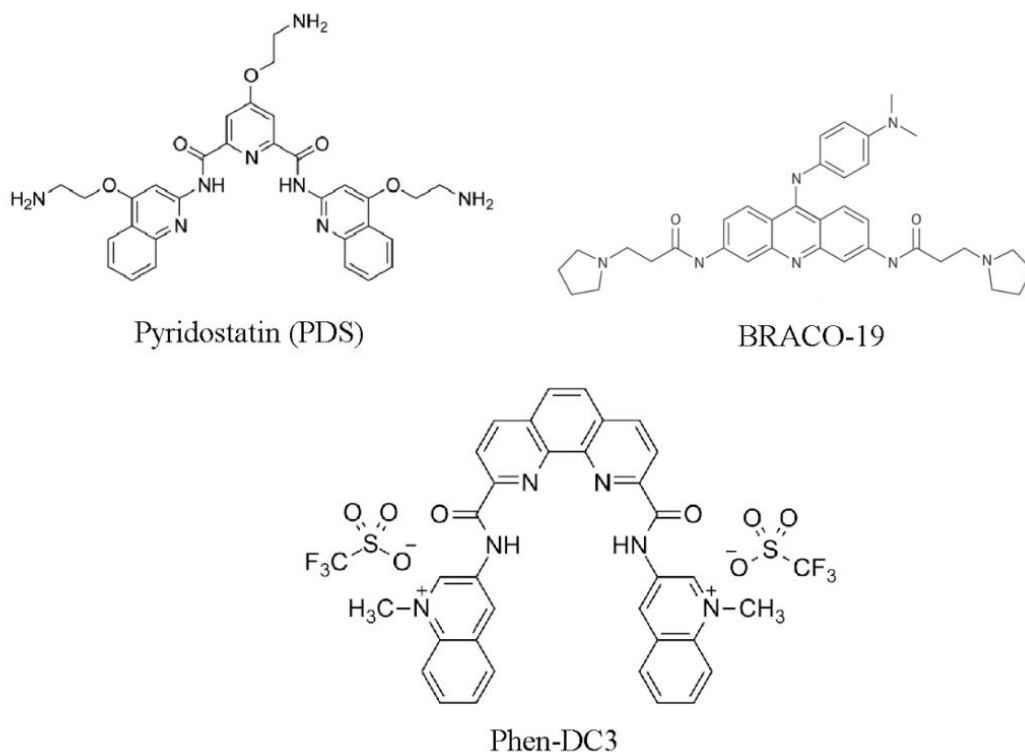


Figure 1.3 Structures of the three main G4 binders: PDS (*top left*), BRACO-19 (*top right*), and Phen-DC3 (*bottom*). Created with Paint.NET

bind G4 structures on both DNA and RNA (Hou et al., 2022) and it exhibits a significant effectiveness in inducing DNA damage by poisoning the transcription-coupled repair pathway (Takebayashi et al., 2001). Although it is still unknown which genes are targeted by this molecule, previous studies revealed that PDS seems to preferentially aim at non-telomeric nucleic acid sequences (Hou et al., 2022).

BRACO-19 is a G4-binder from the family of trisubstituted acridine compounds that seems to be very active against telomerases. It is known to produce specific effects *in vivo*, like growth inhibition and senescence (Burger et al., 2005). It has also been used as a coadjuvant in tumor models, because of its ability to hamper tumor regrowth (Gowan et al., 2002).

Phen-DC3 is a phenanthroline dicarboxamide bisquinolinium, one of the most effective G4-binders known so far. Its strong efficacy is mostly due to its particular V-shape structure that surrounds guanines, avoiding intercalation between the base pairs and restricting any further access to the stacked bases. Phen-DC3 localizes at cytosolic and nucleolar level, indicating a strong affinity for G4 and especially for RNA G-quadruplex (Deiana et al., 2020).

Because of their ability to bind and stabilize G4 structures, thus hampering RNA pol activity, recently a group of G4-binders have also been studied as possible antiviral agents, including PDS, BRACO-19, 360A, Nil, Ber, and TMPyP4, among others. Interestingly, they have shown a certain antiviral activity against viruses like herpes simplex 1, Epstein-Barr, Hepatitis B, Zika, and HIV1 (Zou et al., 2021).

In light of the fact that a change in the stability of G4s or in the way they form can alter the function of telomerase (Bryan, 2020; Tan and Lan, 2020), induce genome instability, (Bryan, 2019), hinder DNA replication (Lerner and Sale, 2019), and inhibit or promote transcription (Kim, 2017; Varshney et al., 2020), research has looked to chemical or molecular ways to induce said changes. Therefore, researchers have tried to develop G4 binders to stabilize G4s or shape their structure, in order to block cellular replication or

oncogene expression and hence use them as a cancer treatment strategy (Ruggiero and Richter, 2018; Carvalho et al., 2020).

To date, over 3000 G4 binders have been identified (Wang et al., 2022), exhibiting a wide range of features, specificity, and cell permeability (Haider et al., 2011). Although these molecules show promising perspectives in the development of new anti-cancer drugs, their use is yet to be approved in clinical applications (Ruggiero and Richter, 2018). Therefore, studies are currently underway to examine further G4 binders that are able to selectively target G4 structures, as it is the case of the molecules investigated in this PhD dissertation (see Chapter 3), in order to identify highly effective anti-tumor activity with lower potential side effects (Felsenstein et al., 2016; Asamitsu et al., 2019).

1.2 DNA Topoisomerases

DNA topoisomerases are highly-conserved enzymes that govern DNA topology in living cells. DNA topoisomerases cut one strand of a DNA duplex to allow a controlled rotation of one strand around the other, in order to relax DNA supercoils. They are active during DNA replication, transcription, chromatin remodeling, chromosome segregation and recombination, in order to resolve topological problems (Capranico et al., 2004). A constant regulation of DNA torsional stress is essential also because different degrees of DNA bending impact the extent to which proteins can access nucleic acid (Rohs et al., 2010) and DNA can endure high temperature in hyperthermophilic bacteria (Grogan, 1998). Topoisomerase enzymes come into action when a condition of topological stress occurs, for instance in the proximity of a transcribing RNA polymerase or a DNA replication fork. Indeed such structures imply the presence of positive supercoils in front of polymerases and negative supercoils behind RNA polymerases or catenated daughter duplexes behind replication forks. Torsional forces applied to the DNA duplex can alter the natural B-form of the DNA and a large number of phenomena can alter DNA winding number, exposing a

larger or smaller DNA portion to the interactions with DNA-binding proteins therefore determining relaxation or stretching (Corless and Gilbert, 2016). All the processes that require DNA denaturation and a facilitated access to DNA are more effective on negatively-supercoiled DNA duplexes (Champoux, 2012). Moreover, negative supercoils could also favour different, non-B structures, like cruciform DNA, triplex-DNA, G-quadruplexes, Z-DNA, and R-loops (Corless and Gilbert, 2016).

In mammals there are seven different topoisomerases (Figure 1.4). Four are defined as type I topoisomerases (TOP1), while the other three are type II topoisomerases (TOP2). They are distinguished based on the number of strands they are able to cut, one single

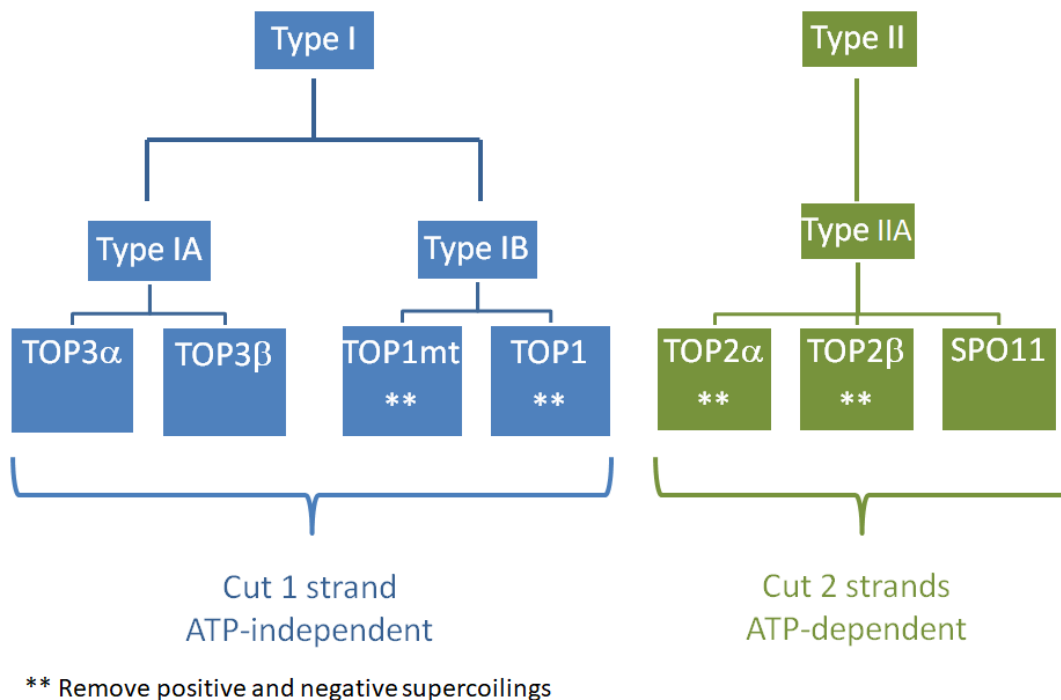


Figure 1.4 DNA Topoisomerases in mammals

DNA strand in the case of TOP1 and two strands for TOP2. While TOP1s are able to perform their enzymatic cut in an ATP-independent mode, TOP2s require ATP hydrolysis to remove DNA supercoils. Among the four TOP1, we can further identify type IA topoisomerases (TOP3 α , and TOP3 β), and type IB topoisomerases, namely the strictly

mitochondrial form mtTOP1 and the nuclear form TOP1. As for the three TOP2, they include TOP2 α , TOP2 β , and SPO11. TOP2 enzymes are able to relax supercoils during transcription and replication events, segregation of chromosomes, and removal of DNA catenanes (Roca, 2009).

1.2.1 Topoisomerase 1

Topoisomerases 1 are versatile enzymes since they are able to resolve both positive and negative supercoils; they remove one supercoil at once, so that a large number of reaction may be required in order to restore a normal supercoiling state (Pommier et al, 2016). The role of topoisomerase 1 is crucial for cell survival; as a matter of fact, an inadequate TOP1 activity can lead to a higher frequency of genomic breaks (Miao et al, 2007). Furthermore, TOP1 are also able to prevent the formation of unscheduled R-loops, thus reducing the risk of genome instability and DNA damage (Manzo et al., 2018).

When DNA is highly stretched, TOP1 enzymes can intervene to (i) induce a transient DNA break, (ii) stimulate a controlled rotation of the cut strand around the uncut one to reduce the number of windings, and (iii) re-ligate the DNA nick (Champoux, 2001; Capranico et al., 2017). The enzymatic catalytic site where this process takes place is always a tyrosine residue. The amino acid performs a nucleophilic attack targeting the 3'-hydroxyl end of the phosphodiester DNA backbone, while in TOP2 and TOP3 enzymes the attack aims at the 5'-hydroxyl DNA end (Koster et al, 2005).

After binding DNA, topoisomerases form an intermediate called TOP1 cleavage complex (TOP1cc), characterized by a bond between Tyr723 and the 3'-DNA ends (Stewart et al., 1998). The resulting cut strand of DNA rotates around the fixed one and is followed by the re-ligation of the 5'-free end, which in turn forms a new phosphodiesteric bond (Pommier et al., 2016). For this very last step a perfect alignment between the 5'-OH and the 3'-ends is critical; hence, any factor that may engender a misalignment of DNA ends can block

TOP1cc and prevent the nick from being repaired. In a physiological state, the cleavage complex intermediate exists for a very short period of time because the ligation step is faster than the cutting one and this makes Top1ccs almost undetectable. However, it can be stabilized by different stress conditions, namely oxidative agents, acidic pH, and drugs, leading eventually to frank DNA breaks. For this reason, TOP1cc constitutes an effective target for the development of anticancer drugs, indeed TOP1 poisons are used in standard therapies of certain solid tumors.

1.2.1.1 Topoisomerase and R-loops

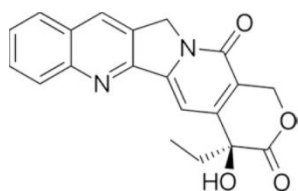
As described in Paragraph 1.1.1., R-loops are non-B DNA structures commonly associated with genomic instability, due to their ability to provoke interferences between the replication and the transcription machinery (Aguilera and García-Muse, 2012; Hamperl and Cimprich, 2014). In case of a high resistance to the rotational motion of transcription, negative supercoils generate behind the advancing polymerase (Liu and Wang, 1987), which are known to facilitate the formation of R-loops, since they promote DNA unwinding and, as a consequence, favor the strand re-annealing (Drolet et al., 1994). DNA Topoisomerase I (TOP1) is a topological homeostasis controlling factor of gene expression (Wang, 2002; Baranello et al., 2013). In bacteria, it has been shown that the relaxation of negative supercoils reduces the co-transcriptional formation of R-loops, thus avoiding their interfering with replication/transcription events and maintaining genome stability. For example, in *E. coli* deletion of bacterial topA gene, which is able to relax negative supercoils, results in the emergence of hypernegative DNA supercoils, which significantly promote the formation of R-loops and can only be reverted by means of RNaseH (an endonuclease that specifically degrade RNAs annealed to DNA strands) (Drolet et al., 1995; Massé et al., 1997). TOP1 can modulate R-loops either by reducing or increasing

their levels in living cells, depending on the genomic context (Manzo et al., 2018). In particular, Top1 gene depletion affects the amount of R-loops at a high number of transcribed loci, thus distinguishing between gene-poor regions characterized by R-loop gains and gene-rich regions showing R-loop losses (Manzo et al., 2018).

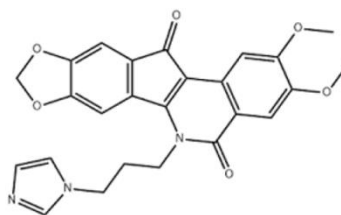
1.2.2 Top1 poisons

In light of the essential role played by Topoisomerases, a number of studies has investigated their activity in cancer cells and observed their overexpression in these aberrant cellular types (Ashour et al. 2015; Chen et al., 2015). For this reason, extensive research has looked for possible molecules that could inhibit the activity of TOP1, labeled as TOP1 poisons (Pommier, 2006; Pommier, 2013; Bailly 2012).

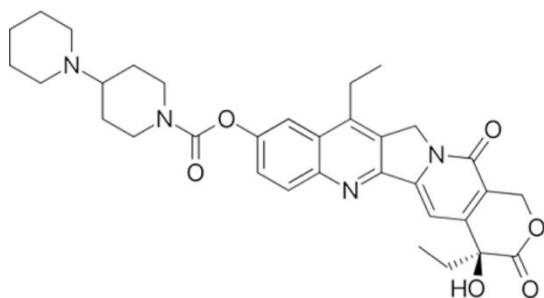
One of the first and most known TOP1 poisons is the alkaloid CPT, which was isolated



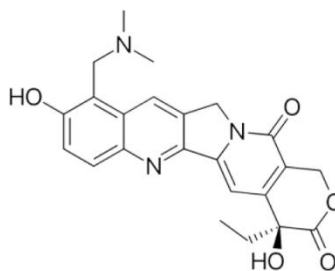
Camptothecin



Indimitecan (LMP-776)



Irinotecan



Topotecan

Figure 1.5 Molecular structures of TOP1 poisons. Created with Paint.NET

from a Chinese tree, the *Camptotheca acuminata* and employed in clinical tests as an anti-tumoral drug already in the 1970s (Wall and Wani, 1995). Since then, many other drugs were synthesized, including Irinotecan, (LMP-776, from the Indenoisoquinoline family), Irinotecan and Topotecan (Figure 1.5). Specifically, Irinotecan has been approved by US FDA for colorectal cancer, while Topotecan for lung and ovarian cancer. CPT targets exclusively TOP1 and achieves this goal in a very fast process (minutes after drug administration), although cleavage complexes are equally rapid in reverting this effect after drug removal (Pommier, 2016).

The cytotoxic effect of TOP1 poisons is mainly due to their ability of positioning right in between DNA and topoisomerase I, forming a stable ternary complex. In so doing, they manage to stop the cleavage complex and produce a single strand break (SSB), which can eventually evolve in a double strand break (DSB) if the stalled cleavage complex collides with a replication fork (Capranico et al., 2004; Pommier and Cushman 2009). As a consequence, they are able to kill cells while they are undergoing the S-phase (D'Arpa et al., 1990).

Their anticancer activity is also enhanced by their ability to originate stalled replication forks and contribute to the inhibition of the transcription process, which proves particularly efficient in longer genes which contain several introns (Martino et al., 2017). Furthermore, a stalled TOP1cc can also produce a sort of transcriptional stress, involving a more exposed chromatin together with a disproportion between sense and antisense strands (Baranello, 2010). This aspect is even more poignant considering that, as mentioned above, cancer cells are more susceptible to TOP1 poisons' action in respect to non-cancer cells, since they tend to overexpress TOP1 and are generally defective for DNA damage response (Pommier et al., 2010), making TOP1 poisons a rich object of investigation and one of the major objects studied in this work, with reference to their participation in the production of DNA damage.

1.3 DNA damage and DNA damage response

A common outcome of CPT administration is the enhancing of SSBs and DSBs due to the collision between the overt top1cc and the transcription/replication machinery. When these events occur, a number of cellular mechanisms are put in place in response to this damage, in order to signal, react and repair it. In the first place, the response to DNA damages mediated by TOP1 poisons elicits the activation of several important genes, like PARP1, PARP2, CSA, CSB, TDP1, p53, H2AX, ATM, and ATR, which can often undergo mutations in tumor cell lines, improving tumor survival. These proteins trigger the reaction of a wide range of other proteins, including: replication protein A2 (RPA2), p53, BLM, the two checkpoint kinase CHK1 and CHK2, and ATM.

Once the damage is inflicted to the DNA, the DNA-dependent protein kinase (DNAPK) is activated and phosphorylates RPA2, H2AX, and ATM (Gorgoulis et al., 2005; Shao et al., 1999). As a consequence, the kinase can also induce the activation of ATM-CHK2-p53 pathway (Pommier, 2006; Takemura et al., 2006). In case of high doses of CPT, DNA damage can also trigger the degradation of both TOP1 and RNAPOL2 mediated by proteasome (Desai et al., 2003). In the presence of a blocked TOP1cc, it is likely that negative supercoils tend to accumulate upstream with respect to the transcription blocked site, resulting in the emergence of unscheduled R-loops. The transcription block can also affect the splicing regulation capability, generating errors in the alternative splicing system and leading to altered mRNA constructs (Soret et al., 2003).

In order to resolve the block caused by TOP1ccs, cells can set off different pathways. If the DNA damage happens during transcription, cells can resort to XRCC1 and Base Excision Repair (BER) (El-Khamisy et al., 2005; Miao et al., 2006). On the contrary, if DNA damage occurs during replication, cells can rely on homologous recombination (HR) or non-homologous end-joining (NHEJ). HR uses the sequence of the homologous chromosome as an intact template that can be replicated on the disjointed one. A high-fidelity restoration process that usually takes place if the damage is inflicted during the S/G2 phase, when

chromosomes are duplicated (Sung and Klein, 2006; Wright et al., 2018). NHEJ comes into place when DSBs occur in not replicated DNA. In order to ligate the nick, NHEJ resorts to groups of exo- and/or endo-nucleases that resect small (≤ 4) amounts of nucleotides to restore compatibility between the separated strands (Davis and Chen, 2013; Weterings and Chen, 2008). NHEJ is often described as an “error-prone” system, since the nucleotide resection operated by exo- and endo-nucleases is likely to produce altered DNA sequences, resulting in small insertions/deletions (Rodgers and McVey, 2016). However, NHEJ repair can also occur without generating erroneous insertions/deletions in the DNA sequence but it is seldom observed since it cannot be detected by standard assays (Betermier et al., 2014).

DNA damage is detected by few main cleavage sensors: PARP1, which recognizes SSBs, and KU antigen and MRN, which recognize DSBs. PARP1 is a nuclear protein which is able to bind DNA by means of a dedicated 2 zinc finger N-terminus domain. Subsequent to DNA binding, poly(ADP-ribose) are attached to PARP1 and DNA histones. This change result in the recruitment of proteins like XRCC1 aiming to repair SSBs (El-Khamisy et al., 2003). The KU complex is able to create the conditions that favors the recruitment of key proteins involved in DNA DSB repair. Specifically, the KU complex intervenes on the end resection of DNA breaks by binding it, thus promoting the action of repair factors involved in non-homologous end joining repair process (Chang, Pannunzio et al., 2017). The MRN complex is formed by three factors: MRE11, NBS1, and RAD50. This complex recruits the ataxia-telangiectasia mutated (ATM) protein, a kinase which is able to phosphorylate the H2AX histone by forming γ H2AX in a region that spans from 0.5 to 2 Mb around the DSB site. The ATM kinase phosphorylates periodically the 0.03% of H2AX histones in this area (Berkovich et al., 2007) and is able to initiate the phosphorylation process within few minutes after the exposition to the stimulus (Furuta et al., 2003). This phosphorylated histone form can load the Mediator of DNA damage Checkpoint 1 (MDC1), which in turn, amplifies the response by means of a positive feedback mechanism that recruits more ATM and MRN. In the event of DNA DSBs, in order to strengthen the signal mechanism,

the p53 binding protein (53BP1) also rushes on damaged sites, forming foci that usually co-localize with γ H2AX ones (Anderson et al., 2001).

Replication inhibition or stress are instead recognized by RPA, which can bind ssDNA fragments, an excess of which is generated by the uncoupling of DNA polymerase from replication helicase activity during replication stress. Then, RPA together with the ATR-interacting protein (ATRIP), is responsible for the recruitment of ataxia-telangiectasia and RAD3 related complex (ATR) (Zou and Elledge, 2013). DNA damage exposes ssDNA that has been covered with RPA. At the same time, structures formed by ssDNA joined to dsDNA are detected by RAD9–RAD1–HUS1 (9-1-1). Subsequent to these two processes of exposure and detection, topoisomerase-binding protein-1 (TOPBP₁) creates a bond with the site of the damage, thus activating ATR by means of ATRIP (Mordes et al., 2008).

1.3.1 Micronuclei

Micronuclei (Figure 1.6) are cytoplasmic bodies containing fragments of broken

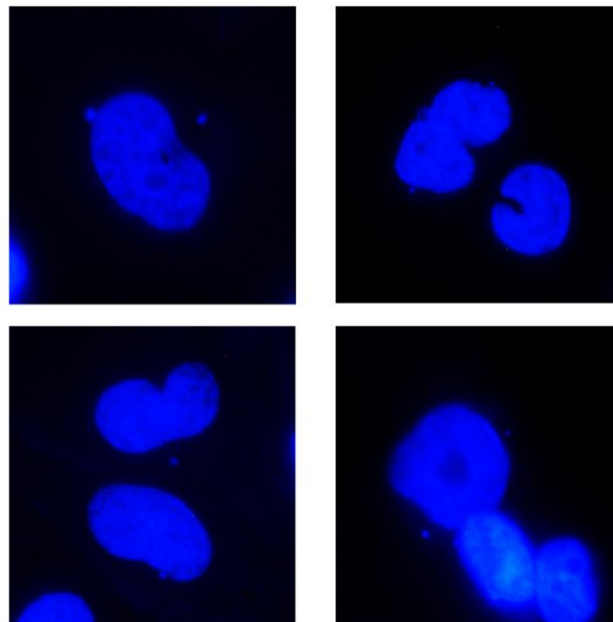


Figure 1.6 Examples of micronuclei observed by immunofluorescence microscopy with DAPI staining.

chromosomes and small sections of chromatin, which are separated from the main nucleus after cell division. Micronuclei are enveloped in a full double-layer nuclear membrane (MacKenzie et al., 2017; Harding et al., 2017), which enables the compartmentalization of cytosolic chromatin structures. Although micronuclei can successfully endure several cellular divisions, a lack of their lamina integrity can result in the collapse of the nuclear envelope during the G2 phase (Hatch et al., 2013). The integrity of the nuclear envelope is maintained by the action of the membrane-remodeling complex ESCRT-III, which is responsible of re-forming the nuclear envelope during mitosis and repairing it during the interphase (Raab et al., 2016; Robijns et al., 2016). This process is initiated by ESCRT-III subunit CHMP7 (Olmos et al., 2016) and regulated by the AAA ATPase, VPS4 (Vietri et al., 2016). Studies on the role played by these proteins in the collapse of nuclear envelope have revealed that their depletion causes severe defects or discontinuities in the nuclear lamina (Willan et al., 2019). This results in the loss of compartmentalization, letting cytosolic enzymes access the micronucleus, thus exposing DNA to the cytosol, which eventually produces DNA damage and chromothripsis (Zhang et al., 2015) and triggers innate immune response (Chen et al., 2016; Mackenzie et al., 2017). Micronuclei have been shown to increase as a consequence of CPT administration (Marinello et al., 2022), thus contributing to inflict further DNA damage and genome instability to daughter cells (Chan et al., 2009; Liu et al., 2014; Holmström and Winters, 1992). Their formation is a well-known marker of genome instability and genotoxicity (Shelby, 1988). Since micronuclei are a source of dsDNA at a cytosolic level, they are able to activate the signaling cGAS/STING pathway that eventually leads to the initiation of innate immune response (MacKenzie et al., 2017). This phenomenon was also observed in cells with other types of DNA damage or cells deficient for repair mechanisms, such as BRCA2- or BLM-depleted cells (Heijink et al., 2019; Gratia et al., 2019).

1.4. Innate immune response triggered by the cGAS/STING pathway

Innate immunity can be considered as the first line of defense against a wide range of pathogenic infections. It can be triggered in a number of different ways, all involving the recognition of the pathogenic agent or elements hinting to its presence, followed by a cascade mechanism triggering the defensive reaction. Such recognition of exogenous dangerous agents takes place by means of sensors including, among others, pattern recognition (PRRs) and NOD-like receptors (NLRs), and cytosolic DNA sensors (Takeuchi and Akira, 2010; Barber, 2014).

The cGAS/STING pathway (Figure 1.7) is an important biochemical pathway devoted to the recognition and signaling of the presence of nucleic acids in the cytosol (Chen et al., 2016). This situation does not occur in physiologic conditions and can result from microbial invasion or the expulsion of damaged DNA from nucleus, which is why cells must react quickly to avoid worse consequences. Because of its role in inducing innate immune response, as a consequence of DNA damage detection, a number of different tumors have been shown to constitutively downregulate this pathway to create an immune escape (Khoo and Chen, 2018; Su et al., 2019; Marinello et al., 2022). For this reason, it constitutes an important object of study for cancer-related research (Decout et al., 2021).

This pathway includes a cytosolic sensor, the cyclic GMP-AMP synthase (cGAS) that specifically recognizes and binds dsDNA. Two cGAS molecules bind two dsDNA sites to form a quaternary complex (Li, 2013; Zhang, 2014) and, as a consequence, the binding

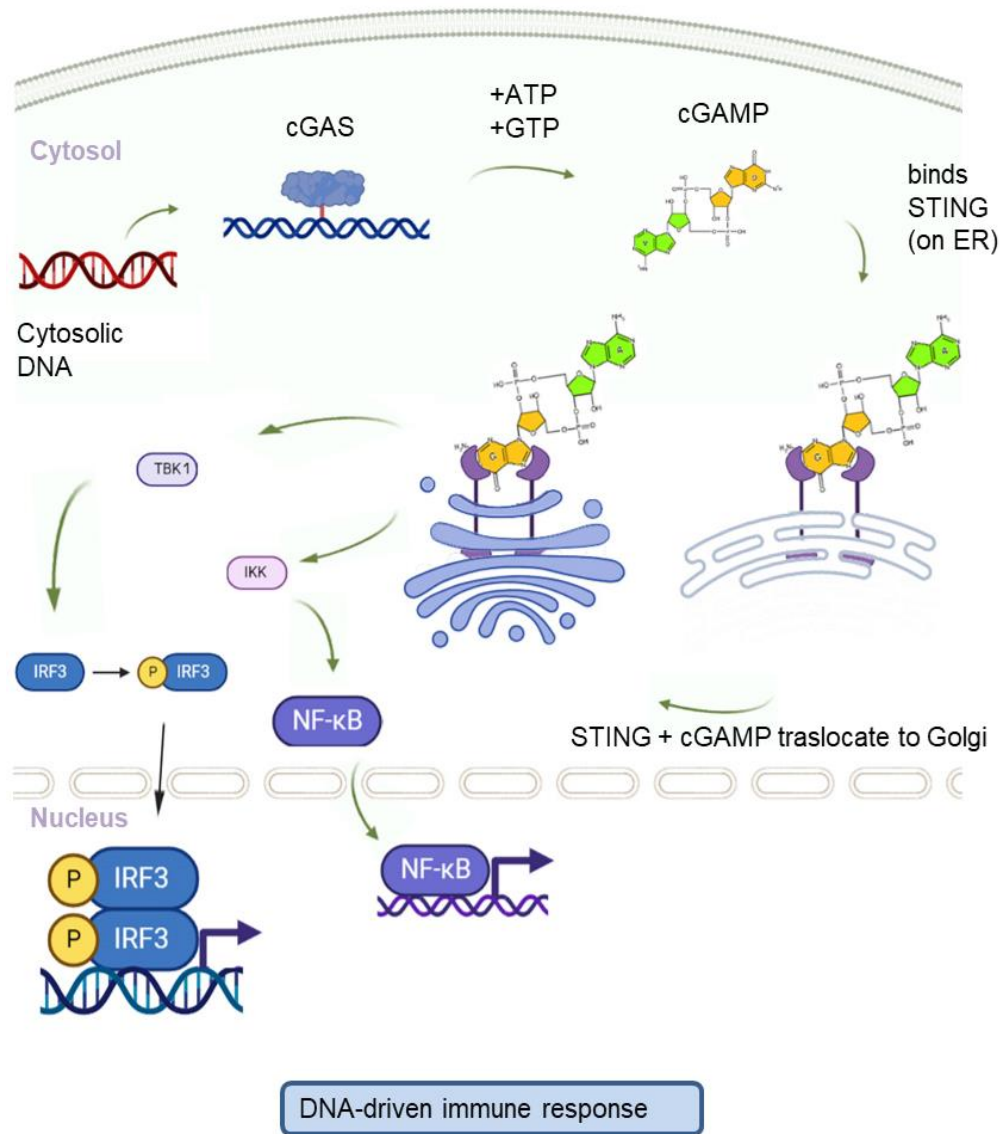


Figure 1.7 Short cGAS/STING pathway scheme reporting the cascade of events that goes from the recognition of cytosolic DNA by means of cGAS sensor, to the formation of a cGAMP molecule via ATP and GTP and eventually to the binding between cGAMP and STING. After this binding, the active form of STING promotes the production of 2 nuclear transcription factors that, once in the cell nucleus, are able to stimulate the transcription of interferon-family genes. Created with BioRender.com.

promotes the synthesis of the second messenger cyclic guanosine monophosphate-adenosine monophosphate (cGAMP). cGAMP, then, is specifically bound by the stimulator of interferon genes (STING), a transmembrane, adaptor protein originally situated on the endoplasmic reticulum. The binding event entails two main consequences: the complex STING-cGAMP moves to the Golgi apparatus (Ishikawa et al., 2009) and STING itself changes its conformation by exposing the C-terminal domain. This protein region is able to bind and activate the tank-binding kinase1 (TBK1) (Gao et al., 2013) which, in turn, phosphorylates the interferon regulatory factor 3 (IRF3). IRF3 then eventually enters into the nucleus and activates type 1 interferon genes (Fitzgerald et al., 2003; Liu et al., 2015) and, with a cascade mechanism, a large number of genes of the interferon-stimulated gene (ISGs) family (Schneider et al., 2014). These immune genes are valuable because they perform an antiproliferative and immunomodulatory activity. STING can also trigger the activation of I κ B kinase (IKK), an enzyme that activates NF- κ B, which is able to enter the nucleus and promote the transcription of over 150 genes.

cGAS/STING pathway can also be activated via a non-canonical method that occurs when the neo-synthesized cGAMP binds and activate PERK, a kinase located on the endoplasmic reticulum. Following this, the activated form of PERK phosphorylates eIF2 α , and in so doing starts the inflammatory response (Zhang et al., 2022). This alternative pathway results to be more primitive than the canonical one but nonetheless has a relevant role in senescence and organ fibrosis. Recent studies indeed demonstrate that it is possible to observe a reduction in the lung and kidney fibrosis by administering patients a treatment based on the STING-PERK targeting (Zhang et al., 2022).

When the signaling mechanism is not needed anymore, STING protein is degraded and, to this purpose, it is redirected to lysosomes and autophagosomes (Gonugunta et al., 2018).

1.5 TOP1 poisons and Small Cell Lung Cancers

Innate immune response constitutes one of the major areas of investigation when it comes to clinical studies aiming to develop immunostimulatory treatments targeting cancers. For this reason, several molecules are being studied in order to understand if the modulation of non-B DNA structures can be employed to activate an innate immune response to effectively fight cancer. Among these drugs, TOP1 poisons have long been used in cancer treatments, with special reference to colon, ovary, and SCL cancers.

Indeed, TOP1 plays a critical role in the development of several different types of cancer, characterized by a high cellular proliferation and high replication levels, which require high involvement of TOP1. For this reason, a number of cancer treatments have already employed TOP1 as a target (Naumann and Coleman, 2011; Hartwell et al., 2011; Van Cutsem et al., 2002), although some types of cancer, like NSCLC, seem to exhibit some resistance to TOP1 drugs (Vennepureddy et al., 2015; Yang et al., 2015). However, some studies have found that other factors might concur to the effectiveness of TOP1 targeting in cancer treatment, like the repair protein XPF (Liu et al., 2007) and TDP1 activity (Jakobsen et al., 2022). Thus, therapeutic approaches targeting TOP1, also in combination with other targeted proteins, constitute promising methods to fight lung cancers.

Lung cancers are a heterogeneous category of cancer diseases, with cell populations that come from different histological locations, including central lung positions, such as squamous cell carcinomas, small cell lung cancers (SCLC) or from outermost ones, like adenocarcinomas (Sun et al., 2007). Out of all these different types of lung cancers, with an estimated 7% 5-year survival, SCLC is widely known for its lethality and high metastatic activity, to the point that it is responsible for the death of over 200,000 people all over the world every year (American Cancer Society, 2015; Rudin et al., 2016).

SCLC cell lines generally exhibit short doubling times, a pronounced neuroendocrine differentiation and are often suspension-growing cells (Gazdar et al., 2017). The region on chromosome 19, where LKB1 and BRG1 tumor suppressor genes are located, is often lost

in this cancer cell lines (Rodriguez-Nieto et Sanchez-Chespedes, 2009). Furthermore, these cells bear a homozygous deletion on the long arm of chromosome 2, which determines the inactivation of CASP8 (Shivapurkar et al., 2002), a main actor from the caspase family involved in the death-inducing signaling complex. As for highly expressed genes, SCLC cells are characterized by the overexpression of MYC proteins (Jahchan et al., 2016) and SOX2, a regulator of pluripotent stem cells and neural differentiation (Rudin et al., 2012). This is extremely relevant, in light of the fact that the stem cell fraction is greatly represented in these cancer cells, since the respiratory epithelium hosts many stem cell niches, involved in the emergence of SCLC cell lines that are known to sprout starting from stem cells committed in the neuro-endocrine differentiation path (Semenova et al., 2015).

Besides these common and frequent features, variants can also be observed, including slightly larger cells with noticeable nucleoli, partial loss of neuroendocrine properties, a marked tendency to epithelial-mesenchymal transition, and a rather-adherent grown pattern (Stewart et al., 2017).

In this PhD thesis project, 3 SCLC cell lines were used, namely H889, H209, and DMS114. H889 is a human, carcinoma cell line from the lung epithelium, stage E, obtained from a 69-years old European female, growing in suspension. H209 is a human lung carcinoma characterized by small, rounded cells that grow in suspension with a tendency to form floating aggregates. The line is from a European, 55-years old male patient. Finally, DMS114 are a human lung carcinoma cell line, from a European, 68-years old male and they grow in adhesion. All three cell lines are grown in the same culture medium, RPMI.

SCLC cell lines were selected as they have been observed to resist checkpoint immune inhibitors, which are currently investigated as an antitumor treatment (Thomas and Pommier, 2016). Therefore, an approach based on the enhancement of cancer cell-internal innate immune response, rather than a cell-mediated one might offer interesting outcomes.

Aim of the project

This project focuses on gaining a better understanding of the process triggered by the mis-regulation of non-B DNA structures (R-Loops and G4s) that leads to the initiation of innate immune response in cancer cells. In order to achieve this goal, the phenomenon was studied over two different research lines. The first one explored the effects of TOP1 poisons in 4 SCLC cell lines, namely: H209, H889 and DMS114 as compared to HeLa cells, while the second one aimed at establishing structure-activity relationships of G4 stabilizers in relation to cytotoxicity, ability to stabilize G4 structures and activation of immune genes in living cells.

In order to study the effects of TOP1 poisons, two different drugs were used (CPT and LMP776). After drug administration, we determined that TOP1 poisons were able to stimulate the production of R-loops and micronuclei. We observed that micronuclei production could indeed be ascribed to R-loops stimulation. Then, we assessed the activation level of cGAS/STING pathway in the four cell lines and consequent innate immune response activation by analyzing a panel of cytokines with real time-PCR. The findings have been published in the British Journal of Cancer (Marinello et al. 2022).

The second part of my PhD work dealt with the study of a group of different neo-synthesized G4 binders to evaluate *in vivo* their G4-binding effectiveness, cytotoxicity and ability to induce DNA damage and IFN β production. The phase of drug design and synthesis was performed by prof. Rita Morigi from University of Bologna, while studies concerning G4 stabilization, affinity, and selectivity *in vitro* were performed by the research team of proff. Antonio Randazzo and Jussara Amato from Federico II University of Naples. The results of this study have been published in Journal of Medicinal Chemistry (Marzano et al., 2022).

CHAPTER II

Methods

2.1 Cell lines, cultures and treatments

The cell lines used for this PhD project were: U2OS, MCF7, HeLa, H209, H889, DMS114, MNMCA1, and B16. U2OS (RRID:CVCL_0042) and HeLa (RRID:CVCL_0030) were bought from ATCC (LGC Standards SRL, Milan, Italy), while H209, H889, and DMS114 were kindly provided by Anish Thomas from NCI, NIH (Pommier, 2006). MCF-7 were purchased by the American Type Culture Collection (ATCC), while wild type and STING gene CRISPR knockout B16 were kindly provided by R. Greenberg (Harding et al., 2017).

We also employed a cell line obtained in our laboratory starting from an U2OS cell strain (De Magis et al., 2019) with an inducible RNaseH1. RNaseH1 induction was realized by administering 2 μ g/mL doxycycline to the cell culture for 48 hours, before other treatments.

All cell cultures were grown in a humidified incubator at 37 °C, with 20% O₂ and 5% CO₂, they were periodically tested for Mycoplasma and for cell identity with Cell ID System (Promega, Madison, WI, USA) by BMR Genomics (Padua, Italy).

Drugs and compounds we used were dissolved in dimethyl sulfoxide (Sigma-Aldrich #472301) by realizing 10mM concentration stock aliquots, stored at -20°C and diluted at the final concentration just before use, unless otherwise stated. Drug treatments were administered to exponentially growing cells.

Cell line	Species	Disease	Growing conditions	Culture characteristics
U2OS	Human	Osteosarcoma	DMEM + 10%FBS + 2mM L-glutamine	Adhesion, monolayer
U2OS-RH	Human	Osteosarcoma	DMEM + 10%FBS + 2mM L-glutamine + 500µg/mL Hygromycin B + 1.5µg/mL puromycin + 100µg/mL Pen/Strep	Adhesion, monolayer
MCF7	Human	Invasive breast carcinoma	DMEM + 10%FBS + 2mM L-glutamine	Adhesion, monolayer
HeLa	Human	Papilloma-virus related endocervical adenocarcinoma	DMEM + 10%FBS + 2mM L-glutamine	Adhesion, monolayer
H209	Human	Small Cell Lung Cancer	RPMI + 10%FBS + 100µg/mL Pen/Strep + 2mM L-glutamine	Suspension
H889	Human	Small Cell Lung Cancer	RPMI + 10%FBS + 100µg/mL Pen/Strep + 2mM L-glutamine	Suspension
DMS114	Human	Small Cell Lung Cancer	RPMI + 10%FBS + 100µg/mL Pen/Strep + 2mM L-glutamine	Adhesion, monolayer
MNMCA1	Mouse	Fibrosarcoma	DMEM + 10%FBS + 2mM L-glutamine	Adhesion, monolayer
B16	Mouse	Melanoma	DMEM + 10%FBS + 2mM L-glutamine	Adhesion, monolayer

Table 2.1 Cell line characteristics and their growing conditions. We purchased DMEM, RPMI, FBS, L-glutamine, Penicillin/Streptomycin from Gibco (Thermo Fisher, Waltham, MA, USA) and Hygromycin B from Invitrogen (Thermo Fisher, Waltham, MA, USA).

2.2 Immunofluorescence

2.2.1 TOP1 poisons and S9.6

2×10^5 cells were seeded on a microscope glass slide in a 6-well multiwell dish. After a 24-hour TOP1 treatment cells were let to recover for 48 hours and then they were fixed by

administering ice-cold methanol for 10 minutes at room temperature. After this, cells were washed twice with PBS and permeabilization was performed by treating cells with Acetone for 1 minute on ice. At this point cells were washed 3 times with cold PBS for 5 minutes under gentle shaking. Therefore, in case of S9.6 staining, glass slides were incubated for 2 hours at room temperature with primary antibody against nucleolin (anti-nucleolin antibody, Abcam Cat# ab22758, 1:1,000) and S9.6 (S9.6 antibody, 5 µg per slide) to stain, respectively, nucleoli and R-loops. We incubated glass slides by positioning them upside down on a parafilm strip where 70 µL of antibody solution were spotted. After primary antibody administration, we washed the glass slides 3 times with saline-sodium citrate buffer 4X (SSC 4X buffer) for 5 minutes, gently shaking. The secondary antibody staining was performed by using Alexa Fluor 594 goat anti-mouse IgG (Thermo Fisher Scientific Cat#A-11032) and Alexa Fluor 488 goat anti-Rabbit IgG (Thermo Fisher Scientific at# A-11032).

Then, for both TOP1 poison and S9.6 staining, we incubated cells with a 3.3µg/mL aqueous DAPI solution for 20 minutes. Finally glass slides were mounted by means of Mowiol and observed by Nikon Eclipse 90i Microscope. Acquired data were analyzed with ImageJ software and we evaluated R-loops immunofluorescence by subtracting the nucleolin signal from the total nuclear staining.

2.2.2 U2OS overexpressing RNaseH1

U2OS overexpressing RNaseH1 require to add Hygromycin B and Puromycin for the maintenance in a DMEM medium and doxycycline for RNaseH1 induction. In order to start our immunofluorescence experiments, 3×10^4 cells were seeded on a cover glass slide in a 6-well and they were cultured in a Hygromycin- and Puromycin-free DMEM medium. The induction of RNaseH1 began 24 hours after the seeding and was obtained by administering 2µg/mL of doxycycline to cells for 48 hours. On the last culturing day, TOP1

poisons were provided to cells in order to stabilize and enhance R-loops (10 μ M of CPT or LMP-776 for 5 or 10 minutes in case of short-period treatments, or 100nM of CPT or 200nM of LMP-776 for 24 hours in case of long-period treatments). Then we fixed our cells with ice-cold methanol and we proceeded as previously described in this chapter.

2.2.3 γ H2AX

As for the γ H2AX immunofluorescence procedure, we fixed our cells for 15 minutes with 4% formaldehyde in PBS, then we permeabilized them with 0.5% Triton X-100 in PBS for 15 minutes and we performed 3 washes in PBS lasting 5 minutes. Following, we performed the blocking by using 8% BSA in PBS for 30 minutes at room temperature. At this point, slides were incubated with the primary antibody directed against γ H2AX (Anti-phospho-histone H2AX (Ser139) antibody, Millipore, Cat# 05-636), 1:1,000 in 1% BSA/PBS for 2 hours at room temperature. We performed 3 washes in PBS (lasting 5 minutes) and then we incubated with the secondary antibody Alexa Fluor 488 goat anti-mouse IgG Secondary antibody (Thermo Fisher Scientific Cat# A-11011) dissolved in 1% BSA/PBS for 1 hour. Finally we performed 3 further washes and finally DAPI staining with a 3.3 μ g/ μ L DAPI solution in water. The last step was to mount glass slides with 15 μ L of Mowiol as previously described.

2.2.4 STING and cGAS

We seeded cells directly on a cover slide. The STING immunofluorescence protocol requires an initial fixing incubation for 10 minutes with 4% paraformaldehyde at room temperature, followed by a permeabilization/blocking incubation performed with 1% BSA, 10% FBS, 0.1% glycine, and 0.1% Tween-20 for 1 hour, at room temperature, under gentle

shaking. To follow, we performed the primary antibody incubation with an anti-STING antibody (TMEM173 Antibody, Abcam Cat# ab92605, RRID:AB_10562137) overnight at 4°C.

As for the cGAS immunofluorescence, we realized a 20-minute fixation by using 4% formaldehyde at room temperature, then we permeabilized cells for 5 minutes with 0.5% Triton X-100 in PBS and, finally, we blocked them with 1% BSA in PBS for 30 minutes at room temperature. Therefore we used an antibody against cGAS (cGAS (D1D3G) antibody, Cell Signaling Technology Cat#15102, RRID:AB_2732795) incubating glass slides for 1 hour at room temperature. For both protocols we used the same secondary antibody: Alexa Fluor 488 anti-rabbit IgG (Thermo Fisher Scientific Cat# A-11008, RRID:AB_143165) and a final DAPI staining step, at 2µg/mL for 20 minutes.

2.2.5 Micronuclei Immunofluorescence

Following the procedure for adherent cells, 2×10^5 cells were seeded on cover slides in a 6-well multiwell. The day after seeding we performed a 24-hour treatment by administering 100 nM CPT or 200 nM LMP-776. After this treatment we let cells to recover for 48 hours and then we proceeded with a 15-minute fixation by treating with 4% paraformaldehyde at room temperature and, subsequently, with permeabilization, by administering 0.5% Triton X-100 in PBS for 15 minutes at room temperature and finally we realized a 20 minutes DNA-staining with DAPI. On the other hand, cells growing in suspension required an initial concentration of at least 7×10^4 cells/mL and we performed the same treatments, plus, this cell type needs an additional step before the fixation. Indeed it was necessary to make cells adhere to the slide in a more stable manner and, to do this, we cytopinned 2×10^5 cells by means of Cytospin 4 (Thermo Shandon, Runcorn, UK) onto a glass slide and there we performed fixation, permeabilization and DAPI staining as already described for

adherent cells. Representative images were taken by Nikon Eclipse 90i Microscope to perform micronuclei count and related statistics.

2.2.6 BG4 immunofluorescence

S. Balasubramanian kindly provided our laboratory with the plasmid expressing the BG4 antibody and we transfected BL21 (DE3) E. Coli cells. Antibody expression was obtained by means of autoinduction in said cells and the purification was performed by means of Protino Ni-IDA (Machery-Nagel ref#745250.10) pre-charged with Ni²⁺ and subsequently eluted with a 250 mM Imidazole solution dissolved in a PBS buffer pH 8.0 containing: 1.37 mM NaCl, 27 mM KCl, 100 mM Na₂HPO₄*7H₂O, and 18 mM KH₂PO₄. The solution containing the BG4 was concentrated with Amicon Ultra-15 Centrifugal Filter Units (Millipore ref #UFC903024). The excess of Imidazole was removed by washing many times with PBS pH 8.0. Finally the antibody solution was stored at 4 °C in a 0.02% sodium azide solution.

We seeded 3.5x10⁵ U2OS cells onto a glass slide in a 6-well and the following day we administered G4-binders at a 10µM concentration for 10 minutes. After drug administration the medium was replaced with a pre-fixation mix, composed by 50% DMEM and 50% fixing solution (methanol/acetic acid 3:1) that was left in wells for 10 minutes. After this time, one quick wash in fixing solution was performed, followed by a 10-minute incubation at room temperature. Subsequently, cells were permeabilized by treating them with 0.1% Triton X-100 in PBS for 3 minutes at room temperature under gentle rocking. Afterwards, they were washed 3 times in PBS for 5 minutes. Then cells were subjected to blocking for 1 hour at room temperature under gentle rocking by administering 2% milk in PBS. The incubation with both primary and secondary antibodies was performed as already described, by placing the glass slide upside down on a parafilm slice where 70 µL of antibody solution in blocking buffer was previously spotted. Washes

indicated in this protocol were always three 5-minute washes performed with a washing solution made of 0.1% Tween-20 in PBS. We dispensed 2 μg of BG4 per slide and left the slides on the antibody for 2 hours. Thereafter, three washes were carried out and the secondary antibody was used. Since the BG4 antibody is equipped with a 8-aminoacid tag (DYKDDDDK), we administered a secondary antibody directed against this epitope. Indeed we incubated glass slides with a rabbit, anti-FLAG antibody (Cell Signaling ref #2368) diluted 1:800 in blocking buffer for 1 hour at room temperature. Next, another wash session was realized, followed by a 1 hour incubation with a goat anti-rabbit Alexa Fluor 488 IgG 1:1,000 (Life Technologies ref #A11008) and then other 3 washes. Finally, we performed the nuclear staining by means of a 3.3 $\mu\text{g}/\mu\text{L}$ DAPI solution in water for 20 minutes, we realized a last quick water wash and mounted the glass slide upside down in presence of 15 μL of Mowiol.

2.3 RNA extraction, retrotranscription and qrt-PCR

Cells designated for RNA analysis were pelleted after a 48-hour recovery in drug-free medium following a 24-hour TOP1 poison treatment (100 nM CPT, or 200 nM LMP). Cell pellets were lysed by using TRIzol (Ambion, Life Technologies, Carlsbad, CA, USA) following manufacturer's instruction, then extracted RNA was quantified by Nanodrop 2000 (Thermo Fisher Scientific, Waltham, MA, USA) and checked by electrophoresis. The RNA was retrotranscribed in cDNA by using Superscript III Reverse Transcriptase (Invitrogen, Thermo Fisher Scientific, Waltham, MA, USA) in a mix containing oligo-deoxythymidines, random hexamers, and dNTPs. After having obtained cDNA, we performed a series of Real-Time PCR in order to analyze a panel of cytokines with a Biorad CFX Connect Real-Time System and a mix containing SsoAdvanced Universal SYBR Green Supermix (#1725274, Bio-Rad, Hercules, CA, USA) and the primers indicated in table 2.2.

Gene	Species	Type	Sequence
IFIT1	Human		Bio-Rad validated primer 460680247; qHsaCED0034841
DDX60	Human		Bio-Rad validated primer 460680232; qHsaCID0006241
CCL5	Human		Bio-Rad validated primer 460680239; qHsaCID0011644
CXCL10	Human		Bio-Rad validated primer 460680254; qHsaCED0046619
IL6	Human		Bio-Rad validated primer 460680246; qHsaCID0020314
CCL20	Human		Bio-Rad validated primer 460680233; qHsaCID0011773
CytB	Human		Bio-Rad validated primer 460680241; qHsaCED0048354
TNF	Human		Bio-Rad validated primer 460680240; qHsaCED0037461
IL1B	Human		Bio-Rad validated primer 460680238; qHsaCID0022272
IL1A	Human		Bio-Rad validated primer 460680243; qHsaCID0016254
IL8	Human		Bio-Rad validated primer 460680259; qHsaCED0046633
ISG15	Human		Bio-Rad validated primer 460680253; qHsaCED0001967
IFI44	Human		Bio-Rad validated primer 460680258; qHsaCED0044799
IFNA1	Human		Bio-Rad validated primer 460680251; qHsaCED0048248
IFNB1	Human		Bio-Rad validated primer 460680231; qHsaCED0046851
CXCL1	Human		Bio-Rad validated primer 460680252; qHsaCED0046130
CCL5	Mouse	FOR	TGCTCCAATCTTGCAATCGT
		REV	TCTTCTCTGGGTTGGCACAC
CXCL10	Mouse	FOR	CCAAGTGCTGCCGTCATTTT
		REV	AGCTTCCCTATGGCCCTCAT
IFIT1	Mouse	FOR	TGCTCTGCTGAAAACCCAGA
		REV	AGGAACTGGACCTGCTCTGA
IFI44	Mouse	FOR	TACCCATGACCCACTGCTGA
		REV	ATCAGATCCAGGCTATCCACG
ISG15	Mouse	FOR	GACCTAGAGCTAGAGCCTGC
		REV	ACCAGGAAATCGTTACCCCC
CytB	Mouse	FOR	ATTCCTTCATGTCCGACGAG
		REV	ACTGAGAAGCCCCCTCAAAT
cGAS#1	Human	FOR	TGCACGAGTGTTGGAATATTCT
		REV	GAGAAGTTGAAGCTCAGCCG
cGAS#2	Human	FOR	AAAGAAGGCAGTTTTACATGAT
		REV	ACCCAAGCATGCAAAGGAAG
STING	Human	FOR	GCAGTTTATCCAGGAAGCG
		REV	AAGGGAATTTCAACGTGGCC

Table 2.2 Primers used for qRT-PCR

The amplification protocol was designed following manufacturer's instructions, we finally checked our PCR products by means of electrophoresis and by analyzing melting curves.

We expressed the results of our analysis by calculating genes' fold increases by means of $\Delta\Delta\text{Ct}$ comparison and the obtained values were normalized on CytB.

2.4 RNaseH1 overexpression

RNaseH1 overexpression was performed in HeLa cell line. We seeded 5×10^5 cells into a 6-well plate. The day following the seeding, transfection was performed by using 2.5 $\mu\text{g}/\text{well}$ of RNaseH1 overexpression plasmid (pRH1, kindly provided by F. Chedin, University of California, DAVIS) and 5 $\mu\text{L}/\text{well}$ of Lipofectamine 2000 (Invitrogen, Thermo Fisher Scientific, Waltham, MA, USA) in OPTIMEM (Gibco, Thermo Fisher Scientific). The day following the transfection we replaced the medium and administered a 24-hour TOP1 poison treatment, with 100nM CPT or 200nM LMP-776. After treatment, cells were let recover for 48 hours in a fresh, drug-free medium, before initiating RNA extraction.

2.5 Western blot

We pelleted our harvested cells and lysed them in a lysis buffer containing 4% SDS, 20% glycerol, and 0.125M TRIS-HCl. Then, we quantified the protein concentration by using a Lowry assay and we used 60 μg of protein lysate for each well of a precast Bolt 4 to 12% Bis-Tris Mini Protein Gel (Thermo Fisher, Waltham, MA, USA). After the electrophoresis we transferred proteins onto a nitrocellulose membrane, we performed a Red Ponceau staining in order to visualize protein bands and have a normalization standard for protein quantification. Then we blocked our membrane for 1 hour at room temperature by using a blocking buffer containing TBS, 0.5% Tween-20, and 5% milk under gentle rolling. Subsequently, we incubated our membranes overnight, at 4 °C, by using a primary antibody diluted in blocking buffer. We used 3 different primary antibodies, directed

against: STING (Abcam Cat# ab92605, dilution 1:1000), cGAS (cGAS (D1D3G) antibody, Cell Signaling Technology Cat#15102, dilution 1:1000), and TOP1 (Santa Cruz Biotechnology Cat# sc-5342, dilution 1:500). The following day we performed 3 washes with TBS 0.5% Tween-20 and then membranes were incubated for 1 hour at room temperature with secondary HRP-conjugated antibodies, diluted in blocking buffer, directed against: rabbit (Abcam Cat# ab205718, 1:10,000), or goat (Santa Cruz Biotechnology Cat# sc-2922, 1:2,000), under gentle rolling. The final detection was performed by using Pierce ECL Plus Western Blotting Substrate (Thermo Fisher Scientific, Waltham, MA, USA) and the Scanner Storm 840 (Amersham Biosciences, Sunnyvale, CA, USA).

2.6 cGAMP ELISA

HeLa cell line were treated with TOP1 poisons for 24 hours and cGAMP levels were measured upon drug removal and 24, 48, and 72 hours after drug removal. We quantified the second messenger amount by analyzing the whole cellular extract. HeLa cell pellets were resuspended in RIPA buffer containing: 150mM NaCl, 0.5mM PMSF, 1mM EDTA, 2mM DTT, 1% NP-40, 1mM EGTA, 20mM Tris-HCl pH 7.5, and Halt Protease Inhibitor Cocktail. Lysed cells were incubated for 30 minutes on ice and, subsequently centrifuged at 12,000xg at 4°C for 20 minutes. At that point we collected supernatants and used them to evaluate cGAMP quantity by using the Direct 2'3'-Cyclic GAMP Enzyme Immunoassay kit (#K067-H1, Arbor Assay) following manufacturer's instruction.

2.7 STING gene silencing

We seeded 3×10^6 HeLa cells onto a 10 cm dish and during this operation we transfected cells with Lipofectamine RNAiMax Transfection Reagent (Invitrogen, Thermo Fisher

Scientific, Waltham, MA, USA) and 2 different siRNAs directed against STING mRNA (Ambion siRNA #1 128591, Ambion siRNA #2). Then we checked STING protein levels every 24 hours until 96 hours after transfection by means of Western Blot. TOP1 poison treatment was administered 48 hours post-silencing and a new siRNA transfection was performed at the end of TOP1 poison treatment, upon medium replacement, 72 hours after the first transfection.

2.8 STING chemical inhibition

Chemical STING inhibition was realized in H209 cell line by using H151 (Cat. 6675, Tocris Biosciences; Bristol, UK) at 2 μ M concentration. We seeded 40x10⁶ cells in a T-175 flask with a density of about 600,000 cells/mL and just after seeding, H151 was administered. One hour after H151 administration, TOP1 poison treatment started and lasted for 24 hours (100nM CPT or 200nM LMP-776). At the end of treatment the medium was replaced, H151 was added again, and cells were let recover for 48 hours. Finally cells were collected and RNA was extracted as previously described.

2.9 DNA demethylation by 5'-Azacytidine

DNA demethylation was performed on DMS114 cell line with the aim of demethylating STING promoter and reactivating its transcription. In order to do this, we seeded 3x10⁶ DMS114 cells onto a 10cm dish and after 24 hours we administered 5 μ M 5'-Azacytidine (Cat. A2385 Sigma-Aldrich; Darmstadt, Germany). Since 5'-Azacytidine is highly unstable, we replace medium daily. To this purpose, we set up 10mM water stock solutions stored at -80°C and from said stocks we prepared freshly operating solution just before use, diluting to the final concentration directly in the medium. Cells were then treated for 24

hours with Top1 poisons (100nM CPT or 200nM LMP-776), 48 hours after the first 5'-Azacytidine administration and they were let recover for 48 hours before performing RNA extraction.

2.10 STING overexpression in DMS114

We performed STING overexpression by means of a plasmid (NET23 pEGFP-N2-1174; plasmid #62037 Addgene, Watertown; MA, USA) in DMS114 cell line. In order to do this, 10^6 DMS114 cells were seeded in a 6-well and, the day after seeding, cells transfection was performed by administering 2.5µg/well of said plasmid together with 5µL/well of Lipofectamin 2000 (Invitrogen, Thermo Fisher Scientific, Waltham, MA, USA) in OPTIMEM (Gibco, Thermo Fisher Scientific). The transfection mix was left to act for 24 hours and then it was replaced with a fresh medium containing TOP1 poison treatment, as already reported (100nM CPT or 200nM LMP-776 for 24 hours). Finally cells recovered for 48 hours at the end of TOP1 poison treatment in a free-drug medium and they were harvested to extract and analyze RNA.

2.11 Viability assay (MTT assay)

The MTT assay was used to evaluate the viability of cells after performing a drug treatment. At the end of the assay, for each tested compound, the IC_{50} was calculated in order to choose the drug concentration to be used in the following experiments. This is a colorimetric test in which succinate dehydrogenase reduces tetrazolium ring to formazan, an insoluble blue salt that precipitates in the well by giving the cell culture a purple color. The amount of produced formazan can be measured by means of spectrophotometry at

540nm. Since only living cells can perform the enzymatic reaction, the absorbance measurement is directly proportional to the number of survived cells.

We seeded 3×10^4 cells in a 24-well and the day after seeding we administered increasing concentrations of the same drug for 24 hours. After this time we replaced medium with a fresh one and we let cells recover for 48 hours in a drug-free medium. After recovering, the medium was replaced again with a $0.45 \mu\text{g}/\text{mL}$ MTT (Merck #2128) solution in complete DMEM and cells were incubated at 37°C for 2 hours. Subsequently, MTT solution was carefully removed without disturbing formazan salt crystals and $300 \mu\text{L}$ of DMSO were added to each well in order to resuspend formazan by incubating plates at room temperature under gently shaking for 1 hour. Finally $100 \mu\text{L}$ of formazan solution were laid in a 96-well to read absorbance and realize graphs of IC_{50} by means of Graph Pad software (Graph Pad Prism 8.0, Graph Pad Software Inc.).

2.12 IFN β ELISA

The IFN β ELISA test was performed on several cell lines (MNMCA1, HeLa, MCF-7, and U2OS) in order to measure the amount of IFN β produced in the supernatant of these cell lines as a consequence of innate immune response activation due to the administration of G4-stabilizers. To this purpose we used a human IFN-B Quantikine ELISA kit (MIFNB0, R&D Systems), following manufacturer's indications. To perform this experiment, we seeded 10^6 cells in a 10cm dish. The following day we started a 24-hour G4-binder treatment and when it ended, cells were provided for fresh, drug-free medium and were left recover for 48 hours. After this time supernatants were collected and added with a protease inhibitors mix made of: 2mM DTT, 1mg/mL aprotinin, leupeptin, and pepstatin, 0.5mM PMSF. Subsequently we make supernatants to concentrate about 25-folds by means of a Pierce Protein Concentrator PES, 3k MWCO, 5-20mL (#88525, Thermo Fisher Scientific) and finally we calculated the IFN β produced as $\text{pg}/\text{mL}/10^6$ cells.

CHAPTER III

Results

3.1 Top1 poisons induce micronuclei production mediated by R-Loop stabilization

TOP1 poisons are known to induce DNA damage mediated by Top1cc stabilization when administered to cells (Pommier, 2006; García-Muse and Aguilera, 2016; Hamperl et al., 2017). Moreover, early studies have found that TOP1 poisoning by CPT can stimulate the production of micronuclei in murine bone marrow cells (Holmström and Winters, 1992). Hence, we wondered whether DNA damage can lead to micronuclei formation in human cancer cells. In order to answer to this question, we evaluated the effects of TOP1 poisons by administering 100nM CPT and 200nM LMP-776 (sub-cytotoxic doses) to HeLa, H209, H889, and DMS114 cells for 24 hours. Then, subsequent to drug removal, cells were let recover for 48 hours in fresh medium and micronuclei were then detected by immunofluorescence microscopy (Figure 3.1c). The observation of non-treated cells revealed the presence of only 3-4 micronuclei/100 cells (Figure 3.1a), while treated cells showed an increase in the number of micronuclei: 4 times higher in HeLa and H209 cell lines, 3 times in H889 cell line, 4 to 6 times in DMS114 cell line (Figure 3.1b). Both the treatments with CPT and LMP-776 produced quite similar results across all of the 4 examined cell lines, even though a difference could be observed in DMS114, where the number of CPT-induced micronuclei was slightly higher than the one induced by LMP-776 but this increase was not sufficient to be statistically significant. This result implies that both the TOP1 poisons tested are able to induce the formation of significantly

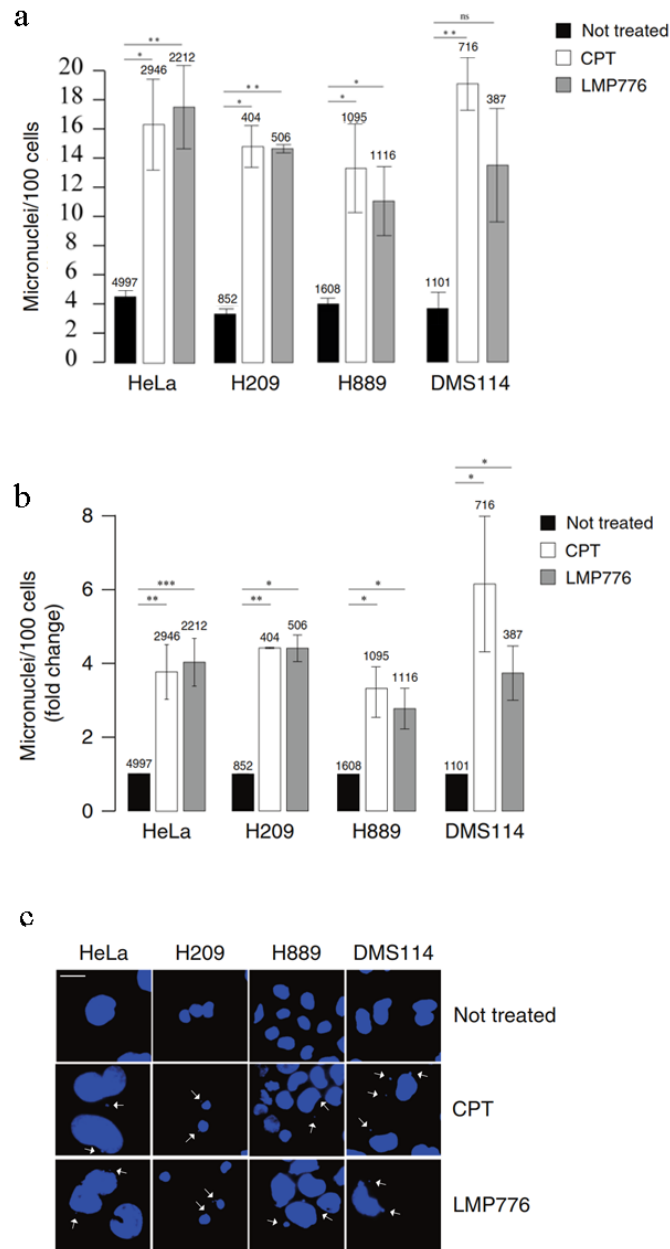


Figure 3.1 Micronuclei in HeLa, H209, H889, and DMS114 cell line after a 24-hour treatment with CPT or LMP-776, followed by 48-hours recovery. **(a)** Non-normalized micronuclei count/100 cells. **(b)** Normalized micronuclei count in HeLa, H209, H889, and DMS114. In both graphs, columns indicate mean values \pm SEM (5 biological replicates for HeLa, 2 for H209, and 3 for both H889 and DMS114). The numbers above indicate the sample size and asterisks show statistical significance calculated by t-test. $*P < 0.05$, $**P < 0.01$, $***P < 0.001$. **(c)** Representative images of micronuclei, as observed by IF in the 4 different examined cell lines. Adapted from Marinello et al., 2022. Image licensed under the Creative Commons Attribution 4.0 International License. To view a copy of this license, visit <http://creativecommons.org/licenses/by/4.0/> or send a letter to Creative Commons, PO Box 1866, Mountain View, CA 94042, USA.

higher amounts of micronuclei, which can be observed in all of the 4 cancer cell lines under investigation.

A second step aimed to determine whether TOP1 poisons were able to enhance R-loop production. In order to do so, we used S9.6 antibody to detect R-loops. S9.6 antibody is a monoclonal antibody able to bind DNA:RNA hybrid duplex in a highly specific manner. It demonstrated a higher specificity for hybrid DNA:RNA rather than dsDNA or dsRNA (Sanz and Chédin, 2019; Bou-Nader et al., 2022). The main players involved in the recognition of R-loops are the aromatic and basic residues belonging to heavy chains of this antibody, which strictly bind the minor groove in the hybrid DNA:RNA structure (Bou-Nader et al., 2022). We prepared this antibody in our laboratory and we checked the binding ability of each batch.

We cultured a murine HB-8730 hybridoma cell line able to express this antibody, collected the supernatant and then used it to purify the antibody by means of Sepharose-based columns. The eluate was subsequently concentrated and quantified by Lowry protein assay and, finally, we performed 2 tests in order to control the presence, the quality and the binding-capability of the purified antibody.

First, we controlled the antibody purity degree by running the purified eluate fraction on a polyacrylamide gel (Figure 3.2a). Then, we conducted an immunofluorescence microscopy (IF) experiment by comparing the R-loop signal between cells treated with CPT for 10 minutes and non-treated cells. In these IF experiments we verified that the newly produced antibody was able to effectively bind R-loops, by evaluating the nucleoplasmic signal increase between treated and non-treated cells (Figure 3.2b). In addition, we compared the results obtained with previous ones in order to check whether each batch produced exhibited a high binding efficiency.

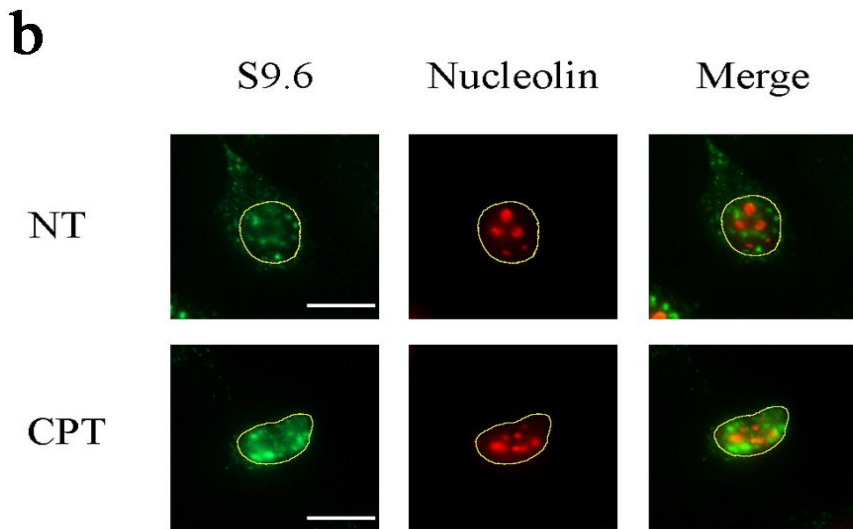
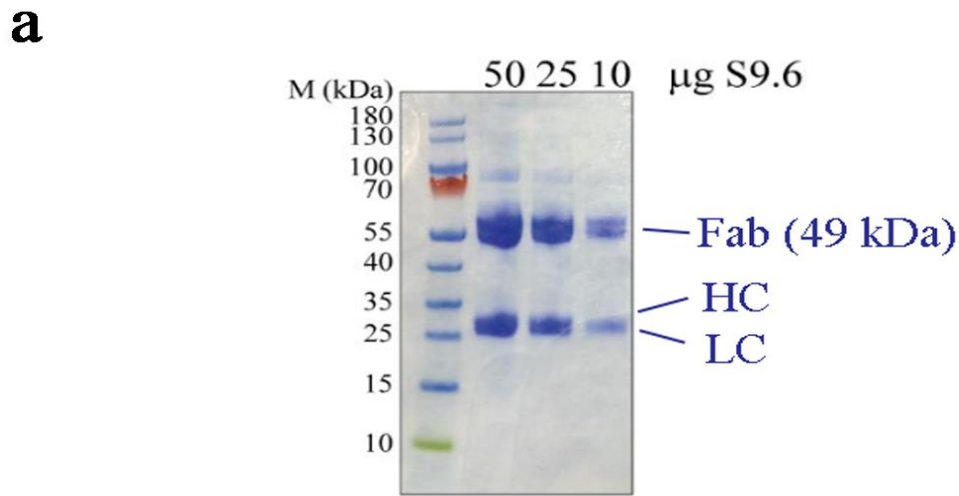


Figure 3.2 S9.6 antibody validation. **(a)** S9.6 antibody on a polyacrylamide gel. Different amounts of antibody were loaded in each lane (50, 25, and 10 μ g). Antibody fragments can be identified in the most evident bands, namely Fab (49kDa) and heavy and light chain at about 25kDa. The purity level of this tested sample is about 80%. **(b)** Representative images of S9.6 validation in HeLa cells. In the first line non-treated cells, in the second line cells treated with CPT for 5 minutes. On the left, green S9.6 staining, in the middle, red staining for the nucleolin and, on the right, their merge. Scale bar = 10 μ M. Adapted from Marinello et al., 2022. Image licensed under the Creative Commons Attribution 4.0 International License. To view a copy of this license, visit <http://creativecommons.org/licenses/by/4.0/> or send a letter to Creative Commons, PO Box 1866, Mountain View, CA 94042, USA.

In order to check whether TOP1 poison administration resulted in an increase of R-Loop signals, we performed an IF experiment on HeLa cells by administering an equimolar concentration of our 2 TOP1 poisons, namely 10 μ M, and checking for different short treatment times. After cell staining with both S9.6 and anti-nucleolin antibodies, we determined the nucleoplasmic R-loop signal by subtracting the nucleoli signal from the total signal for each cell. As a result, we were able to observe that TOP1 poisons exercise a transient stimulation of the R-loop signal, which is considerably intense, although more for LMP-776 than CPT, following a short-period treatment, especially after 5-10 minutes of

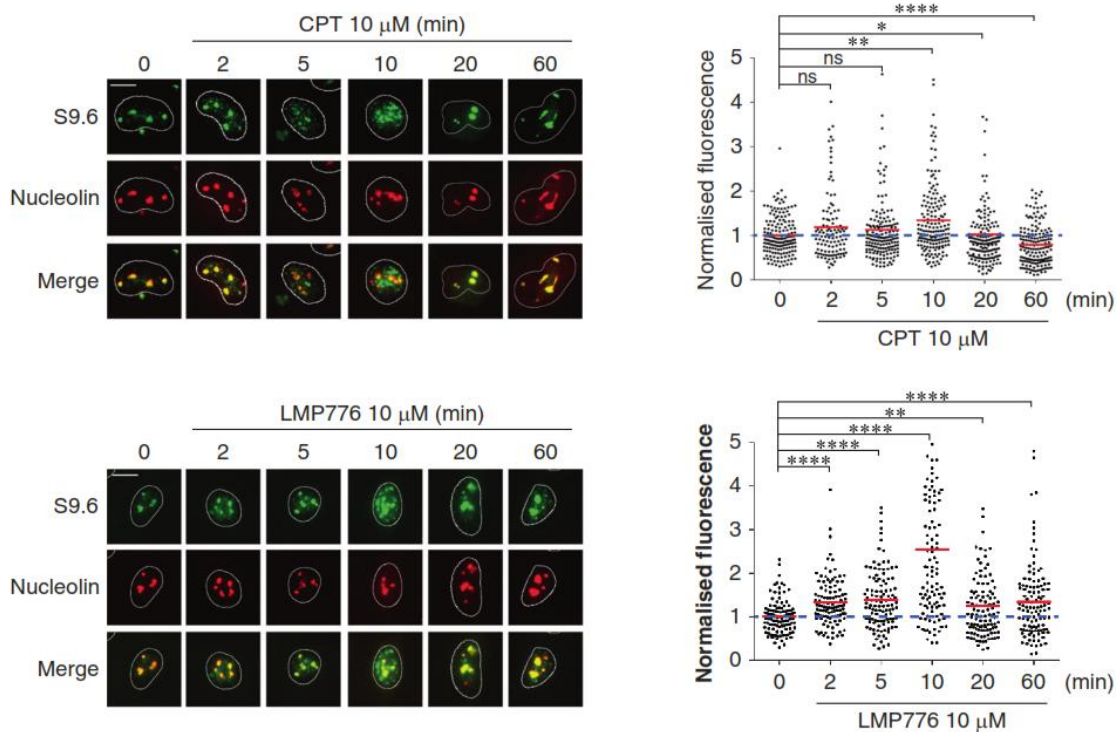


Figure 3.3 (Left) Immunofluorescence images of cells stained with S9.6 antibody (green) and nucleolin (red) and treated for specified times with CPT or LMP-776. (Right) Dot-plot reporting nucleoplasmic S9.6 signal normalized on non-treated cells, each dot stands for a single cell. Asterisks over the graph show the significance of treated vs. non-treated cells calculated by Kolmogorov-Smirnov statistical test. * $P < 0.05$, ** $P < 0.01$, *** $P < 0.001$, **** $P < 0.0001$. Adapted from Marinello et al., 2022. Image licensed under the Creative Commons Attribution 4.0 International License. To view a copy of this license, visit <http://creativecommons.org/licenses/by/4.0/> or send a letter to Creative Commons, PO Box 1866, Mountain View, CA 94042, USA.

drug administration (Figure 3.3). Although both the TOP1 poisons proved effective in stimulating transient R-loop formation, LMP-776 seems to produce a stronger effect than CPT, which might be explained to differences in their chemical structure and, as a consequence, TOP1ccs originated by LMP-776 exhibit a longer half-life than the ones elicited by CPT (Antony et al., 2007).

In light of the demonstrated ability of both CPT and LMP-776 to induce micronuclei and R-loop formation, we asked whether micronuclei formation was directly correlated to the R-loops observed. In order to provide a plausible answer, IF was performed on a U2OS cell line that was stably transfected with a vector bearing a doxycycline-inducible RNaseH1 gene. Hence, the exogenous RNaseH1 has an 8-aminoacid FLAG, so that it can be easily detected in immunofluorescence by a specific antibody. Cells were treated with 100nM CPT or 200nM LMP-776 for 24 hours and then were left to recover for 48 hours. Results from these experiments demonstrate that micronuclei formation is dependent on DNA:RNA hybrids as RNaseH1 expression reduces micronuclei levels (Figure 3.4 a, c). Specifically, high RNaseH1 levels are associated with the least micronuclei production, while micronuclei slightly increase in case of intermediate RNaseH1 levels, and when RNaseH1 is totally absent, micronuclei increase is at the highest level (Figure 3.4a, b). This shows that micronuclei formation likely depends on R-loops in a dose-dependent manner. Interestingly, the non-normalized micronuclei number in non-treated cells grew in tandem with doxycycline administration (Figure 3.3c), thus underlining the importance of R-loops in reparation of DSBs (Ohle et al., 2016). In light of the fact that treated and non-treated cells do not exhibit saturation in terms of micronuclei/100 cell ratio, it is reasonable to infer that RNaseH1 exogenous overexpression has hindered CPT's and LMP's ability to boost the baseline levels of micronuclei.

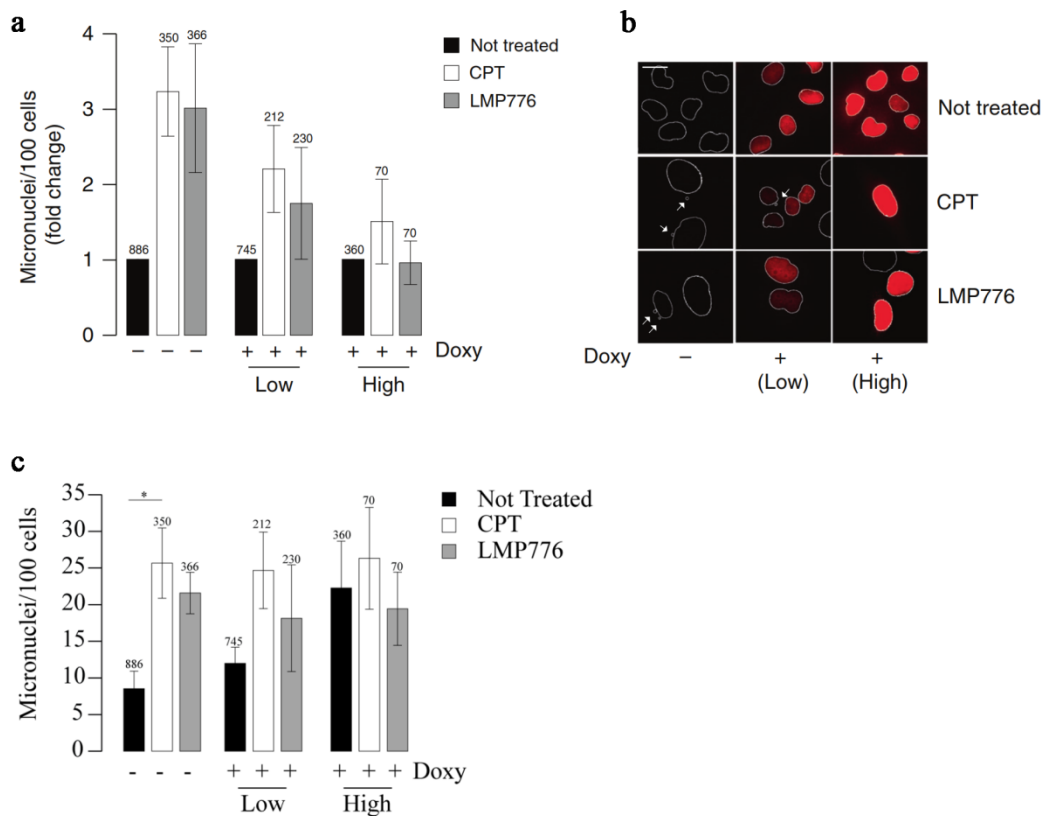


Figure 3.4 U2OS cells stably transfected with a vector bearing a doxycycline-dependent RNaseH1 after a 24-hour TOP1 treatment (100 nM CPT, 200 nM LMP-776), followed by a 48-hour recovery. Cells were administered with (+) or without (-) doxy for the 48 hours preceding TOP1 treatment and, in the end, categories “low” and “high” were created in order to indicate a low or high exogenous RNaseH1 induction. **(a)** Histograms reporting micronuclei/100 cells \pm SEM, counted after doxycycline induction (+), or without doxy (-), normalized on non-treated cells. Numbers above bars indicate sample size of 3 biological replicates and statistical significance was evaluated by t-test. Statistically significant values of tested samples are $p=0.054$ and $p=0.191$, for “low” category CPT and LMP-776, respectively, and $p=0.068$ and 0.058 , for “high” CPT and LMP-776, respectively. **(b)** Representative immunofluorescence images of doxycycline-induced cells exhibiting no/low/high RNaseH1 levels. **(c)** Histogram reporting non-normalized micronuclei/100 cells \pm SEM. Numbers above bars indicate sample size of 3 biological replicates and statistical significance was evaluated by t-test. Only the comparison between CPT-treated cells and their non-treated control sample, without doxycycline administration, originated a statistically significant ratio ($p=0.019$); a near-limit value was obtained for the LMP-treated sample vs. non-treated cells, again without doxycycline exposure ($p=0.055$). Adapted from Marinello et al., 2022. Image licensed under the Creative Commons Attribution 4.0 International License. To view a copy of this license, visit <http://creativecommons.org/licenses/by/4.0/> or send a letter to Creative Commons, PO Box 1866, Mountain View, CA 94042, USA.

Considering the role played by R-loops in causing genome instability, we wondered whether, besides impacting micronuclei formation, R-loops can also elicit DNA damage. In order to test this hypothesis, we performed an IF assay in U2OS_RH cell line, aimed at studying the phosphorylation of Serine 139 of histone H2AX (γ H2AX). We could observe that long treatments with TOP1 poisons originated high levels of DNA damage as detected by γ H2AX foci. To make this phenomenon more evident we decided to analyze cells in accordance with their RNaseH1 signal level in the following groups: low/intermediate/high (Figure 3.5a-c). Similarly to what we observed for R loops, RNaseH1 overexpression results in a dose-dependent reduction of γ H2AX foci caused by

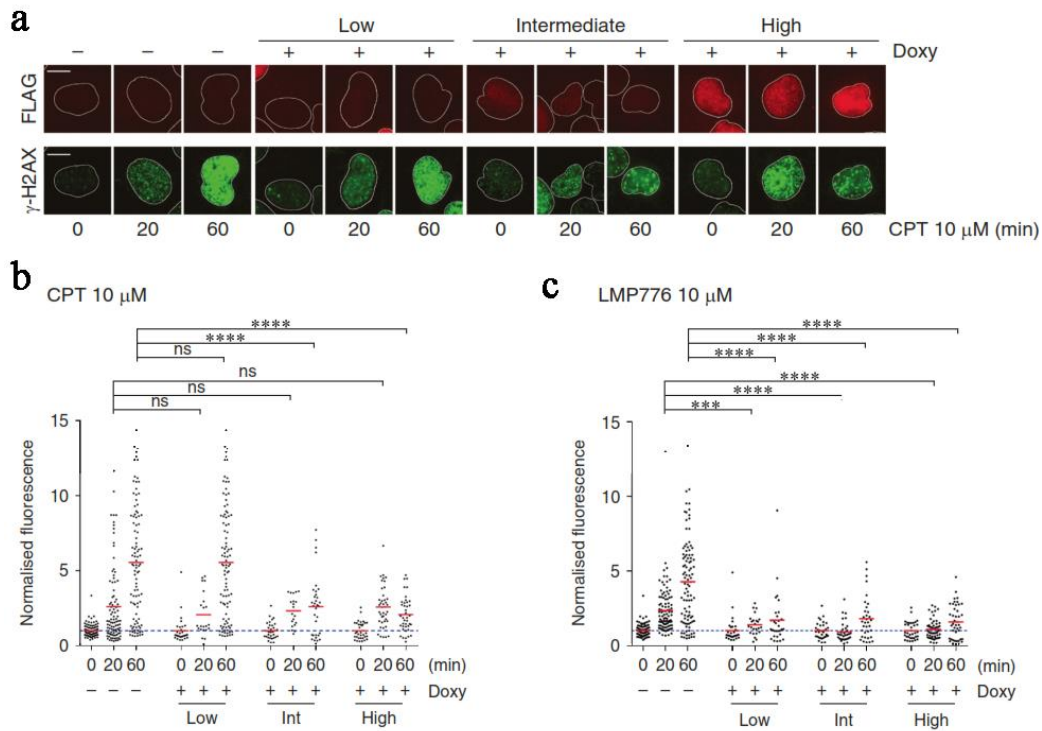


Figure 3.5 Immunofluorescence performed on U2OS_RH cell line treated with CPT 10 μ M for indicated times. **(a)** Illustrative images of staining. RNaseH1 (red), and γ H2AX (green). Scale bar: 10 μ m. Dot plots of cells treated with **(b)** CPT and **(c)** LMP regarding the nuclear γ H2AX signal. Asterisks show significance level, calculated by Mann-Whitney test, where * P < 0.05, ** P < 0.01, *** P < 0.001, **** P < 0.0001. Cells treated with doxycycline were grouped according their RNaseH1 expression level, that could be low/intermediate/high. Adapted from Marinello et al., 2022. Image licensed under the Creative Commons Attribution 4.0 International License. To view a copy of this license, visit <http://creativecommons.org/licenses/by/4.0/> or send a letter to Creative Commons, PO Box 1866, Mountain View, CA 94042, USA.

TOP1 poisons, implying that R loops are likely involved in the mechanisms of DNA damage induction by Top1 poisons. The reduction is much more evident in cells treated with LMP-776 as compared to those treated with CPT. Moreover, the levels of DNA damage observed in cells that were not treated with doxycycline tend to increase over time, reaching their peaks at 60 minutes. Cells that were treated with both TOP1 poisons and doxycycline tend to exhibit a lower DNA damage even at longer treatment times (Figure 3.5b, c). Thus, it is likely that RNaseH1 expression has lowered the level of R-loop production, thus eradicating the main source of γ H2AX foci, showing a critical role of R-loops in mediating TOP1 poison-induced DNA damage.

3.2 Micronuclei trigger innate immune gene activation

Micronuclei are a source of cytosolic dsDNA deposits that can trigger cGAS/STING signaling pathway, as discussed in the Introduction. After having observed a considerable micronuclei formation in each cell line resulting from TOP1 poison treatments, we decided to assess whether Top1 poisons could activate an innate immune response in the SCLC cell lines. Therefore, we decided to analyze a panel of cytokine genes belonging to the innate immune response cascade by means of qRT-PCR. We selected 15 cytokines and divided them in two groups, one constituted by genes activated mainly by NFkB (CCL20, CXCL1, IL1A, IL1B, IL6, IL8, and TNF) and a second group constituted by genes activated by NFkB as well as IRF3 (CCL5, CXCL10, DDX60, IFI44, IFIT1, ISG15, IFNB1, and IFNA1). The second group includes genes known as IFN- β -stimulated genes (ISG). It is worth to point out that NFkB-stimulated cytokines can be triggered by both the cGAS/STING pathway and other cellular pathways that are not related to the presence of micronuclei. On the contrary, ISGs are more specific for cGAS/STING pathway.

Among the studied cytokine genes (Figure 3.6 a-d), CCL20 and CXCL1 seem to be more responsive to treatment because their transcription levels are very high, especially in HeLa cells. On the contrary, TNF, IL1A and IL1B appear to be the least transcribed cytokines. Furthermore, the results suggest that LMP-776 is somewhat more effective than CPT in inducing an innate immune response. qRT-PCR analyses reveal that HeLa cells exhibit the

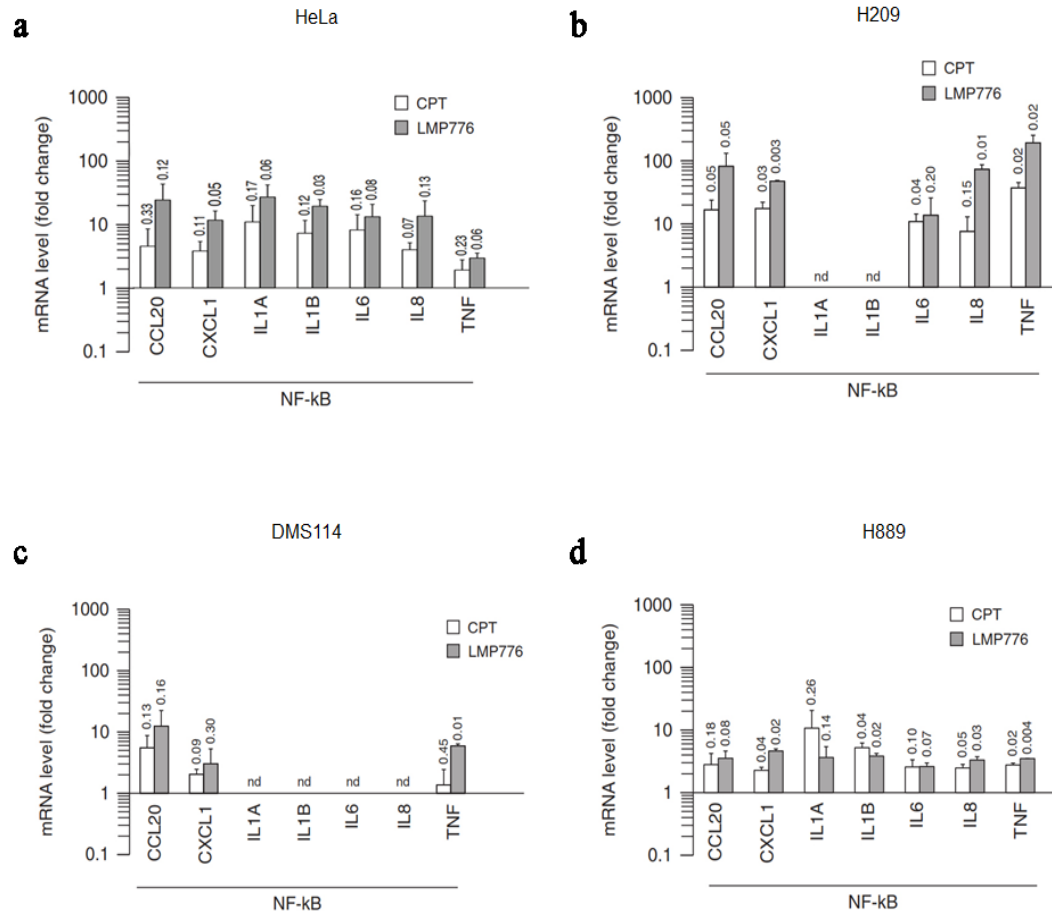


Figure 3.6 NFkB-induced innate immune gene activation levels in the 4 cell lines studied. qRT-PCR were performed after a 24 hour-treatment followed by a 48 hour-recovery. Bars indicate the mean of 2 biological replicates \pm SEM and *P* value is shown above each bar, calculated by one-tailed ratio paired t test; nd stands for values below detection levels. **(a)** HeLa, **(b)** H209, **(c)** DMS114, and **(d)** H889 cell lines. Adapted from Marinello et al., 2022. Image licensed under the Creative Commons Attribution 4.0 International License. To view a copy of this license, visit <http://creativecommons.org/licenses/by/4.0/> or send a letter to Creative Commons, PO Box 1866, Mountain View, CA 94042, USA.

overall highest cytokine activation level, H209 show an intermediate cytokine production, while H889 and especially DMS114 display poor cytokine activation (Figures 3.6a-d and 3.7a-d).

In spite of a similar micronuclei production across all the cell lines, we could observe an marked difference of NFkB-and IRF3-stimulated cytokines, with HeLa exhibiting the highest response level, followed by H209, showing an intermediate response level, while H889 and DMS114 revealed a very weak innate immune gene activation (Figures 3.6a-d and 3.7a-d). Therefore, as differences of ISG activation cannot be ascribed to Top1-

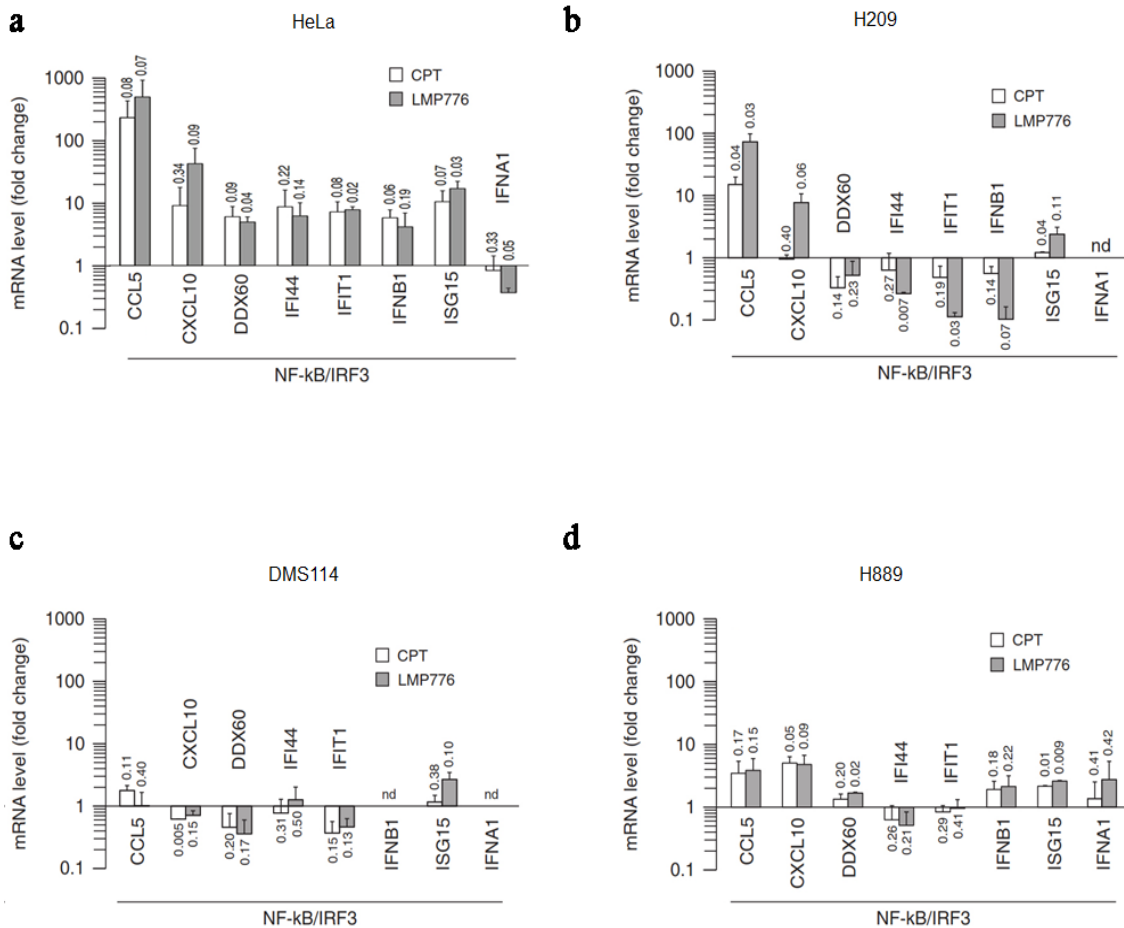


Figure 3.7 NFkB and IRF3-stimulated innate immune gene activation levels in the 4 cell lines studied. qRT-PCR were performed after a 24 hour-treatment followed by a 48 hour-recovery. Bars indicate the mean of 2 biological replicates \pm SEM and *P* value is shown above each bar, calculated by one-tailed ratio paired t test; nd stands for values below detection levels. **(a)** HeLa, **(b)** H209, **(c)** DMS114, and **(d)** H889 cell lines. Adapted from Marinello et al., 2022. Image licensed under the Creative Commons Attribution 4.0 International License. To view a copy of this license, visit <http://creativecommons.org/licenses/by/4.0/> or send a letter to Creative Commons, PO Box 1866, Mountain View, CA 94042, USA.

induced micronuclei levels, the findings indicate that the functionality of the cGAS/STING pathway may be altered in the studied SCLC cell lines.

Next, we asked whether immune gene activation was dependent on R-loop and performed experiment investigating the effects of RNaseH1 expression on cytokine gene expression. We selected HeLa cells as they exhibit a fully functional signaling pathway and a high level of innate immune response. Since RNaseH1 is able to resolve R-loops (Drolet et al., 1995; Massé et al., 1997), it can reduce DNA damage, thus weakening micronuclei formation (as we have seen earlier in this Chapter, see paragraph 3.1) and eventually leading to a decreased innate immune response activation. In order to do this, we used the plasmid pRH1 (pcDNA3 – RNaseH1-ML5) to transiently express RNaseH1 in HeLa cells. Then, we compared immune gene expression in control and transfected cells. The data showed that RNaseH1 expression induced an increase in CCL20, CXCL1, IL1A, and IL8 expression in comparison to control cells, whereas we found a decrease of CCL5, DDX60,

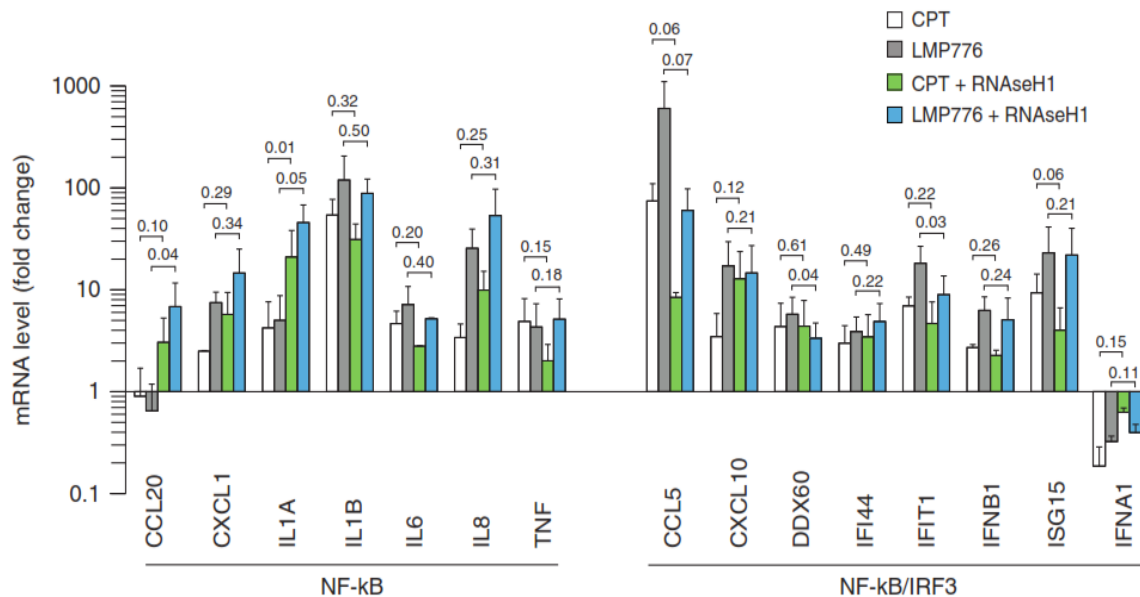


Figure 3.8 Innate immune response gene activation in HeLa cells after the administration of TOP1 poisons and RNaseH1. Bars are mean \pm SEM of 2 biological replicates and p-values are indicated above each bar. Significance was calculated by using one-tailed ratio paired *t*-test. Adapted from Marinello et al., 2022. Image licensed under the Creative Commons Attribution 4.0 International License. To view a copy of this license, visit <http://creativecommons.org/licenses/by/4.0/> or send a letter to Creative Commons, PO Box 1866, Mountain View, CA 94042, USA.

IFIT1, and ISG15 gene transcription; no significant variations could be noticed for other cytokines (Figure 3.8). It is worth to point out that CCL5, DDX60, IFIT1, and ISG15 belong to a group of genes stimulated by both NFkB and IRF3, implying that they are more indicative of the activated cGAS/STING pathway. These experimental results underline a strong role of R-loops in the induction of the innate immune gene response.

3.3 cGAS/STING pathway impairment and its effects

Despite the fact that the micronuclei production observed does not show significant variation across the 4 cell lines under investigation, the same homogeneity is not found when it comes to the activation of innate immune response. In order to determine whether these differences might be due to alterations of the cGAS/STING pathway, we have then investigated the main factors of the pathway in the studied SCLC cell lines.

Considering that HeLa cells exhibit the highest innate immune cytokine response, they were used as a control and reference in the experiments. By means of western blot, we verified that both cGAS and STING proteins are expressed in the cell lines, in both non-treated and TOP1 poison-treated cells (Figure 3.9a and Figure 3.11a,c). The results showed an over-production of these proteins in treated cells, possibly due to a positive feedback-loop regulation. Afterwards, an immunofluorescence assay allowed us to check for the correct localization of cGAS protein in the cell. Data revealed a significant localization of cGAS in micronuclei as detected by signals produced by DAPI and the cGAS-targeting antibody. This means that the cGAS protein likely binds to dsDNA in micronuclei to set off the sequence of events that constitutes the entire pathway. Furthermore, we also observed that non-treated cells exhibit a very low cGAS signal as compared to treated cells, which becomes quite evident in IF images (Figure 3.9b). In order to verify that the pathway was activated in response to TOP1 poison administration, we assessed the

production of the signaling messenger cGAMP by means of an ELISA assay. We analyzed HeLa supernatants from samples collected every 24 hours for 4 days after an initial 24-hour TOP1 poison administration. As a result, we found that non-treated cells did not show any change in cGAMP production, while on days 3 and 4 after the treatment, both

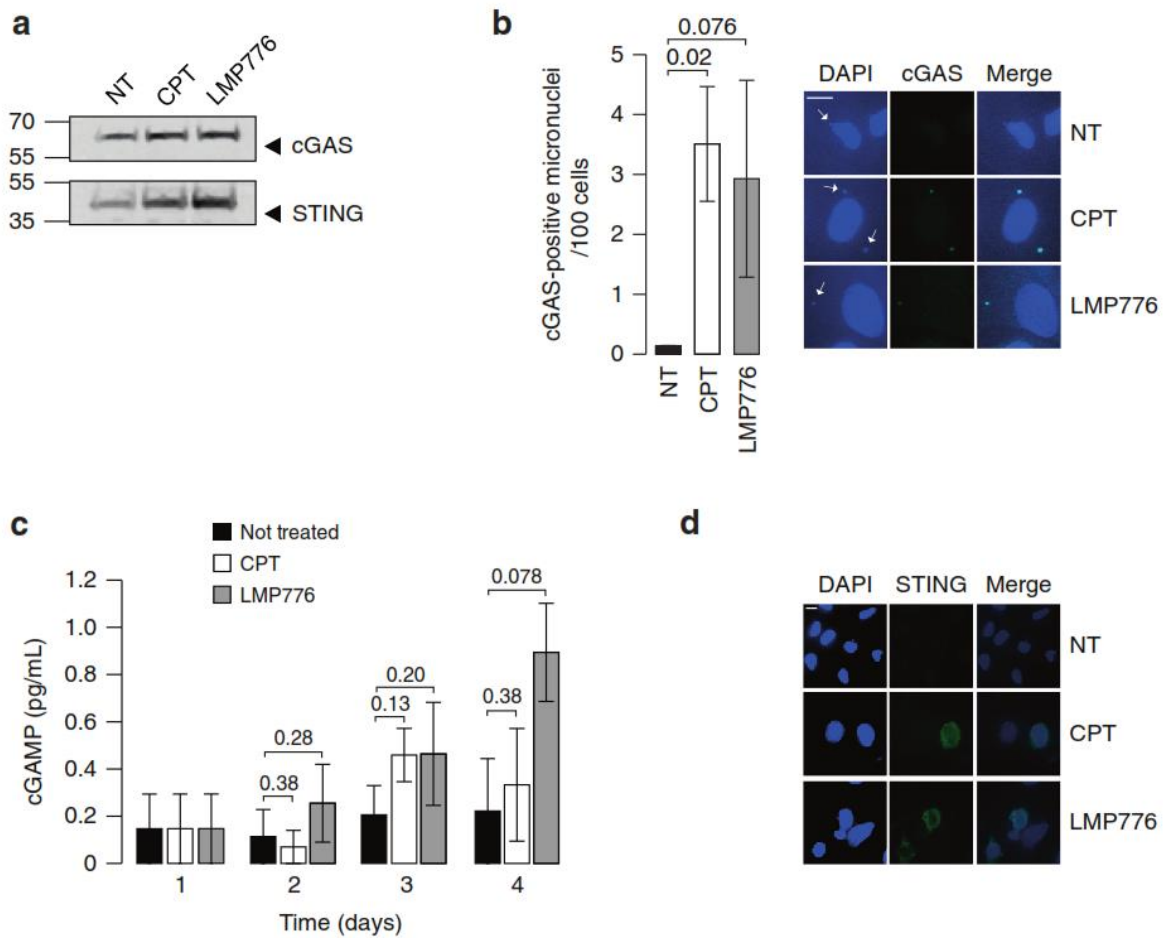


Figure 3.9 cGAS/STING activation level in HeLa cells. **(a)** Evaluation of cGAS and STING protein production by WB after a 24-hours treatment followed by 48-hours recovery. **(b)** IF investigating cGAS activation and localization. Co-staining is located in micronuclei. Scale bar: 10 μ m. Histograms show cGAS-positive micronuclei/100 cells, numbers above bars indicate *p*-values calculated by one-tailed ratio paired *t* test. **(c)** ELISA assay to measure cGAMP amount in treated and non-treated cells; bars represent the mean of 2 biological replicates \pm SEM; numbers above bars indicate *p*-values calculated by one-tailed ratio unpaired *t* test. **(d)** STING activation and localization by IF, representative images with a scale bar of 10 μ m. Adapted from Marinello et al., 2022. Image licensed under the Creative Commons Attribution 4.0 International License. To view a copy of this license, visit <http://creativecommons.org/licenses/by/4.0/> or send a letter to Creative Commons, PO Box 1866, Mountain View, CA 94042, USA.

CPT- and LMP-treated cells demonstrated a relevant increase in the amount of this signaling dinucleotide (Figure 3.9c).

As a final step, we examined the position of the STING protein as well by

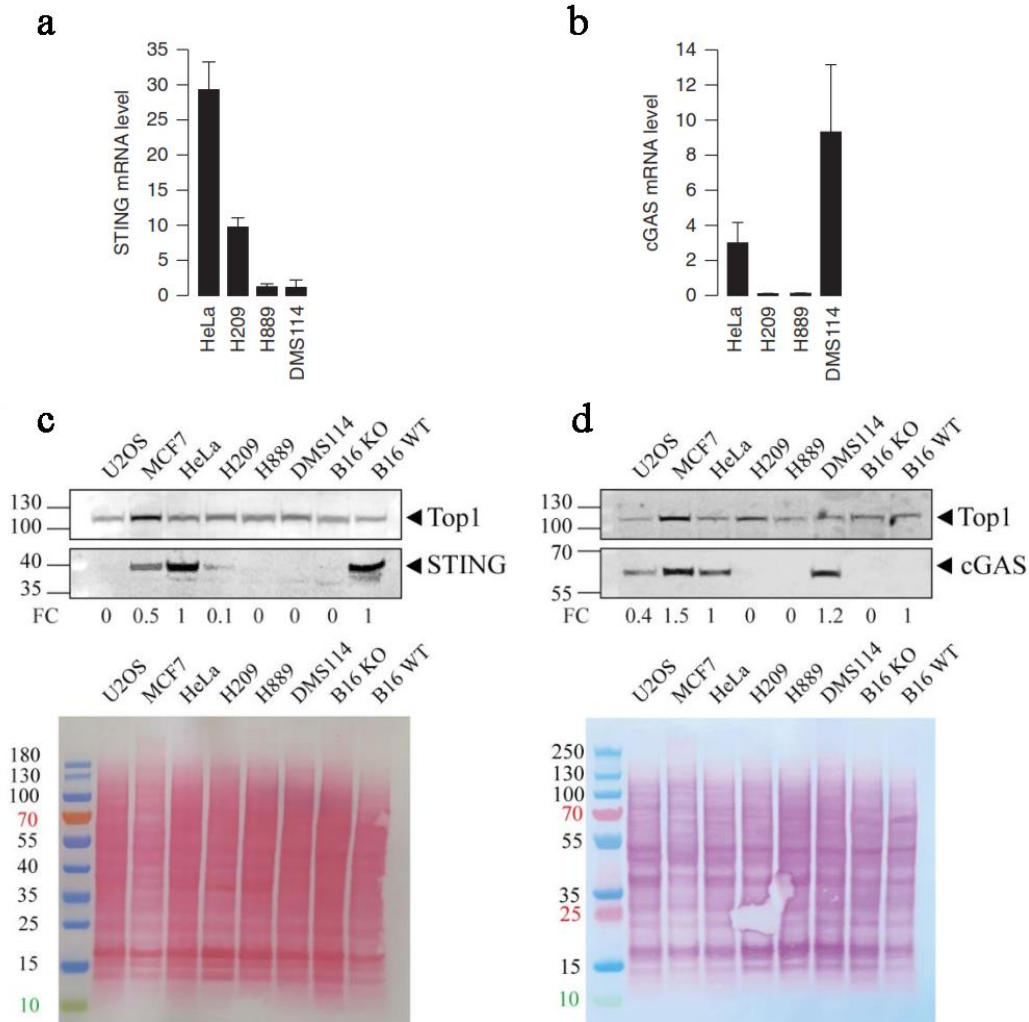


Figure 3.10 STING and cGAS levels in several cell types. **(a)** STING and **(b)** cGAS mRNA quantification by means of qrt-PCR in HeLa and SCLC cell lines. Data are normalized on cytochrome *c* gene. Bars report mean \pm SEM of 2 biological replicates. WB images of: **(c)** STING and **(d)** cGAS proteins in different cell lines together with their Red Ponceau colored blot. Top1 is the loading control and the fold change values indicate the protein band intensity, as compared to the HeLa one for U2OS, MCF7, HeLa and lung cancer cell lines, while B16 are compared to B16 WT cell line. Normalization is achieved by comparing Red Ponceau. Adapted from Marinello et al., 2022. Image licensed under the Creative Commons Attribution 4.0 International License. To view a copy of this license, visit <http://creativecommons.org/licenses/by/4.0/> or send a letter to Creative Commons, PO Box 1866, Mountain View, CA 94042, USA.

immunofluorescence microscopy. STING is a transmembrane protein that is usually found on the endoplasmic reticulum. When bound by cGAS, the cGAS/STING complex moves to the Golgi apparatus at the perinuclear compartment. IF data showed a considerable signal in treated cells and only a poor signal in non-treated cells, and this signal was correctly detectable at a perinuclear level (Figure 3.9d), thus pointing to the fact that STING had been activated. This series of experiments indicate that the HeLa cell line is characterized by a strong activation of the cGAS/STING pathway. All the experimental data allow us to conclude that in HeLa cells the cGAS/STING pathway is fully active.

Once we saw that HeLa cell line demonstrated a high innate immune gene activation together with a fully active cGAS/STING pathway, we decided to explore the activity of this pathway in SCLC cell lines. To this end, we firstly performed qrt-PCR analysis to evaluate mRNA transcript amounts of both STING and cGAS. We observed that HeLa exhibited the highest level of STING gene expression, H209 showed an intermediate gene transcription, while DMS114 and H889 demonstrated only a very low level of mRNA quantity. With regard to cGAS gene expression, surprisingly, DMS114 revealed the highest level of cGAS transcript, whereas HeLa displayed moderate levels of mRNA, while H889 and H209 exhibited very low levels of cGAS transcript (Figure 3.10a,b).

As for the effects observed after TOP1 poison treatment, we performed a qrt-PCR on cGAS mRNA in HeLa cell line after a 24-hour TOP1-poison treatment followed by a 48-hour recovery. As a result, we could record no significant differences in mRNA levels. Then, we assessed STING mRNA levels in each of the 4 cell lines examined. We could detect a statistically significant difference in LMP-treated H209 and in both CPT- and LMP-treated DMS114. Thus, STING is significantly (although at low levels) expressed in H209 cells only, whereas cGAS is expressed in DMS114 cells only. In addition, cGAS and STING were somewhat enhanced by TOP1 poisons in H209 and DMS114 cells (Figure 3.11b).

Then, we proceeded to study the protein yield, so we performed WBs for both the 2 proteins, not only in HeLa and SCLC cell lines, but also in MCF7, U2OS, B16 STING-KO, and B16 STING-WT. These cell lines belong respectively to human breast cancer, human osteosarcoma, and murine melanoma CRISPR-KO for STING or STING-wild type. The experiments conducted showed that HeLa and B16 STING-WT revealed the highest STING

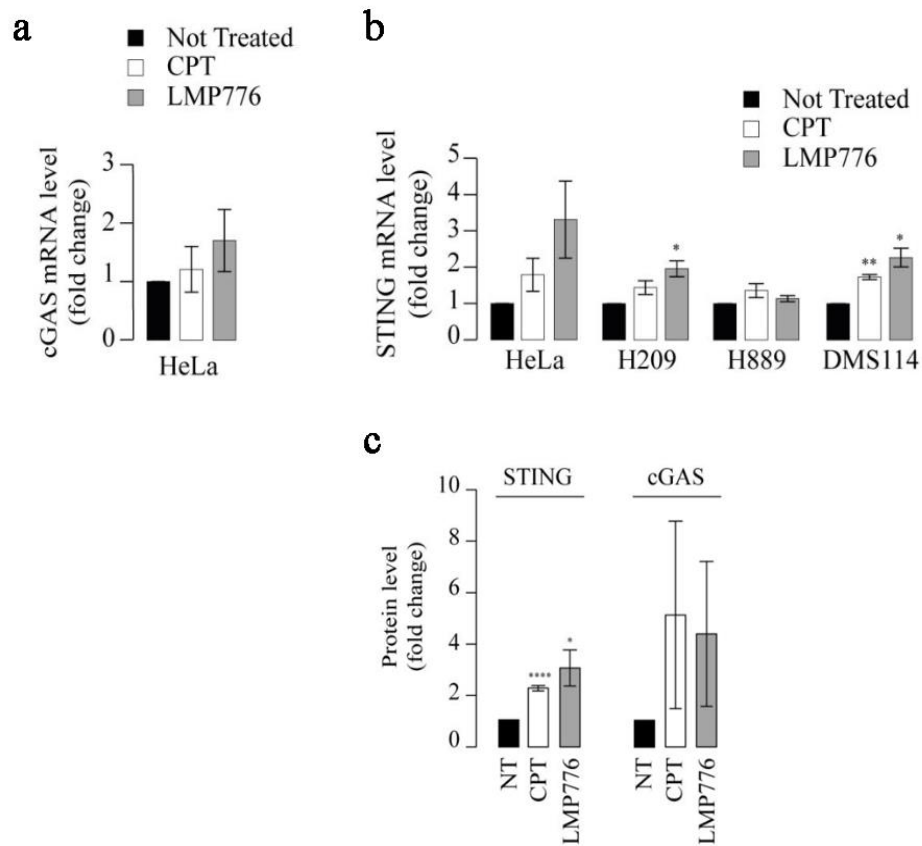


Figure 3.11 cGAS and STING variation after TOP1 poison administration. **(a)** mRNA levels of cGAS as measured by qrt-PCR in HeLa cell line; bars represent the mean of 2 experiments \pm SEM. **(b)** mRNA levels of STING by qrt-PCR in HeLa and SCLC cell lines; bars represent the mean of 2 experiments \pm SEM. Asterisks indicate statistical significance of samples which is calculated by unpaired *t*-test; **p* < 0.05, ***p* < 0.01. **(c)** Histograms showing the mean \pm SEM of 4 biological replications performed to quantify STING and cGAS proteins in HeLa. Again, asterisks indicate statistical significance of samples which is calculated by unpaired *t*-test; **p* < 0.05, ***p* < 0.01. Adapted from Marinello et al., 2022. Image licensed under the Creative Commons Attribution 4.0 International License. To view a copy of this license, visit <http://creativecommons.org/licenses/by/4.0/> or send a letter to Creative Commons, PO Box 1866, Mountain View, CA 94042, USA.

protein level, followed by MCF7. Protein production was lower in H209, while it was below detection levels in the case of U2OS, B16 STING-KO, H889, and DMS114. By examining cGAS blot, the protein band was highly evident in MCF7 and DMS114 and slightly weaker in HeLa, whereas U2OS indicate low amounts of protein and, finally, B16 (both WT and KO), H209, and H889 cell lines demonstrate protein amounts below detection levels (Figure 3.10c,d). Data gathered so far by both qrt-PCR and WB indicate that an increase in mRNA transcription is reflected by a parallel increase in protein levels, thus showing a certain consistency of expression data. To sum up, we can say that H209 cell line only exhibits a moderate production of STING. DMS114 cell line only shows a very high level of cGAS, in terms of both mRNA and protein. Finally, we could not detect any transcript or protein production of either STING or cGAS in H889. These results are interesting in light of the fact that some tumors are known to constitutively downregulate this pathway for tumor immune escape (Khoo and Chen, 2018; Su et al., 2019). Moreover, bioinformatics data have revealed that human SCLCs show a substantial reduction of both STING and cGAS expression in comparison to normal lung tissues (Marinello et al., 2022), in agreement with the described experimental findings on SCLC cell lines.

3.4 STING expression alteration affects the initiation of innate immune response

Experiments performed so far depict a multi-faceted picture regarding HeLa and SCLC cell lines in terms of protein amounts and transcript quantities, with some cell lines having defective expression of cGAS and/or STING. In light of the results presented in the previous paragraphs, only HeLa cells exhibit a high level innate immune response activation, while H209 show low levels of STING protein and, as a consequence, a weaker innate immune response activation. The other 2 cell lines, namely DMS114 and H889 seem not to express STING protein, resulting in extremely low levels of immune response stimulation. These results point to a preponderant role for STING in the stimulation of innate immune response, as it will be further discussed in the next Chapter.

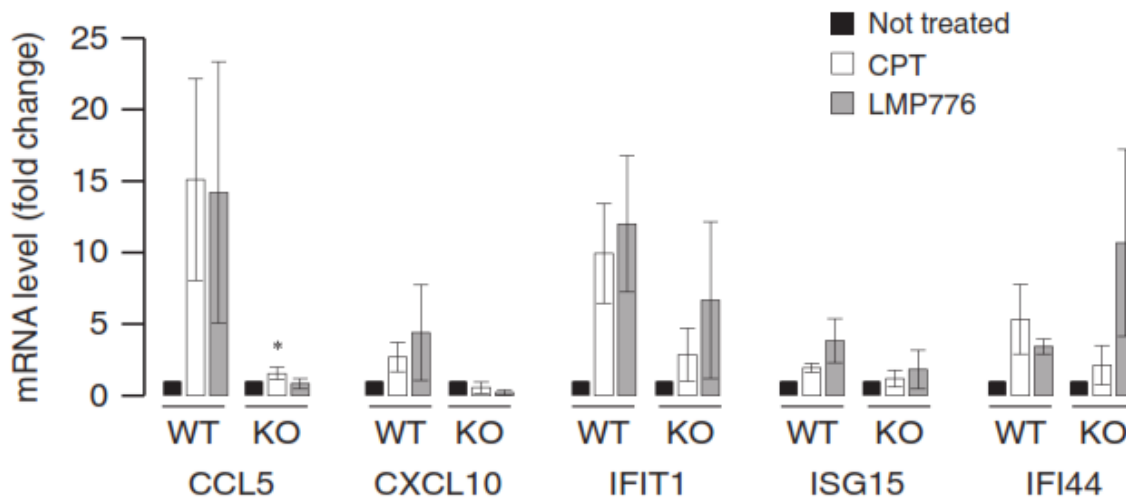


Figure 3.12 Innate immune response gene activation in B16 STING-WT and –KO cell line. Histograms reporting genes fold change of treated cells compared to non-treated cells. Bars are the mean \pm SEM of 2 biological replicates. Asterisks mark statistically significant samples; significance was calculated by using *t* test and $*P < 0.05$. Western blot regarding the STING protein expression in these 2 cell lines are reported in fig. 3.10c.

Adapted from Marinello et al., 2022. Image licensed under the Creative Commons Attribution 4.0 International License. To view a copy of this license, visit <http://creativecommons.org/licenses/by/4.0/> or send a letter to Creative Commons, PO Box 1866, Mountain View, CA 94042, USA.

In order to further support this hypothesis, more experiments were needed on STING, so we decided to modulate the pathway activity in SCLC cell lines by silencing STING when expressed or expressing an exogenous STING gene when absent. To this purpose, we started from observing the differences in innate immune response between the B16 STING-WT and B16 STING-KO cell lines after TOP1 poison treatment. Similar to other previous experiments, we performed RNA extraction after a 24-hour drug treatment followed by 48-hour recovery. We examined 5 cytokines belonging to NFkB and IRF3-stimulated genes, namely CCL5, CXCL10, IFIT1, ISG15, and IFI44. In equal treatment conditions, most of the STING-KO cell line tends to show a much lower increase than that observed in the WT strain. After CPT administration the entity of cytokine transcription is particularly evident for all of the cytokines, whereas only four out of five were relevantly

expressed after LMP-776 treatment (Figure 3.12). This underlines once more the importance of STING in eliciting a high-level innate immune response.

The STING gene was then silenced in HeLa cells with 2 different, specific siRNAs targeting STING mRNA or with scrambled siRNA in control samples. After silencing STING, we checked the protein levels by WB every 24 hours. We observed that STING protein levels began to decline 48 hours after transfection and remained steadily down for at least 96 hours post-transfection, which constitutes the end of our experiment (Figure 3.13b). By quantifying STING protein levels, we were able to verify that both the two siRNAs manage to significantly reduce protein although with different potency (siRNA #1 was more efficient than siRNA#2; Figure 3.13c). As a result of these observations, we decided to administer our TOP1 poisons 48 hours after having performed silencing, so as to be sure that CPT and LMP-776 started to act when the protein levels were already minimized. The TOP1 poison treatment lasted 24 hours, and then we removed the drugs and left cells to recover in a free-drug medium for 48 hours. After this time, we eventually proceeded with RNA extraction, having reached 96 hours post-silencing, a time point at which we were certain that the protein level was still at a minimum. By means of qrt-PCR, we analyzed CCL5, CXCL10, IFIT1, DDX60, CCL20, and IL6. The data obtained demonstrated that there was a strong reduction in all of the cytokines when using siRNA #1, since the baseline stimulation levels of some of the genes involved were initially already low. siRNA #2 exhibited a less striking decrease in cytokine stimulation, in line with their downregulation profile (Figure 3.13a). Thus, the data with both siRNA #1 and siRNA#2 show that cytokine gene activation by Top1 poisons was dependent on STING expression.

Then, we performed another experiment aimed at inhibiting STING activity by means of a specific compound, H151. This is an irreversible and selective STING-binder that covalently joins the cysteine-91 residue, preventing reactions of palmitoylation and clustering, thus hampering the starting of the signaling mechanism (Haag et al., 2018). This inhibitor is

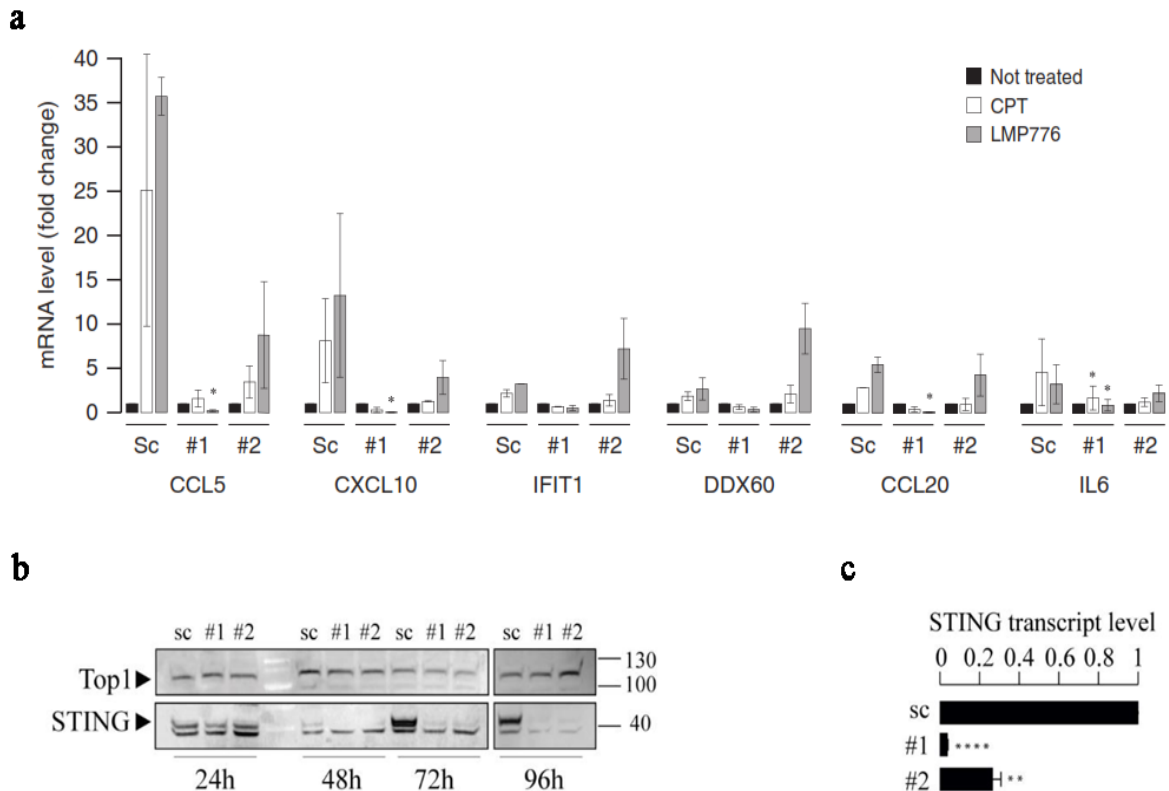


Figure 3.13 HeLa cell line transfected with scrambled siRNA (Sc) or 2 different siRNAs specific for STING (#1 and #2). **(a)** Innate immune gene expression analysis. Histogram bars show mean \pm SEM of 2 biological replicates and asterisks underline the statistically significant samples; significance was calculated by using *t* test and $*P < 0.05$. **(b)** WB of STING protein resulting from transfection. Data represent the situation every 24 hours. **(c)** Evaluation of silencing effectiveness by qrt-PCR. siRNA STING transcript levels were confronted to scramble's ones. Bars show mean \pm SEM of 2 biological replicates and asterisks underline the statistically significant samples; significance was calculated by using *t* test and $*P < 0.05$, $**P < 0.01$, $***P < 0.001$, $****P < 0.0001$. Adapted from Marinello et al., 2022. Image licensed under the Creative Commons Attribution 4.0 International License. To view a copy of this license, visit <http://creativecommons.org/licenses/by/4.0/> or send a letter to Creative Commons, PO Box 1866, Mountain View, CA 94042, USA.

rather unstable, so it degrades quite quickly and, in order to keep an effective concentration in culture medium, we daily replaced the medium with a fresh one containing new H151. H209 is a cancer cell line bearing only a moderate level of STING and apparently no cGAS, therefore an exogenous activation/introduction of STING in this cell line allows to investigate this protein. Despite this, after administering TOP1 poisons, it exhibits an intermediate level of innate immune response. We chose to use a H151 concentration of 2 μ M since it had already worked in previous experiments performed in our laboratory (Miglietta et al., 2021). We administered H151 with the aim of verifying if it indeed lowered the innate immune cytokines expression. After seeding cells, we administered 2 μ M H151 and, after 1 hour, TOP1 poisons, leaving them to act for 24 hours.

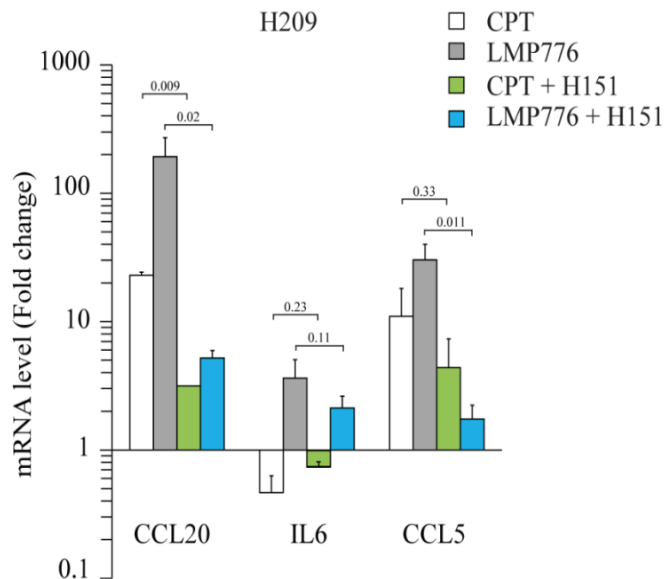


Figure 3.14 STING inhibitor (H151) effect in H209 cell line treated with CPT or LMP-776. H151 was administered daily at 2 μ M concentration. The graph shows the 3 cytokines' expression levels in cells treated with TOP1 poisons with or without H151. Bars indicate mean \pm SEM of 2 biological replicates and p-values are indicated above each bar. Significance was calculated by using one-tailed ratio paired *t*-test comparing treated samples to non-treated ones. Image from Marinello et al., 2022. Image licensed under the Creative Commons Attribution 4.0 International License. To view a copy of this license, visit <http://creativecommons.org/licenses/by/4.0/> or send a letter to Creative Commons, PO Box 1866, Mountain View, CA 94042, USA.

Afterwards, cells were left to recover for 48 hours in drug-free medium. At the end of the recovery process, RNA extraction was performed. In so doing, we tested H151 on 3 cytokines, namely CCL20, IL6, and CCL5 and in all of them we could observe a marked reduction in cytokine stimulation, in both CPT- and LMP-treated samples. Best results were generally achieved in LMP-treated samples, with a more evident reduction in CCL20 and CCL5 (Figure 3.14).

DMS114 is a cell line showing relevant levels of cGAS, but STING is under the detection level. A bioinformatics survey performed on this cell line by means of the Cancer Cell Line Encyclopedia (CCLE project) shows that the STING promoter in DMS114 is highly methylated (Figure 3.15a). Starting from this observation, we tried to induce a significant STING production by using a general demethylating agent, namely 5'-Azacytidine. We tried 3 different concentrations in order to decide which one eventually worked (2, 5, and 10 μ M) and we could observe STING reactivation with 5 and 10 μ M, while 2 μ M did not result in any reactivation (Figure 3.15b,c). We decided to use a 5 μ M concentration because this concentration was well tolerated, while a 10 μ M concentration resulted in considerable cell death. After identifying the proper drug concentration, we performed our experiment by treating DMS114 cells with TOP1 poisons for 24 hours and then letting them to recover for 48 hours in order to eventually extract RNA samples. Since we wanted to ensure high levels of STING during and especially at the end of TOP1 poison treatment, we administered TOP1 poisons 48 hours after the first 5'-Azacytidine dispensation, so as to end TOP1 poison treatment after 72 hours of 5'-Azacytidine administration.

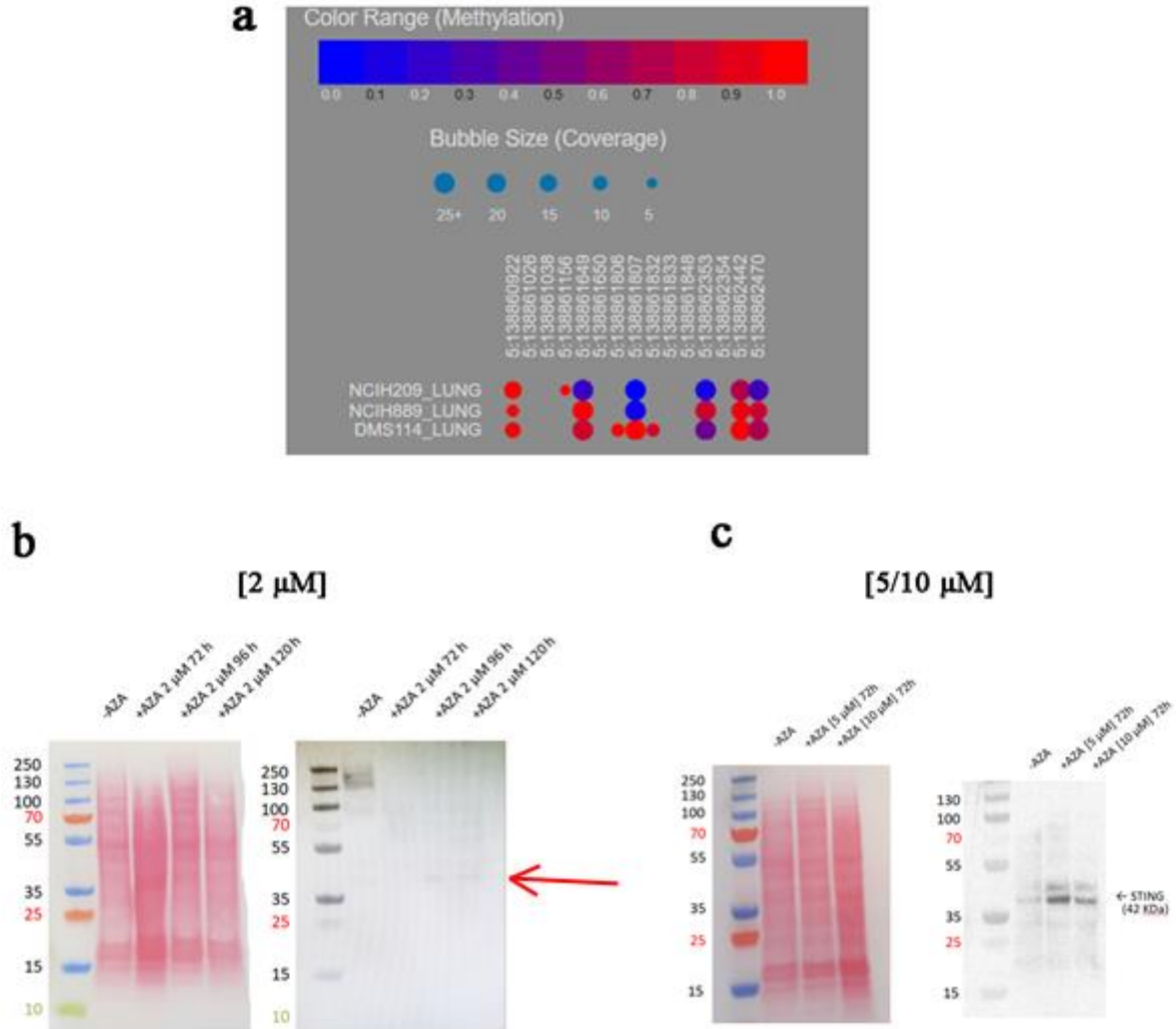


Figure 3.15 Effects of 5'-Azacytidine on STING in DMS114 cell line. **(a)** The bioinformatics analysis performed on the CCLE project website aimed to verify the methylation levels of the promoters belonging to the studied SCLC cell lines. Vertical numbers above the bubbles indicates genomic coordinates of specific CpG islands targeted by methylation. The more red-colored the bubbles, the more methylated. Larger bubbles correspond to a greater coverage for that position. Panels **b** and **c** show administration of 5'-Azacytidine, with (*left*) Red Ponceau staining and (*right*) antibody against STING. 5'-Azacytidine was administered at the concentration of **(b)** 2 μ M (red arrow points to the STING band), **(c)** 5/10 μ M. This latter WB shows a comparison between 5 and 10 μ M concentrations.

Although we could observe an increase in the protein, this did not result in any observable effect and, after treating DMS114 with the aforementioned demethylating agent and TOP1 poisons, we could not notice a real improvement in immune innate cytokine production. Only IL1A exhibits an increase, whereas all the others show values similar to the ones obtained in absence of 5'-Azacytidine (Figure 3.16).

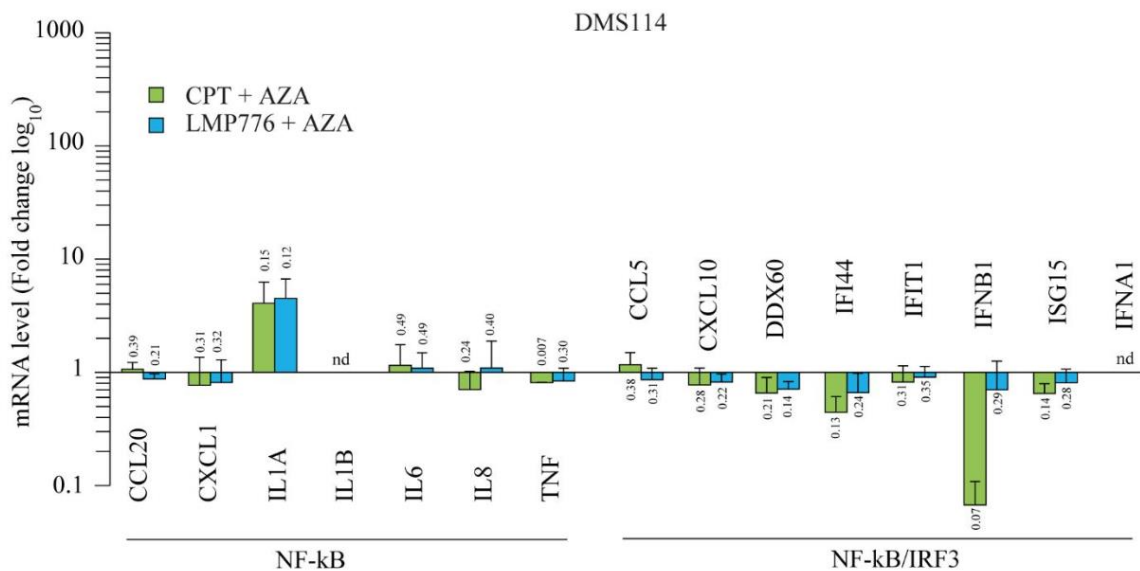


Figure 3.16 Innate immune response cytokines in DMS114 after 5'-Azacytidine administration. Bars indicate mean \pm SEM of 2 biological replicates and p-values are indicated above each bar. Significance was calculated by using one-tailed ratio paired *t*-test comparing treated samples to non-treated ones. Nd stands for non-detectable samples. Adapted from Marinello et al., 2022. Image licensed under the Creative Commons Attribution 4.0 International License. To view a copy of this license, visit <http://creativecommons.org/licenses/by/4.0/> or send a letter to Creative Commons, PO Box 1866, Mountain View, CA 94042, USA.

After attempting with 5'-Azacytidine we tried to produce exogenous STING overexpression by using a plasmid, namely NET23 pEGFP-N2 (Addgene), bearing a sequence in which the STING gene was fused to a GFP. In this way, transfected cells are able to elicit STING overexpression and their amount can be directly and quickly observed by a UV microscope. Then, we proceeded performing a transient transfection of DMS114

with this plasmid. We tested 3 different combinations of Lipofectamin and plasmid, namely 2.5µg plasmid + 2.5µL Lipofectamin, 2.5µg plasmid + 5µL Lipofectamin, 5µg plasmid + 5µL Lipofectamin. Then we measured the increase in STING protein by WB (Figure 3.16b,c) at T2 and T5 of the experimental design (Figure 3.17a).

By means of WB (Figure 3.17c), we could observe more than one single band in each lane, including a lighter one, with an approximate weight of about 40KDa, which is absolutely compatible with the molecular weight of STING (42KDa), and 2 more bands, weighting about 45 and 70Kda. The lower band seems not to appear in every lane, thus leading to the assumption that it might be a proteolized form of STING or an exogenously

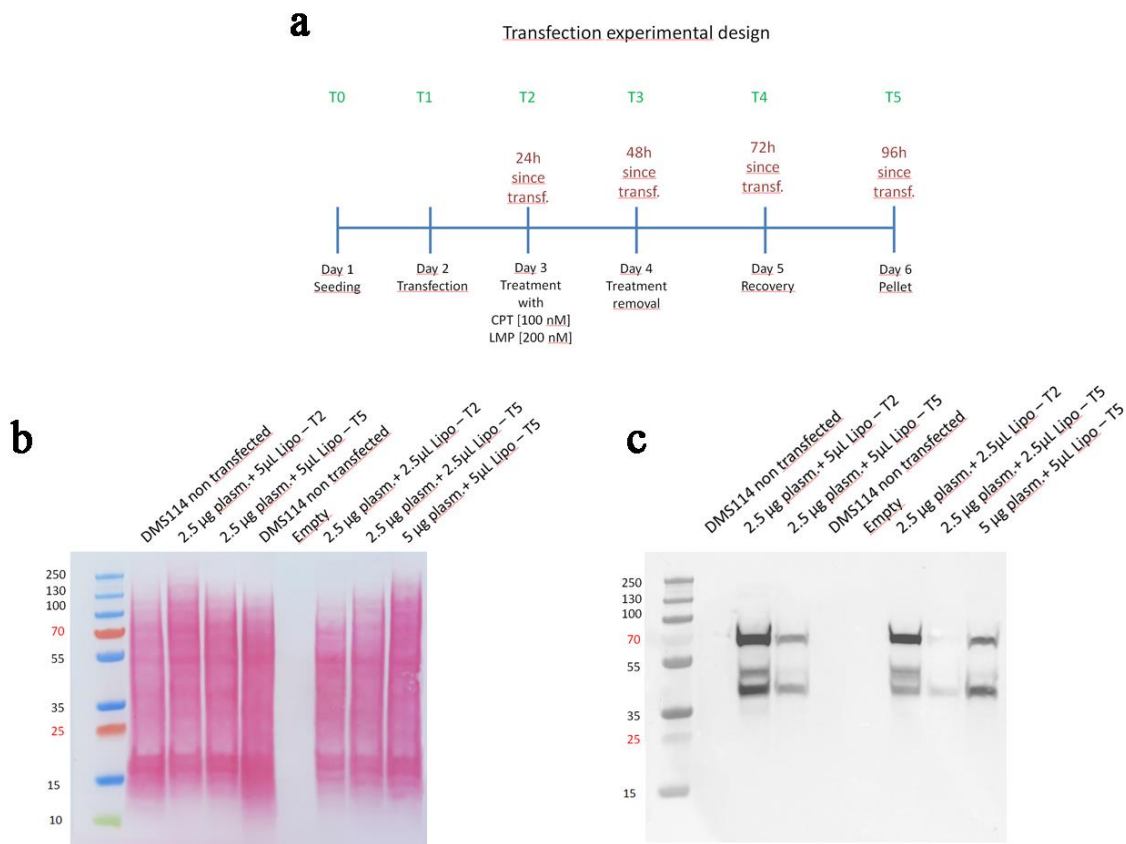


Figure 3.17 DMS114 transfection by using a STING-GFP-conjugated plasmid. **(a)** The timeline of this experiment shows transfection performed the day after seeding and administration of TOP1 poison treatment on the second day post-seeding. This treatment lasts 24 hours and is followed by 48 hours of recovery, at the end of which, cells are pelleted for RNA or protein extraction. **(b)** Red Ponceau image of the **(c)** WB testing of: non-transfected DMS114, 2.5µg plasmid + 5µL Lipofectamin transfected DMS114 at T2 and T5, non-transfected DMS114, an empty lane, 2.5µg plasmid + 2.5µL Lipofectamin transfected DMS114 at T2 and T5, and 5µg plasmid + 5µL Lipofectamin transfected DMS114 at T5.

stimulated form of STING. Because STING has a molecular weight of 42KDa, while GFP weights 27KDa, this makes it reasonable to assume that the 70KDa protein could be the form conjugated with the GFP. We can also note that the treatment performed with 2.5 μ g plasmid + 5 μ L Lipofectamin produced the most remarkable and durable results since the bands are very evident at the studied times and more detectable than 2.5 + 2.5 ones. As for the 5 + 5 treatment, in light of great cell mortality observed during the treatment, we only analyzed the T5 timing to ensure that we could check the final result, but we eventually decided to discard that combination due to said mortality. To conclude, we

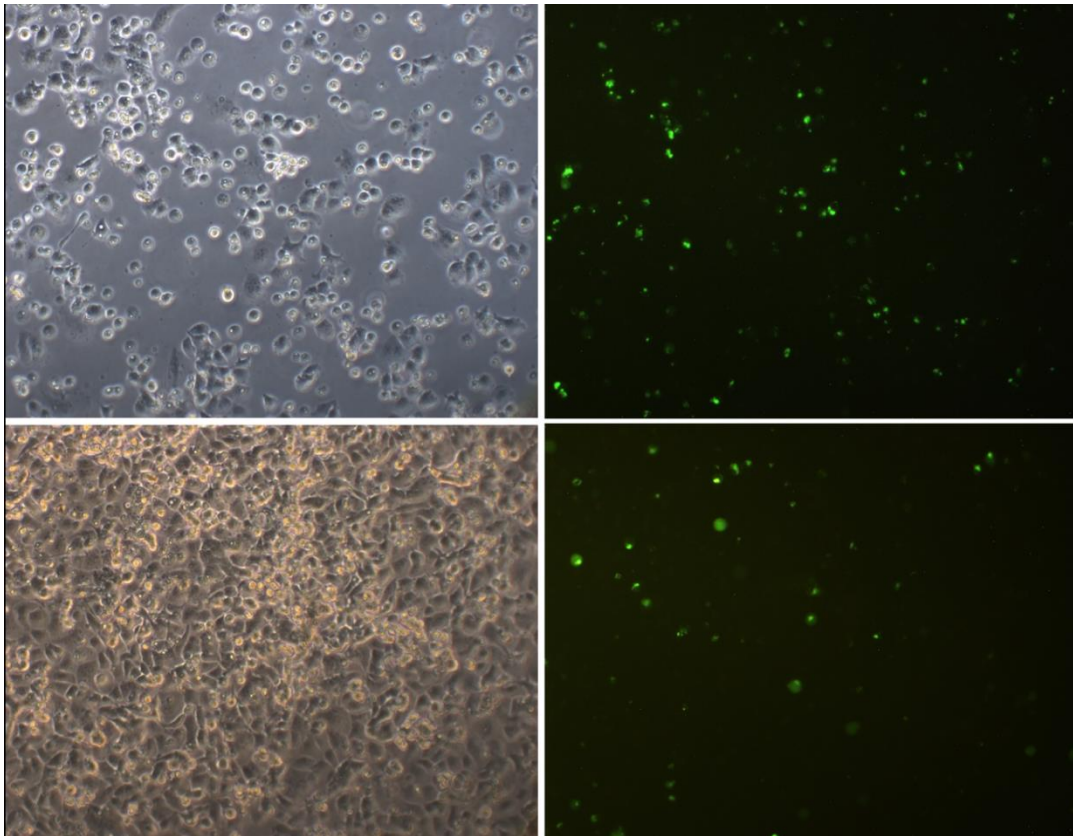


Figure 3.18 Microscopy images of DMS114 transfected with the plasmid bearing STING protein conjugated with GFP. Top pictures represent cell status at T2 (24 hours post transfection), while bottom ones stand for T5 (96 hours post transfection). Cells are shown in visible light (*left*) and in fluorescence emitted by GFP (*right*).

evaluated the 2.5 + 5 combination as the most effective treatment, a choice that was also confirmed by microscope observation of our samples that allowed us to detect a significant number of successfully transfected cells (Figure 3.18).

The exposure times needed to visualize the protein bands resulting from the 2 treatments performed on DMS114 are indeed very different, less than a minute for the plasmid-treatment and several minutes for the 5'-Azacytidine treatment. What we have said so far indicates very different levels, with a much better outcome in the case of the transfection treatment. Finally, we measured innate immune gene activation in DMS114 treated with plasmid transfection and TOP1 poisons altogether. Unfortunately, not even after the transfection was there an increase in cytokine transcription, which still exhibited low activation levels, similar to those observed in absence of transfection. In particular, interleukins (IL1A, IL1B, IL6, and IL8), together with IFNA1, were again below detection levels (Figure 3.19). Overall, the results on DMS114 indicate that the cGAS/STING pathway

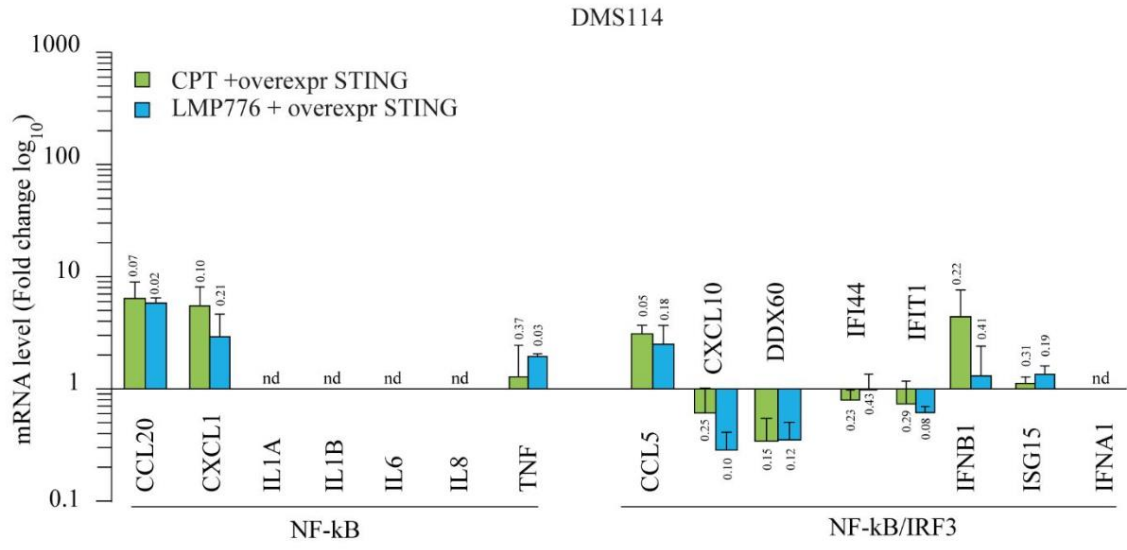


Figure 3.19 Innate immune response cytokine activation was measured in DMS114 cancer cell line after exogenous STING overexpression combined with TOP1 poison treatment. Bars represent the mean of 2 biological replicates \pm SEM. *P* values are reported above each bar and are calculated by one-tailed ratio paired *t*-test. Nd stands for “non detectable” for values below detection levels. Adapted from Marinello et al., 2022. Image licensed under the Creative Commons Attribution 4.0 International License. To view a copy of this license, visit <http://creativecommons.org/licenses/by/4.0/> or send a letter to Creative Commons, PO Box 1866, Mountain View, CA 94042, USA.

is likely impaired by several distinct mechanisms in this SCLC cell line.

Altogether the experimental findings in SCLC cell lines allow us to conclude that TOP1 poisons induce a marked increase of unscheduled R-loops, that are able to produce both DNA damage and micronuclei in cancer cells. Micronuclei are then recognized by the cGAS/STING pathway which, in so doing, trigger the activation of innate immune response. The entity of the innate immune response is much stronger in those cell lines that exhibit a fully active cGAS/STING pathway, whereas it is weak or inactivated in those cell lines showing an impaired cGAS/STING pathway. Moreover, the presented findings show that human SCLCs are often characterized by an impairment of the cGAS/STING pathways, and this feature likely suggest a reduction of Top1 poisons therapeutic activity in those cancer cell lines showing similar impairments.

3.5 G4 stabilization and cytotoxicity properties of hydrazone derivatives impact IFN-B stimulation

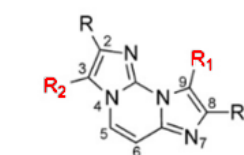
G4 binders are a class of molecules that have drawn the attention of researchers as attractive and promising anticancer drugs. Recent studies from our lab have shown their ability to increase the production of micronuclei and innate immune gene activation (Miglietta et al., 2021; De Magis et al., 2019; Amato et al., 2020). As discussed earlier in this thesis, micronuclei favor the emergence of dsDNA in the cytosol, which in turn can activate the cGAS/STING pathway, eventually triggering an innate immune response.

In 2010, two neo-synthesized strong G4-binders were discovered and named “1” and “3” (Sparapani et al., 2010); subsequently these compounds were renamed “FG” and “FIM” in Marzano et al., 2022. In 2016, more effective derivatives were produced and studied (Amato et al., 2016). These molecules belong to the hydrazone-based family and exhibit a central nuclear core called diimidazo [1,2-a:1,2-c]-pyrimidine. Out of all the molecules

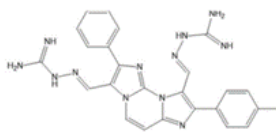
examined, FG was one of the most effective and it was able to identify and bind G4 structures in several cancer cell lines. Nonetheless, the mono-hydrazone FIM was evaluated as the most selective of the group and it was able to (i) strongly bind the promoter of c-myc, (ii) tie bonds with oxygen atoms of the G4 stack's backbone phosphate, and (iii) tie hydrogen bonds with the first upper lateral base of the pile of guanosines. However, it is not able to produce G4 stacks *ex novo*. It also showed a very high cytotoxicity if compared to other molecules (Amato et al., 2016). Prof. R. Morigi, University of Bologna, and her team have recently synthesized a new series of modified hydrazones that we have extensively studied. Within a partnership with Prof. A. Randazzo and his team at the University of Naples, I aimed at showing the activity of selected new hydrazone analogs in living cancer cells. In order to gather thorough information, these new compounds were analyzed in terms of cytotoxicity, efficiency in binding nuclear G4 structures, ability to cause DNA damage as detected by H2AX histone phosphorylation, micronuclei production and effectiveness in inducing Interferon β production.

The studied analogs included 7 compounds: "1", "2", "8", "15", "19", "20", and "FIM" (Figure 3.20) (Marzano et al., 2022). Furthermore, PDS served as a term of comparison as it is a well-known and characterized G4 binder. Among the selected compounds, 1, 2, and 8 are FG-derivatives and exhibit two identical chemical groups bound to the central Diimidazo [1,2-a: 1,2-c] pyrimidine core in R1 and R2 positions (Figure 3.20). In compound 1, these identical ligands include a couple of imino-guanidines, in compound 2 and 8 two imidazolines, and compound 8 exhibits a chlorine atom expected to act as a reactive region in this molecule. With regards to compounds 15, 19 and 20, they are FIM analogues. They show different substituent groups in positions R1 and R2 of the central Diimidazo [1,2-a: 1,2-c] pyrimidine core. In compounds 15 and 20 an imino-guanidine is located in position R1, while in compounds 19 and FIM the same position is occupied by an imidazoline. As for position R2, in compounds 19 and 20 it hosts a hydroxyl group, while in compounds 15 and FIM an aldehyde (Figure 3.20).

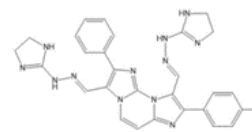
Diimidazo [1,2-a: 1,2-c] pyrimidine



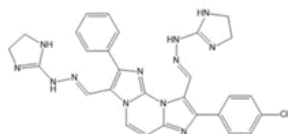
1



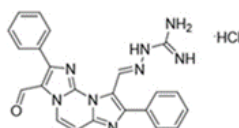
2



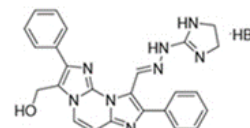
8



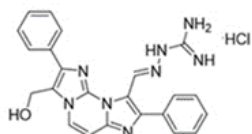
15



19



20



FIM

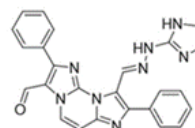


Figure 3.20 Chemical structures of studied Hydrazone derivatives. In red, R₁ and R₂ positions where substituents groups can bind to the core.

3.5.1 Cytotoxicity correlates with chemical structure in hydrazone derivatives

The first step in the study of these compounds was to evaluate their cytotoxicity, so a series of MTT assays was performed in order to evaluate IC₅₀ values, that is to say the drug concentration inhibiting the 50% of cell viability in the sample. This value is useful to establish the drug cell-killing potency and it can be employed as a threshold because the use of subcytotoxic concentrations allows to evaluate possible immune-modulatory effects. These assays were performed by administering drugs for the preset times (shown in Table 3.1) and, after drug removal, letting them to recover for 48 hours before

conducting MTT to determine how many cells were killed. The experiments were performed in U2OS and in MNMCA1 cell lines, the first being a human well-known osteosarcoma cancer cell line, while the second one a murine fibrosarcoma cancer line that is known to express high levels of IFN- β . We tested U2OS under both a short-period treatment (1 hour) and a long exposure (24 hours), while MNMCA1 cell line was only tested for the 24-hour treatment. Data indicate that in U2OS, after the short-treatment, the most cytotoxic compounds are FIM and 15. As for the others, 19 seems to be slightly less cytotoxic and, finally, compounds 1, 2, 8, and 20 do not display significant levels

	U2OS cell line		MNMCA1 cell line
	1 h-treatment	24-h treatment	24-h treatment
PDS	N.D.	> 50	27 \pm 16
1	148.85 \pm 25.65	46.84 \pm 12.7	38.49 \pm 5.76
2	223.13 \pm 141.64	108.26 \pm 35.4	28.62 \pm 8.43
8	343.30 \pm 181.63	20.2 \pm 1.01	23.52 \pm 5.08
FIM	5.65 \pm 0.56	4.01 \pm 0.33	2.29 \pm 0.92
15	6.80 \pm 0.91	2.56 \pm 0.87	1.87 \pm 0.33
19	44.44 \pm 2.87	24.47 \pm 1.19	12.08 \pm 2.51
20	356.39 \pm 143.08	14.26 \pm 9.31	35.65 \pm 0.67

Table 3.1. Cytotoxicity of the hydrazone derivatives in U2OS and MNMCA1 cancer cell lines. IC₅₀ concentrations of the studied hydrazone derivatives in 2 different cancer cell lines (U2OS and MNMCA1) after 1 and 24 hours of treatment. IC₅₀ (μ M) are reported as the mean \pm SEM of two independent experiments performed in triplicate. N.D. = not determined

of cytotoxicity. The 24-hour-treatment performed in U2OS showed, once again, that FIM and 15 are the most cytotoxic molecules, followed by less cytotoxic

compounds 20, 8, and 19, with no great differences in cytotoxicity among each other. Compound 1 exhibits rather a low level of cytotoxicity, whereas compound 2 turned out to be the least cytotoxic molecule. In MNMCA1, the most cytotoxic compounds are 15 and FIM, followed by 19. All other compounds have a rather similar cytotoxicity level, ranging from 23 ± 52 (compound 8) to 38.49 ± 5.76 (compound 1). These experiments (Table 3.1) indicate that FIM and 15 are, in general, the 2 most cytotoxic G4-binders and this can be explained by the fact that they bear an aldehyde group, which is an intrinsically-reactive functional group.

As for compounds 19 and 20, they both possess a hydroxyl group and their cytotoxicity levels are very similar to each other but slightly lower if compared to FIM and 15. Out of the remaining group that includes 1, 2, and 8, the latter seems to show high cytotoxicity levels. Finally, 1 and 2 are equipped with the planar lateral chains imino-guanidine and imidazoline, respectively, and rank as the least cytotoxic of all the molecules tested.

3.5.2 G4 stabilization and DNA damage induction in U2OS cells

Then, we wanted to determine the extent to which these molecules are able to selectively bind nuclear G4 structures *in vivo*. To achieve this goal, we carried out IF by using BG4, an antibody able to specifically bind G4s with high affinity (De Magis et al., 2019; Biffi et al., 2014). Prior to immunofluorescence microscopy examination, the experimental design required to treat U2OS cells for 10 minutes with an equimolar $10\mu\text{M}$ concentration of the studied G4 binder. To our purpose, we deemed it convenient to divide our compounds into 2 groups: the FG-derivatives (compounds 1, 2, and 8) and the FIM-analogues (FIM, 15, 19, and 20). In each group, we compared the means of all the spot signals in cell nuclei and we designed our experiments to include, besides the drug-treated samples, a non-

treated control and a PDS positive control, so as to compare the results obtained with those of a well-known G4-binder.

IF data revealed that the best G4-stabilizer is 20, with a fold increase of 2.45 ± 0.48 times vs. non-treated cells, followed by compound 1 (2.43 ± 0.81), compound 2 (2.37 ± 0.11), compound 15 (2.32 ± 0.32), PDS (mean fold-increase of 2.06 ± 0.20), compound 19 (1.91 ± 0.24), FIM (1.55 ± 0.25), and finally compound 8 (0.77 ± 0.46). All but compound 8 proved to be effective stabilizers. In fact, the effects produced by 8 were measured as being even lower than those found in non-treated cells. This can probably be due to the presence of a chlorine atom, which interacts with other cellular components (Figure 3.21).

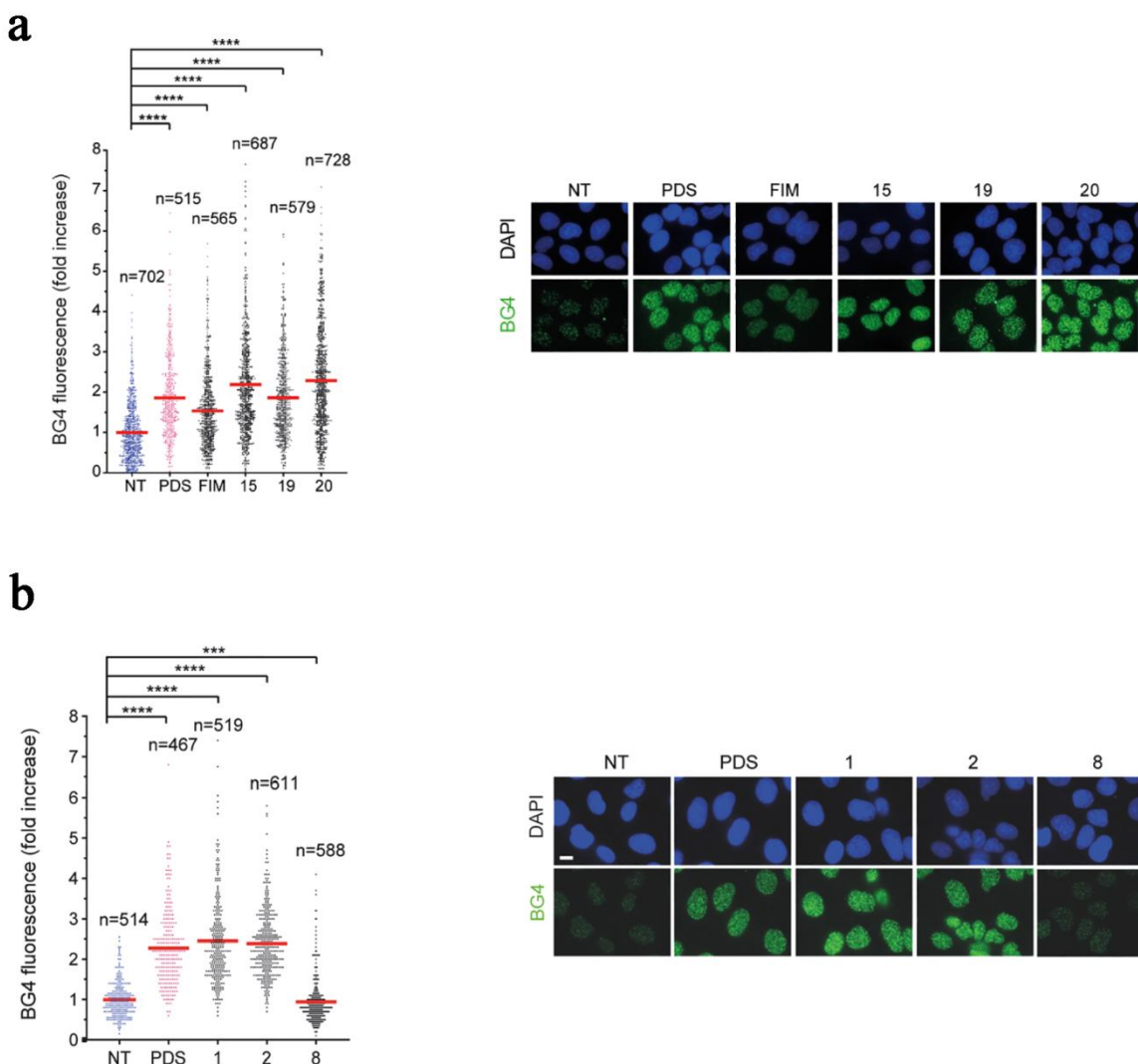


Figure 3.21 (Left) dot-plot representing the G4-stabilization analysis of the studied G4-binders by means of IF, with BG4 staining in U2OS cell line. This graph indicates the mean \pm SEM of 2 biological replicates. Numbers above dots report numerosness of each sample. Significance was calculated by using Kolmogorov-Smirnov test, comparing treated samples to non-treated ones ($*p < 0.05$, $**p > 0.01$, $***p < 0.001$, and $****p > 0.0001$). Cells were treated for 10 minutes with indicated G4-binders at a concentration of $10\mu\text{M}$. (Right) Representative IF images of treated and non-treated cells. Scale bar= $10\mu\text{m}$. (a) Compounds FIM, 15, 19, and 20 with non-treated cells (negative control) and PDS (positive control). (b) FG derivatives: 1, 2, and 8 with non-treated cells (negative control) and PDS (positive control). Image from Marzano et al., 2022. Image licensed under the Creative Commons Attribution-NonCommercial-NoDerivatives 4.0 International License. To view a copy of this license, visit <http://creativecommons.org/licenses/by-nc-nd/4.0/> or send a letter to Creative Commons, PO Box 1866, Mountain View, CA 94042, USA.

The next step was to assess if these molecules are able to induce DNA damage intended as phosphorylation of histone H2AX.

To this purpose we administered these molecules for 24 hours to U2OS by using an equitoxic concentration, with the following values: 10 μ M for PDS, 4 μ M for FIM, 2.5 μ M for compound 15, 24 μ M for compound 19, 14 μ M for compound 20, 46 μ M for compound 1, 100 μ M for compound 2, and 20 μ M for compound 8. To analyze the results, we once again divided samples into 2 groups, similar to what was done for the BG4 IF experiment (FG-derivatives and FIM-analogues) and we included non-treated cells as a negative control *and PDS-treated cells as a positive control in each group. Finally, we calculated the median of 2 biological replicates. This experiment revealed that the highest DNA damage level was caused by compound 20, with a fold increase of 2.25 ± 0.04 times vs. non-treated cells, followed by: FIM (1.69 ± 0.09), 19 (1.69 ± 0.06), compound 2 (1.58 ± 0.06), PDS with a mean fold-increase of 1.58 ± 0.02 , compound 8 (1.40 ± 0.06), compound 15 (1.13 ± 0.09), and finally compound 1 (0.94 ± 0.10). These results are fully shown in Figure 3.22.

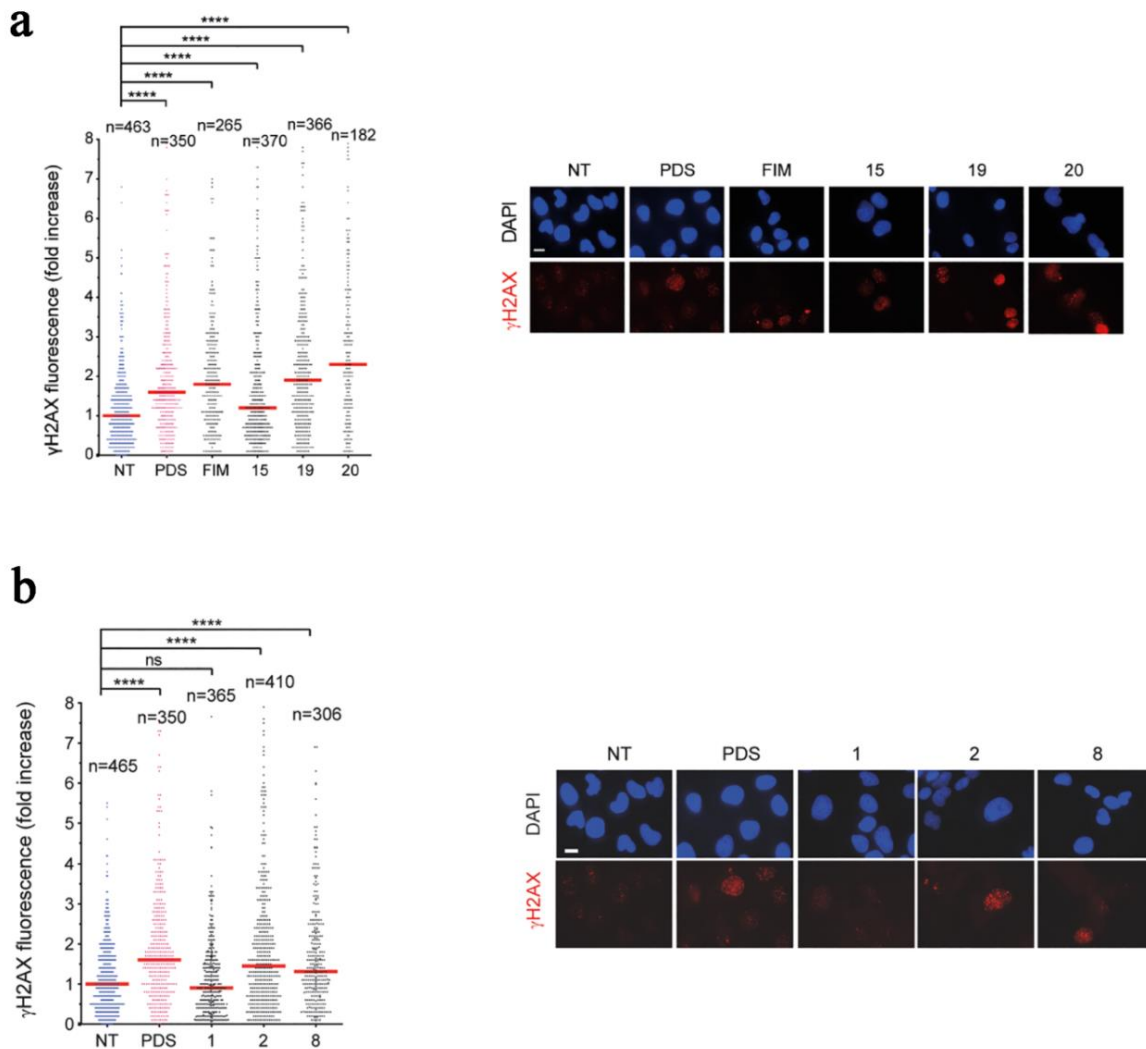


Figure 3.22 Dot-plot representing the phosphorylated histone H2AX analysis of the studied G4-binders by means of IF, in U2OS cell line. This graph indicates median \pm SEM of 2 biological replicates. Numbers above dots report numerosness of each sample. Significance was calculated by using Kolmogorov-Smirnov test comparing treated samples to non-treated ones ($*p < 0.05$, $**p > 0.01$, $***p < 0.001$, and $****p > 0.0001$). Cells were treated for 24 hours with indicated G4-binders at concentrations of: 10 μ M (PDS), 4 μ M (FIM), 2.5 μ M (15), 24 μ M (19), 14 μ M (20), 46 μ M (1), 100 μ M (2), and 20 μ M (8). On the right, representative IF images of treated and non-treated cells. Scale bar= 10 μ m. **(a)** compounds FIM, 15, 19, and 20 with non-treated cells (negative control) and PDS (positive control). **(b)** FG-derivatives: 1, 2, and 8 with non-treated cells (negative control) and PDS (positive control). Image from Marzano et al., 2022. Image licensed under the Creative Commons Attribution-NonCommercial-NoDerivatives 4.0 International License. To view a copy of this license, visit <http://creativecommons.org/licenses/by-nc-nd/4.0/> or send a letter to Creative Commons, PO Box 1866, Mountain View, CA 94042, USA.

3.5.3 Micronuclei production and IFN-B stimulation induced by hydrazone derivatives

Afterwards, we decided to measure micronuclei induction caused by our G4-binder treatments. To achieve this goal, we administered our compounds to MNMCA1 murine cells for 24 hours and then we let them recover for 24 hours in a fresh, drug-free medium. We chose sub-lethal concentrations, about half of IC₅₀ values: 10 μ M for PDS, 1 μ M for FIM and compound 15, 5 μ M for compounds 19 and 20, and finally 15 μ M for compounds

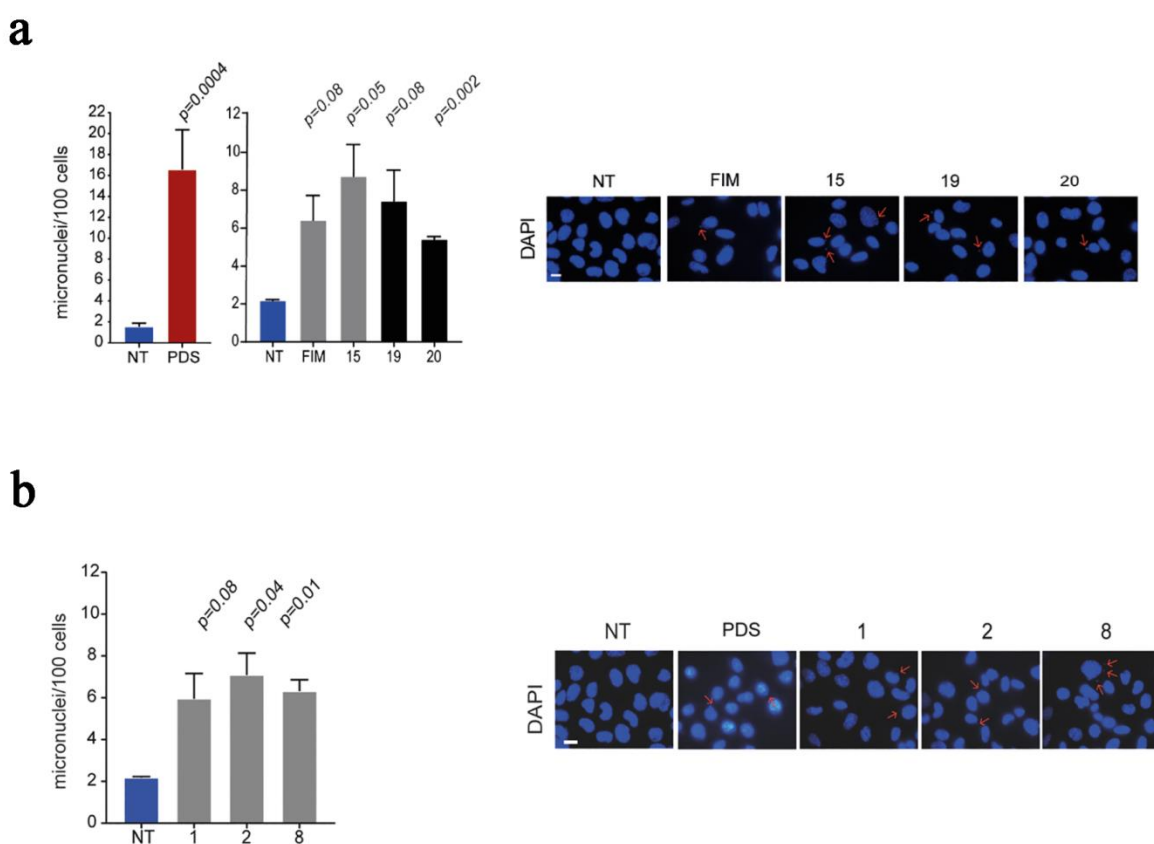


Figure 3.23 Micronuclei production in MNMCA1 cells, after a 24 hour-treatment followed by 24-hour recovery. Concentrations were administered as follows: 10 μ M (PDS), 1 μ M (FIM and 15), 5 μ M (19 and 20), and 15 μ M for (1, 2, and 8). (Left) Histograms reporting micronuclei/100 cells. Bars show the mean \pm SEM of 2 biological replicates. The sample p -value is indicated above each bar. (Right) IF representative images. Scale bar is 10 μ m. (a) Compounds FIM, 15, 19, and 20 with non-treated cells (negative control) and PDS (positive control). (b) FG-derivatives 1, 2, and 8 with non-treated cells (negative control) and PDS (positive control). Image from Marzano et al., 2022. Image licensed under the Creative Commons Attribution-NonCommercial-NoDerivatives 4.0 International License. To view a copy of this license, visit <http://creativecommons.org/licenses/by-nc-nd/4.0/> or send a letter to Creative Commons, PO Box 1866, Mountain View, CA 94042, USA.

1, 2, and 8. We could observe that PDS is much more effective than all other molecules in inducing micronuclei. The comparison of FG-derivatives and FIM-analogues produced rather homogenous results, ranging from 6 to 8 micronuclei/100 cells, with compound 15 reaching the highest level of micronuclei induction and compound 20 originating the lowest amount of micronuclei (Figure 3.23).

Finally, we conducted an experiment devoted to measure IFN- β in the supernatant of MNMCA1 cell line, by means of an ELISA assay. We treated the cells for 24 hours with different concentrations for each compound group, namely 15 μ M and 30 μ M (compounds 1, 2, and 8), 1 μ M (compound 15 and FIM), 5 μ M (compounds 19 and 20), and 10 μ M (PDS). Then, we let cells recover for 48 hours in a fresh, drugless medium. PDS elicited the highest IFN- β level, which is probably related to the remarkable micronuclei production, greater than in other compounds. As depicted in Figure 3.24, out of the compounds tested, compound 1 was able to originate the highest IFN- β amount, at both the concentrations, with a slight signal increase when using the 30 μ M concentration. Compound 2 and FIM showed a very similar IFN- β production amounting to 0.6-0.7 pg/mL/ 10^6 cells. Compound 15 exhibited intermediate power, reaching a value slightly lower than 0.6 pg/mL/ 10^6 cells. The other molecules (8, 19, and 20) turned out to be almost ineffective, showing IFN- β values comparable to those of non-treated cells.

It is noteworthy that compound 8 did not induce the production of IFN- β at a concentration either lower or higher than IC₅₀. This is rather unexpected, since this compound exhibits a micronuclei level similar to the one elicited by other G4-binders studied and proves to be a compound able to induce DNA damage in the form of H2AX histone phosphorylation.

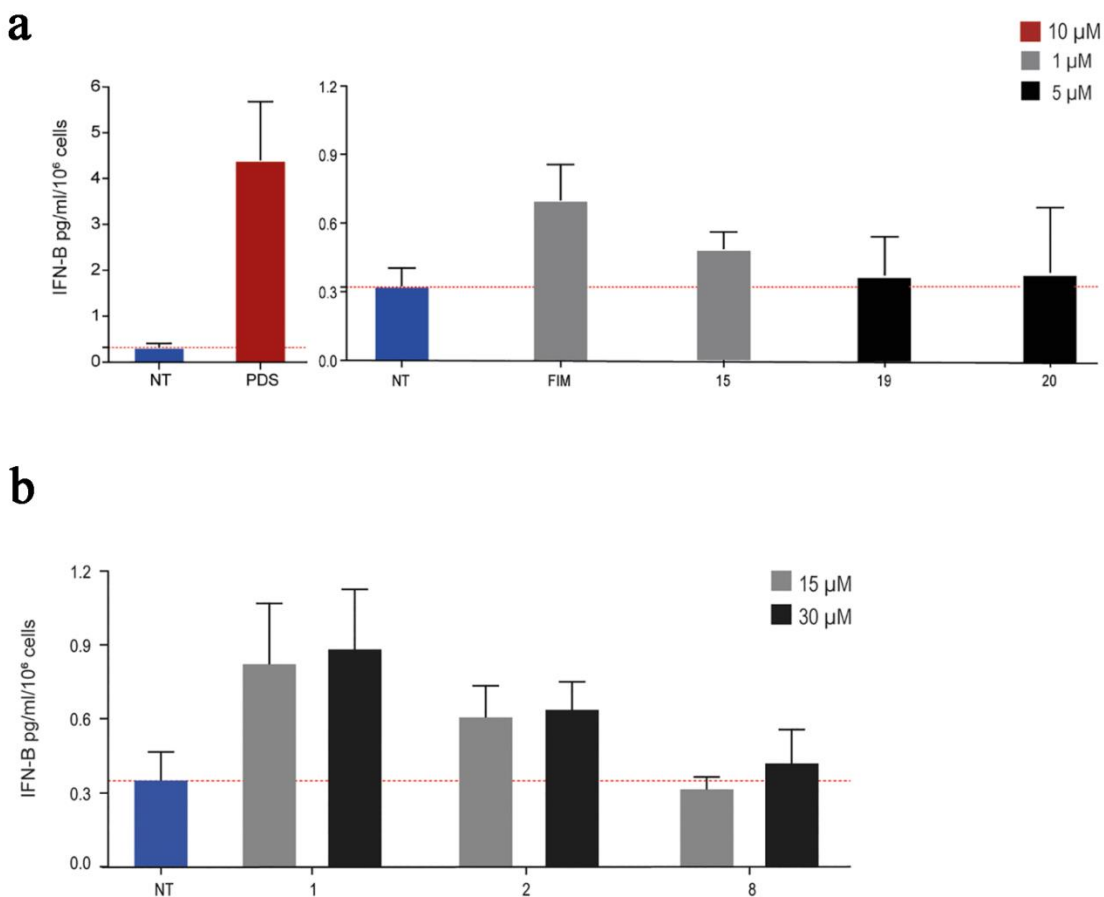


Figure 3.24 IFN-B production after G4 binder treatment in MNMCA1 cell line measured by means of an ELISA assay. Cells were treated for 24 hours at the indicated concentrations and then were left to recover for 48 hours. IFN-B production levels are indicated as pg/mL/10⁶ cells. Image from Marzano et al., 2022. Image licensed under the Creative Commons Attribution-NonCommercial-NoDerivatives 4.0 International License. To view a copy of this license, visit <http://creativecommons.org/licenses/by-nc-nd/4.0/> or send a letter to Creative Commons, PO Box 1866, Mountain View, CA 94042, USA.

On the other hand, compounds 2, 15, and 19 are able to induce IFN-B production and were found to be strong G4-stabilizers. Moreover, they do not seem to provoke a significant phosphorylation of histone H2AX. In light of these observations, we may infer that IFN-B production could be more likely related to G4-stabilizing effectiveness and less to the capability of damaging DNA.

Furthermore, we performed ELISA IFN- β tests by using compounds FIM, 15, 19, and 20 in HeLa, MCF-7 and U2OS cell lines. Each molecule was administered at its IC₅₀ concentration, cells were treated for 24 hours and then let recover for 48 hours. In all of these cell lines, we could not detect any IFN- β production. The values obtained were constantly below detection levels. To overcome this problem, we chose to employ MNMCA1, a cell line exhibiting a higher basal level of IFN- β .

To sum up, IFN- β production elicited by G4 binders could be detected in MNMCA1, which are known to be a cell line characterized by a consistent IFN- β production, but was almost absent in the 3 human cell lines that do not exhibit high basal IFN- β level.

Considering these and previously described results, we can conclude that G4-binders show a good activity to induce the production of IFN- β , although this effect might be strictly dependent on the intrinsic ability of a specific cell line to physiologically produce higher or lower levels of IFN- β . Based on these results it could be possible to infer that the ability of hydrazone-based G4 binders to stimulate IFN- β production depends on a delicate balance between their cytotoxicity and G4-stabilization activity. Other important concurrent factors (although not as critical) are the induction of low DNA damage and a relatively high amount of micronuclei.

CHAPTER IV

Discussion

4.1 TOP1 poisons induce DNA damage and innate immune response activation

This PhD project has resulted in several findings that allow us to highlight the critical role played by TOP1 poisons in the initiation of a consequential path starting from R-loop production and leading to the activation of an innate immune response in cancer cells. We focused on 2 TOP1 poisons, namely CPT and LMP-776, currently used in standard treatment combinations in human cancer patients or in advanced clinical trials. We could observe that both of them are able to transiently enhance R-loops stabilization, starting rather early and peaking 5-10 minutes after drug administration. Furthermore, our findings showed that TOP1 poisons induce a great number of micronuclei in cancer cell lines belonging to different histologies, as a marked micronuclei production was detected in HeLa and 3 SCLC cell lines, namely H209, H889, and DMS114. In line with previous studies (Miglietta et al., 2020; De Magis et al., 2019), the present findings show that the hindrance of R-loop production as an effect of TOP1-poison administration by overexpressing RNaseH1 results in a significant decrease of micronuclei levels (see Chapter 3, Figure 3.1). TOP1 poisons are able to produce a high transcription/replication stress and a dose-dependent increase of unscheduled R-loops, which eventually leads to DSBs (see Chapter 3, Figure 3.3). These results show that R-loops and

transcription/replication stress both play a critical role in the increase of micronuclei production during mitosis.

Micronuclei resulting from TOP1 poison administration can, in turn, stimulate the initiation of cGAS/STING pathway, as shown by mRNA transcription of NF- κ B and IRF3 modulated cytokines.

The experimental data indicate that although TOP1 poisons are able to induce a high micronuclei production in all of the cell lines examined, this effect is not accompanied by a parallel increase in cytokine stimulation, which seems to correlate with cGAS/STING pathway activation/impairment levels and to be strongly dependent on the expression and functionality of the STING protein. Likely, the activation of innate immune response cytokines represents the arrival point of the entire pathway and that STING seems to exert a stronger impact than cGAS on this pathway. In case of STING depletion, as it is the case of H889, DMS114, silenced HeLa, and B16-STING-KO cells, we have not observed any activation of innate immune response, or at least a very reduced one. On the other hand, if this protein is moderately or highly expressed in the cell line, as observed in H209, B16-STING-WT, and above all HeLa, it is easy to obtain a strong innate immune gene activation. In light of these observations, we can say that the level of STING activation is reflected in the degree of subsequent innate immune response. Furthermore, we observed that after TOP1 poison administration, the transcription of STING gene increases, as if more STING would be needed to face the effects of TOP1 poisons, mainly DNA damage. cGAS demonstrated a less impactful role because its levels seem to have a reduced impact on the activation of innate immune response and even when it is highly produced in cells, it is not able to elicit a marked innate immune response activation on itself. These observations are in agreement with the pathway mechanisms, and the central role of STING (Corrales et al., 2017; Galluzzi et al., 2018).

It is noteworthy that HeLa cell line shows a significant innate immune response activation, although its cGAS levels do not increase after TOP1 poison administration, in contrast to what happens with STING. The expression of STING and cGAS varied depending on the

studied cancer cell line, showing extremely low levels, especially in SCLC cells, hampering the activity of cGAS/STING pathway and, as a consequence, of innate immune response. This makes SCLC cell lines generally able to resist immune gene modulation resulting from the action of DNA-damaging agents. However, previous studies have shown that PARP inhibitors can raise the levels of pathway factors and of IFN- β transcription in three SCLC cells bearing highly expressed cGAS and STING (Sen et al., 2019). These observations point to a critical function served by STING to the purpose of an effective functionality of the signaling pathway. Moreover, bioinformatic analyses show that the signaling pathway cGAS/STING is often impaired and STING is underexpressed in cell lines belonging the SCLC group as the STING promoter is frequently methylated the tumors (Marinello et al., 2022; Poirier et al., 2015). These considerations might lead to the assumption that immune gene activation could be empowered by demethylating the STING promoter to restore the functionality of the pathway. However, our results reported in Paragraph 3.4 describe the inactivation of immune cytokines following TOP1 poison administration, in spite of the presence of 5'-azacytidine or STING exogenous overexpression. These findings contradict the above assumption on STING rescue and signal that the impairment of the cGAS/STING pathway in SCLC cells might also be due to other and unknown mechanisms.

Altogether, our findings show that the mechanisms involved in the activation of innate immune response are triggered by the overproduction of unscheduled R-loops resulting from TOP1 poison activity. CPT and LMP-776 show no differences as for their effectiveness in eliciting micronuclei, since they exhibit a similar efficacy, although a slight difference was found their ability to stimulate R-loops. However, this does not deny that both the poisons are effective in transiently stabilizing R-loops and in inducing an innate immune response in those cancer cell lines that exhibit a fully functional cGAS/STING pathway when administered at sub-cytotoxic concentrations. Moreover, CPT and LMP776 at sub-cytotoxic concentrations show the ability to elicit the production of micronuclei and the activation of innate immune response even at longer times after drug removal. These

findings can be of uttermost interest, especially considering that TOP1 poisons exhibit a noticeable cell-killing potential at higher concentrations and immune response modulation power at lower concentrations. This can undoubtedly prove useful in clinical applications, where the use of these molecules can be adjusted by varying the concentration and time of administration, offering physicians different therapeutic effects (Galluzzi et al., 2020).

Previous studies have found that TOP1 poisons result in a number of delayed effects connected to immune response, like the ability of Topotecan to activate STING (Kitai et al., 2017) and stimulate MHC class I genes by overexpressing IFN- β and IFN- β signaling in breast cancer cell lines (Wan et al. 2012). Other research observed the involvement of TOP1 poisons in cancer cell recognition by T cells (McKenzie et al., 2018).

Although our results show a general tendency of cancer cells to under-express the signaling pathway genes, some authors have found that the examined pathway is overexpressed in several cancer types, in order to provoke a permanent inflammatory status (Vashi et Bakhoun, 2021) resulting in a more favorable environment for the progression and resistance of cancer cells to cytotoxic compounds (Cheradame et al., 2021; Ahn et al., 2014). All these aspects and properties are valuable resources and clinicians can take advantage of them when choosing cancer therapies, with the final aim of reaching a patient-tailored treatment, customized on the specific features of a patient and their distinctive cancer cell lines.

To conclude, findings show that TOP1 poisons have interesting effects on the signaling pathway, resulting in the stimulation of innate immune response, thus constituting a profitable area of investigation in order to develop new cancer treatments, which should however take into account the potential downregulation of the pathway that tends to be found in SCLC cell lines.

4.2 G4 stabilization/cytotoxicity balance affects IFN-B stimulation in hydrazone-based G4 binders

The second part of the present PhD project focused on studying a group of hydrazone-based compounds belonging to the family of diimidazo[1,2-a;1,2-c]-pyrimidine derivatives, in order to investigate the features that most affect IFN-B production. Previous published data described them as potent G4-stabilizers, with a high specificity, able to discriminate quadruplex structures from dsDNA (Sparapani et al., 2010). Furthermore they have been shown to increase R-loop and micronuclei levels and induce DNA damage and cell death in cancer cells (Amato et al., 2020). Data also showed that their G4-selectivity significantly improves as a consequence of a lower number of positively charged side chains, while maintaining their ability to stabilize G4s *in vitro* (Amato et al., 2016).

In light of these former studies, we tested *in vivo* these new hydrazones to assess some of their core features like cytotoxicity, G4-stabilization, production of micronuclei, DNA damage, and IFN-B production. Our experiments demonstrate that compound 1 is the most effective molecule (as compared to other studied hydrazones) in terms of IFN-B production, accompanied by a high G4-stabilization ability although with a low cytotoxicity and DNA damage levels. Similarly, FIM shows a high production of IFN-B, intermediate levels of G4-stabilization, micronuclei production, and DNA damage, while exhibiting high cytotoxicity. Compounds 2 and 15 have proven to be very efficient G4-stabilizers, although producing intermediate values of micronuclei, DNA damage and IFN-B and showing different levels of cytotoxicity (compound 2 being less cytotoxic than compound 15). The remaining three compounds (8, 19, and 20) were not able to induce a relevant IFN-B production and displayed low to moderate degrees of cytotoxicity, G4-stabilization, and micronuclei production. All the properties investigated in these hydrazone-based compounds were gathered in an overview reported in Table 4.1.

As for the differences observed in these peculiar characteristics across the compounds under investigation, they are due to the interplay of several aspects discussed as follows.

As for G4-stabilization, out of the G4-binders examined, the one demonstrating the lowest G4-stabilizing power is compound 8 and this is likely due to the presence of a chlorine atom that makes this molecule very reactive to other cellular structures, which decreases its ability to bind G-quadruplexes. Moreover, we confirmed previous findings (Amato et

Compound	Chemical group	Cyto-toxicity	G4-stabilization	Micro-nuclei	DNA damage	IFN-B production
PDS		Low	High	Ve. High	Interm.	Ve. High
1	Imi-Gua	Low	High	Interm.	Low	High
2	Imidazoline	Low	High	Interm.	Interm.	Interm.
8	Imd + Cl	Low	Low	Interm.	Interm.	Low
15	Aldehyde	High	High	High	Interm.	Interm.
19	Hydroxyl	Interm.	Interm.	Interm.	Interm.	Low
20	Hydroxyl	Low	High	Low	High	Low
FIM	Aldehyde	High	Interm.	Interm.	Interm.	High

Table 4.1 Overview of the core features tested in hydrazone-based G4-binders. The table reports the G4-binders tested with a short synthesis of experimental outcomes. The second column shows the substituent group of each molecule. The column “cytotoxicity” considers the IC₅₀ mean value, measured in U2OS cell line, after a 24-hour treatment: IC₅₀ values below 5μM are indicated as “High”, values included between 10μM and 19μM are indicated as “Intermediate”, while values higher than 20μM are indicated as “Low”. The column “G4-stabilization” reports the fold-increase values compared to non-treated cells in U2OS after a 24-hour treatment. Fold-increase values higher than 2 are indicated as “High”, values between 1.0 and 1.99 as “Intermediate” and values below 1 as “Low”. The column “micronuclei” reports the fold-increase values compared to non-treated cells in MNMCA1 after a 24-hour treatment at sub-cytotoxic drug concentrations. Values higher than 15 micronuclei/100 cells (PDS) are indicated as “very high”, values between 15 and 8 micronuclei/100 cells are indicated as “Intermediate”, while values below 8 micronuclei/100 cells are indicated as “Low”. The column “DNA damage” reports fold-increase values compared to non-treated cells in U2OS cell line after a 24-hour treatment. Values higher than 2 (compound 20) are indicated as “High”, values between 1 and 1.99 are indicated as “Intermediate”, while values below 1 are indicated as “Low”. Finally, the column “IFN-B production” reports the IFN-B production measured as pg/mL/10⁶ cells in MNMCA1 after a 24-hour treatment at sub-cytotoxic concentrations. Values higher than 4 (PDS) are indicated as “Very high”, values between 0.75 and 0.90 are indicated as “High”, values between 0.50 and 0.75 are indicated as “Intermediate”, and values below 0.50 are indicated as “Low”.

al., 2016) that those G4-binders bearing 2 side chains (FG-derivatives, namely 1, 2, and 8) are generally more effective in stabilizing G4-structures than 1-side chain molecules (FIM analogues, namely 15, 19, 20, and FIM). Overall, almost every one of the compounds investigated hereby shows a medium-high G4-stabilizing effect, with no relevant differences from one another. However, at this stage it is hard to say whether the G4 structures that were stabilized belong to the same typology or to different ones. Although *in vitro* studies have been conducted on this matter (Marzano et al., 2022), further investigations *in vivo* are needed to gather a deeper understanding of whether and how these hydrazone-based compounds distinguish different G4 structures as their specific targets. In regard to cytotoxicity, high levels exhibited by compounds 15 and FIM are probably due to the aldehyde group they bear. As for compound 20, the high degree of DNA damage observed was not reflected in cytotoxicity levels, which remained rather low, showing that although this compound's activity impacts the breakage of DNA, this does not result in great cell-killing capability and high levels of IFN-B production.

To sum up, the results of the experiments conducted to investigate the effect arisen by the interaction of G4-stabilization, cytotoxicity, and micronuclei production on immune stimulation show that even compounds that are very similar in their structures (like 1, 2, and 8) exhibit important differences in this regard. The high cytotoxicity of compound 8 is accompanied by low G4-stabilization and low IFN-B production, while compound 1 shows low cytotoxicity but a high ability to stabilize G4s *in vivo* and stimulate IFN-B production. Another aspect that is worth to point out is that IFN-B production does not depend uniquely on the number of micronuclei induced, as observed in FIM analogues and, above all, in compound 1. Both of them show relevant levels of IFN-B production but moderate amounts of micronuclei induced. These observations might hint to the fact that immune response requires the emergence of certain amounts of micronuclei but these alone are not enough to produce substantial levels of IFN-B (Crowl et al., 2017; Pilger et al., 2021) and other signaling pathways competing with cGAS/STING might be involved (Miglietta et

al., 2022). For instance, G4 binders are known to stimulate autophagic processes, in which micronuclei and the DNA they contain are recycled in the production of autophagosomes (Gui et al., 2019; Hopfner and Hornung, 2020). Further investigations on the way these processes activate might unveil their possible role in the differences observed in IFN- β production across the compounds studied.

To conclude, the findings obtained allow to infer that IFN- β gene activation can require on the one hand a good G4 binding affinity and stabilization capability, and on the other hand low cytotoxicity levels that allow the cell to function properly without compromising its vital functions. Therefore, the most desirable combination is likely found in those compounds which exhibit a high G4 structure stabilizing capacity together with low cytotoxicity, as summarized by Figure 4.1.

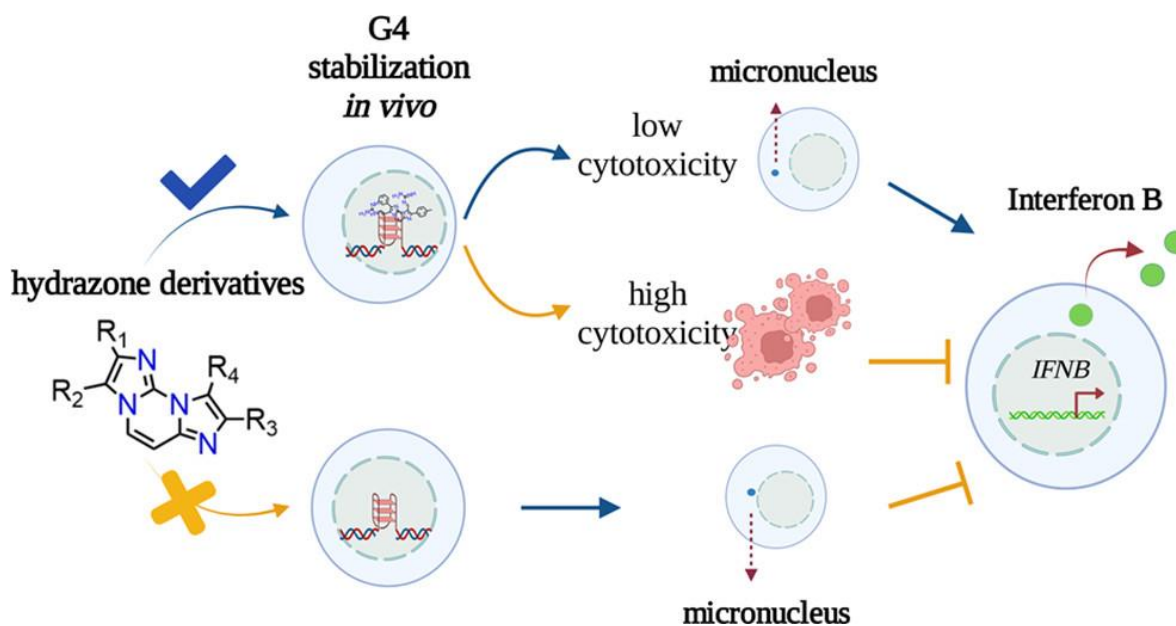


Figure 4.1 Representation of the main features likely needed for a G4-binder to induce IFN- β production. The most desirable features for a G4-stabilizer to induce IFN- β production are: high G4-stabilization capability, high micronuclei induction, and low cytotoxicity. Image from Marzano et al., 2022. Image licensed under the Creative Commons Attribution-NonCommercial-NoDerivatives 4.0 International License. To view a copy of this license, visit <http://creativecommons.org/licenses/by-nc-nd/4.0/> or send a letter to Creative Commons, PO Box 1866, Mountain View, CA 94042, USA.

Conclusions

This PhD project allowed to describe the ways in which TOP1 poisons and some hydrazone-based G4-binders can induce the activation of innate immune response by deregulating 2 non-canonical DNA structures, namely R-loops and G-quadruplexes, respectively.

We observed that the administration of TOP1 poisons results in a significant increase of unscheduled R-loops, which in turn induce the formation of micronuclei, eventually leading to the activation of cytosolic dsDNA signaling pathway cGAS/STING that is able to recognize these extra-nuclear structures. This pathway, with a special role played by the transmembrane protein STING, initiates nuclear transcription factors NFkB and IRF3, thus enabling the transcription of a group of cytokines involved in innate immune response. The way TOP1 poisons affect the activation of the pathway and the long-term effects that they are able to exert represent an interesting area of study that calls for further investigations.

In a similar way, the 7 hydrazone derivatives we examined are able to bind and stabilize G-quadruplexes, with consequences on the physiological regulation of DNA transcription in terms of accessibility, increase or reduction of transcription, and epigenetics. The alteration of this equilibrium influences many main features of cells like cytotoxicity, micronuclei production, DNA damage, and eventually IFN- β production.

Both Top1 poisons and G4-stabilizers possess several features that can be very useful in clinical applications, in light of their ability to stimulate innate immune response factors and exert a certain cell-killing power, plus they offer a broad and diverse range of treatment options in order to face a variety of patient treatment needs. It is for these very reasons that it is of uttermost importance that further studies are conducted on these compounds, in order to synthesize new and increasingly powerful and flexible ones, with fewer side effects to customize therapies on specific cancers' and patients' features.

References

- Ablasser, A., Schmid-Burgk, J. L., Hemmerling, I., Horvath, G. L., Schmidt, T., Latz, E., & Hornung, V. (2013). Cell intrinsic immunity spreads to bystander cells via the intercellular transfer of cGAMP. *Nature*, *503*(7477), 530–534. <https://doi.org/10.1038/nature12640>
- Ahn, J., Xia, T., Konno, H., Konno, K., Ruiz, P., & Barber, G. N. (2014). Inflammation-driven carcinogenesis is mediated through STING. *Nature communications*, *5*, 5166. <https://doi.org/10.1038/ncomms6166>
- Amato, J., Miglietta, G., Morigi, R., Iaccarino, N., Locatelli, A., Leoni, A., Novellino, E., Pagano, B., Capranico, G., & Randazzo, A. (2020). Monohydrazone Based G-Quadruplex Selective Ligands Induce DNA Damage and Genome Instability in Human Cancer Cells. *Journal of medicinal chemistry*, *63*(6), 3090–3103. <https://doi.org/10.1021/acs.jmedchem.9b01866>
- Amato, J., Morigi, R., Pagano, B., Pagano, A., Ohnmacht, S., De Magis, A., Tiang, Y. P., Capranico, G., Locatelli, A., Graziadio, A., Leoni, A., Rambaldi, M., Novellino, E., Neidle, S., & Randazzo, A. (2016). Toward the Development of Specific G-Quadruplex Binders: Synthesis, Biophysical, and Biological Studies of New Hydrazone Derivatives. *Journal of medicinal chemistry*, *59*(12), 5706–5720. <https://doi.org/10.1021/acs.jmedchem.6b00129>
- American Cancer Society. Global Cancer Facts & Figures 3rd edn (American Cancer Society, 2015).
- Anderson, L., Henderson, C., & Adachi, Y. (2001). Phosphorylation and rapid relocalization of 53BP1 to nuclear foci upon DNA damage. *Mol Cell Biol.* 2001 Mar;*21*(5), 1719–29. <https://doi.org/10.1128/MCB.21.5.1719-1729.2001>
- Antony, S., Agama, K. K., Miao, Z. H., Takagi, K., Wright, M. H., Robles, A. I., Varticovski, L., Nagarajan, M., Morrell, A., Cushman, M., & Pommier, Y. (2007). Novel indenoisoquinolines NSC 725776 and NSC 724998 produce persistent topoisomerase I cleavage complexes and overcome multidrug resistance. *Cancer research*, *67*(21), 10397–10405. <https://doi.org/10.1158/0008-5472.CAN-07-0938>
- Ashour, M., Atteya, R. & El-Khamisy, S. Topoisomerase-mediated chromosomal break repair: an emerging player in many games. *Nat Rev Cancer* *15*, 137–151 (2015). <https://doi.org/10.1038/nrc3892>

- Bailly, C. (2012). Contemporary challenges in the design of topoisomerase II inhibitors for cancer chemotherapy. *Chemical reviews*, 112(7), 3611-3640. <https://doi.org/10.1021/cr200325f>
- Baranello, L., Bertozzi, D., Fogli, M. V., Pommier, Y., & Capranico, G. (2010). DNA topoisomerase I inhibition by camptothecin induces escape of RNA polymerase II from promoter-proximal pause site, antisense transcription and histone acetylation at the human HIF-1alpha gene locus. *Nucleic acids research*, 38(1), 159-171. <https://doi.org/10.1093/nar/gkp817>
- Barber G. N. (2014). STING-dependent cytosolic DNA sensing pathways. *Trends in immunology*, 35(2), 88-93. <https://doi.org/10.1016/j.it.2013.10.010>
- Bedrat, A., Lacroix, L., & Mergny, J. L. (2016). Re-evaluation of G-quadruplex propensity with G4Hunter. *Nucleic acids research*, 44(4), 1746-1759. <https://doi.org/10.1093/nar/gkw006>
- Berkovich, E., Monnat, R. J., Jr, & Kastan, M. B. (2007). Roles of ATM and NBS1 in chromatin structure modulation and DNA double-strand break repair. *Nature cell biology*, 9(6), 683-690. <https://doi.org/10.1038/ncb1599>
- Bétermier, M., Bertrand, P., & Lopez, B. S. (2014). Is non-homologous end-joining really an inherently error-prone process?. *PLoS genetics*, 10(1), e1004086. <https://doi.org/10.1371/journal.pgen.1004086>
- Bhattacharyya, D., Mirihana Arachchilage, G., & Basu, S. (2016). Metal Cations in G-Quadruplex Folding and Stability. *Front Chem.* 2016 Sep;9: 4-38. <https://doi.org/10.3389/fchem.2016.00038>
- Bielskutė, S., Plavec, J., Podbevšek, P. (2019). Impact of Oxidative Lesions on the Human Telomeric G-Quadruplex. *J Am Chem Soc* 141(6), 2594-2603. <https://doi.org/10.1021/jacs.8b12748>
- Biffi, G., Di Antonio, M., Tannahill, D., & Balasubramanian, S. (2014). Visualization and selective chemical targeting of RNA G-quadruplex structures in the cytoplasm of human cells. *Nature chemistry*, 6(1), 75-80. <https://doi.org/10.1038/nchem.1805>
- Biffi, G., Tannahill, D., McCafferty, J., & Balasubramanian, S. (2013). Quantitative visualization of DNA G-quadruplex structures in human cells. *Nature chemistry*, 5(3), 182-186. <https://doi.org/10.1038/nchem.1548>
- Biffi, G., Tannahill, D., Miller, J., Howat, W.J., & Balasubramanian, S. (2014). Elevated levels of G-quadruplex formation in human stomach and liver cancer tissues. *PLoS One* 9(7), e102711. <https://doi.org/10.1371/journal.pone.0102711>
- Boguslawski, S. J., Smith, D. E., Michalak, M. A., Mickelson, K. E., Yehle, C. O., Patterson, W. L., & Carrico, R. J. (1986). Characterization of monoclonal antibody to DNA.RNA

- and its application to immunodetection of hybrids. *Journal of immunological methods*, 89(1), 123–130. [https://doi.org/10.1016/0022-1759\(86\)90040-2](https://doi.org/10.1016/0022-1759(86)90040-2)
- Bou-Nader, C., Bothra, A., Garboczi, D. N., Leppla, S. H., & Zhang, J. (2022). Structural basis of R-loop recognition by the S9.6 monoclonal antibody. *Nature communications*, 13(1), 1641. <https://doi.org/10.1038/s41467-022-29187-7>
- Brosh, R. M., Jr, & Cantor, S. B. (2014). Molecular and cellular functions of the FANCD1 DNA helicase defective in cancer and in Fanconi anemia. *Frontiers in genetics*, 5, 372. <https://doi.org/10.3389/fgene.2014.00372>
- Bryan, T.M. (2019). Mechanisms of DNA Replication and Repair: Insights from the Study of G-Quadruplexes. *Molecules* 24(19): 3439. <https://doi.org/10.3390/molecules24193439>
- Bryan, T.M. (2020). G-Quadruplexes at Telomeres: Friend or Foe? *Molecules* 25(16), 3686. <https://doi.org/10.3390/molecules25163686>
- Burger, A. M., Dai, F., Schultes, C. M., Reszka, A. P., Moore, M. J., Double, J. A., & Neidle, S. (2005). The G-quadruplex-interactive molecule BRACO-19 inhibits tumor growth, consistent with telomere targeting and interference with telomerase function. *Cancer research*, 65(4), 1489–1496. <https://doi.org/10.1158/0008-5472.CAN-04-2910>
- Capranico, G., Marinello, J., & Chillemi, G. (2017). Type I DNA Topoisomerases. *Journal of medicinal chemistry*, 60(6), 2169–2192. <https://doi.org/10.1021/acs.jmedchem.6b00966>
- Capranico, G., Zagotto, G., & Palumbo, M. (2004). Development of DNA topoisomerase-related therapeutics: a short perspective of new challenges. *Current medicinal chemistry. Anti-cancer agents*, 4(4), 335–345. <https://doi.org/10.2174/1568011043352885>
- Carvalho, J., Mergny, J.L., Salgado, G.F., Queiroz, J.A., & Cruz, C. (2020). G-quadruplex, Friend or Foe: The Role of the G-quartet in Anticancer Strategies. *Trends Mol Med* 26(9), 848–861. <https://doi.org/10.1016/j.molmed.2020.05.002>
- Chakraborty, P., & Grosse, F. (2011). Human DHX9 helicase preferentially unwinds RNA-containing displacement loops (R-loops) and G-quadruplexes. *DNA repair*, 10(6), 654–665. <https://doi.org/10.1016/j.dnarep.2011.04.013>
- Chambers, V.S., Marsico, G., Boutell, J.M., Di Antonio, M., Smith, G.P., & Balasubramanian, S. (2015). High-throughput sequencing of DNA G-quadruplex structures in the human genome. *Nat Biotechnol* 33(8), 877–881. <https://doi.org/10.1038/nbt.3295>
- Champoux J.J. (2001). DNA topoisomerases: structure, function, and mechanism. *Annual review of biochemistry*, 70, 369–413. <https://doi.org/10.1146/annurev.biochem.70.1.369>

- Champoux, J.J. (2012). Human DNA Topoisomerase I: Structure, Enzymology and Biology. In Y. Pommier (ed.), *DNA Topoisomerases and Cancer* (pp. 53-69). Springer, New York, NY. https://doi.org/10.1007/978-1-4614-0323-4_2
- Chan, K. L., Palmai-Pallag, T., Ying, S., & Hickson, I. D. (2009). Replication stress induces sister-chromatid bridging at fragile site loci in mitosis. *Nature cell biology*, *11*(6), 753–760. <https://doi.org/10.1038/ncb1882>
- Chang, E. Y., Novoa, C. A., Aristizabal, M. J., Coulombe, Y., Segovia, R., Chaturvedi, R., Shen, Y., Keong, C., Tam, A. S., Jones, S., Masson, J. Y., Kobor, M. S., & Stirling, P. C. (2017). RECQ-like helicases Sgs1 and BLM regulate R-loop-associated genome instability. *The Journal of cell biology*, *216*(12), 3991–4005. <https://doi.org/10.1083/jcb.201703168>
- Chang, H.H.Y., Pannunzio, N.R, Adachi, N., Lieber, M.R. (2017). Non-homologous DNA end joining and alternative pathways to double-strand break repair. *Nat Rev Mol Cell Biol* *18*(8), 495–506. <https://doi.org/10.1038/nrm.2017.48>
- Chen, Q., Sun, L. & Chen, Z. (2016). Regulation and function of the cGAS–STING pathway of cytosolic DNA sensing. *Nat Immunol* *17*, 1142–1149. <https://doi.org/10.1038/ni.3558>
- Chen, T., Sun, Y., Ji, P. et al. (2015). Topoisomerase II α in chromosome instability and personalized cancer therapy. *Oncogene* *34*, 4019–4031. <https://doi.org/10.1038/onc.2014.332>
- Cheradame, L., Guerrero, I. C., Gaston, J., Schmitt, A., Jung, V., Goudin, N., Pouillard, M., Radosevic-Robin, N., Modesti, M., Judde, J. G., Cairo, S., & Goffin, V. (2021). STING protects breast cancer cells from intrinsic and genotoxic-induced DNA instability via a non-canonical, cell-autonomous pathway. *Oncogene*, *40*(49), 6627–6640. <https://doi.org/10.1038/s41388-021-02037-4>
- Cogoi, S. & Xodo, L.E. (2006). G-quadruplex formation within the promoter of the KRAS proto-oncogene and its effect on transcription. *Nucleic Acids Res* *34*(9), 2536–49. <https://doi.org/10.1093/nar/gkl286>
- Cogoi, S., Ferino, A., Miglietta, G., Pedersen, E.B., & Xodo, L.E. (2018). The regulatory G4 motif of the Kirsten ras (KRAS) gene is sensitive to guanine oxidation: implications on transcription. *Nucleic Acids Res* *46*(2), 661–676. <https://doi.org/10.1093/nar/gkx1142>
- Corless, S., & Gilbert, N. (2016). Effects of DNA supercoiling on chromatin architecture. *Biophysical reviews*, *8*(Suppl 1), 51–64. <https://doi.org/10.1007/s12551-016-0242-6>

- Corrales L., Matson, V., Flood, B., Spranger, S., & Gajewski, T.F. (2017). Innate immune signaling and regulation in cancer immunotherapy. *Cell Res.* 27(1), 96–108. <https://doi.org/10.1038/cr.2016.149>
- Crabbe, L., Verdun, R. E., Haggblom, C. I., & Karlseder, J. (2004). Defective telomere lagging strand synthesis in cells lacking WRN helicase activity. *Science*, 306(5703), 1951–1953. <https://doi.org/10.1126/science.1103619>
- Cristini, A., Ricci, G., Britton, S., Salimbeni, S., Huang, S. N., Marinello, J., Calsou, P., Pommier, Y., Favre, G., Capranico, G., Gromak, N., & Sordet, O. (2019). Dual Processing of R-Loops and Topoisomerase I Induces Transcription-Dependent DNA Double-Strand Breaks. *Cell reports*, 28(12), 3167–3181.e6. <https://doi.org/10.1016/j.celrep.2019.08.041>
- Crowl, J. T., Gray, E. E., Pestal, K., Volkman, H. E., & Stetson, D. B. (2017). Intracellular Nucleic Acid Detection in Autoimmunity. *Annual review of immunology*, 35, 313–336. <https://doi.org/10.1146/annurev-immunol-051116-052331>
- Davis AJ, Chen DJ. DNA double strand break repair via non-homologous end-joining. *Transl Cancer Res.* 2013 Jun;2(3):130-143. <https://doi:10.3978/j.issn.2218-676X.2013.04.02>.
- D’Arpa, P., Beardmore, C., & Liu, L. F. (1990). Involvement of nucleic acid synthesis in cell killing mechanisms of topoisomerase poisons. *Cancer research*, 50(21), 6919–6924.
- De Magis, A., Manzo, S. G., Russo, M., Marinello, J., Morigi, R., Sordet, O., & Capranico, G. (2019). DNA damage and genome instability by G-quadruplex ligands are mediated by R loops in human cancer cells. *Proceedings of the National Academy of Sciences of the United States of America*, 116(3), 816–825. <https://doi.org/10.1073/pnas.1810409116>
- Decout, A., Katz, J. D., Venkatraman, S., & Ablasser, A. (2021). The cGAS-STING pathway as a therapeutic target in inflammatory diseases. *Nature reviews. Immunology*, 21(9), 548–569. <https://doi.org/10.1038/s41577-021-00524-z>
- Deiana, M., Jamroskovic, J., Obi, I., & Sabouri, N., (2020). Unravelling the cellular emission fingerprint of the benchmark G-quadruplex-interactive compound Phen-DC₃. *Chemical communications*, 56(91), 14251–14254. <https://doi.org/10.1039/d0cc05483f>
- Desai, S. D., Zhang, H., Rodriguez-Bauman, A., Yang, J. M., Wu, X., Gounder, M. K., Rubin, E. H., & Liu, L. F. (2003). Transcription-dependent degradation of topoisomerase I-DNA covalent complexes. *Molecular and cellular biology*, 23(7), 2341–2350. <https://doi.org/10.1128/MCB.23.7.2341-2350.2003>

- Drolet, M., Bi, X., & Liu, L. F. (1994). Hypernegative supercoiling of the DNA template during transcription elongation in vitro. *The Journal of biological chemistry*, 269(3), 2068–2074.
- Drolet, M., Phoenix, P., Menzel, R., Massé, E., Liu, L.F., & Crouch, R.J. (1995). Overexpression of RNase H partially complements the growth defect of an Escherichia coli delta topA mutant: R-loop formation is a major problem in the absence of DNA topoisomerase I. *Proc Natl Acad Sci U S A*. 1995 Apr 11;92(8), 3526–30. <https://doi.org/10.1073/pnas.92.8.3526>
- El-Khamisy, S. F., Saifi, G. M., Weinfeld, M., Johansson, F., Helleday, T., Lupski, J. R., & Caldecott, K. W. (2005). Defective DNA single-strand break repair in spinocerebellar ataxia with axonal neuropathy-1. *Nature*, 434(7029), 108–113. <https://doi.org/10.1038/nature03314>
- El-Khamisy, S.F., Masutani, M., Suzuki, H., & Caldecott, K.W. (2003). A requirement for PARP-1 for the assembly or stability of XRCC1 nuclear foci at sites of oxidative DNA damage. *Nucleic Acids Res* 31, 5526–33. <https://doi.org/10.1093/nar/gkg761>
- Eurostat (2020), *Causes of death statistics*, Statistics explained, September 2020
- Fitzgerald, K. A., McWhirter, S. M., Faia, K. L., Rowe, D. C., Latz, E., Golenbock, D. T., Coyle, A. J., Liao, S. M., & Maniatis, T. (2003). IKKepsilon and TBK1 are essential components of the IRF3 signaling pathway. *Nature immunology*, 4(5), 491–496. <https://doi.org/10.1038/ni921>
- Franklin R. E., and Gosling, R. G. (1953). The structure of sodium thymonucleate fibres I. The influence of water content. *Acta Cryst*, 6 (8), 673–677. <https://doi.org/10.1107/s0365110x53001939>
- Furuta, T., Takemura, H., Liao, Z. Y., Aune, G. J., Redon, C., Sedelnikova, O. A., Pilch, D. R., Rogakou, E. P., Celeste, A., Chen, H. T., Nussenzweig, A., Aladjem, M. I., Bonner, W. M., & Pommier, Y. (2003). Phosphorylation of histone H2AX and activation of Mre11, Rad50, and Nbs1 in response to replication-dependent DNA double-strand breaks induced by mammalian DNA topoisomerase I cleavage complexes. *The Journal of biological chemistry*, 278(22), 20303–20312. <https://doi.org/10.1074/jbc.M300198200>
- Galluzzi, L., Humeau, J., Buqué, A., Zitvogel, L., & Kroemer, G. (2020). Immunostimulation with chemotherapy in the era of immune checkpoint inhibitors. *Nature reviews. Clinical oncology*, 17(12), 725–741. <https://doi.org/10.1038/s41571-020-0413-z>
- Galluzzi, L., Vanpouille-Box, C., Bakhoun, S.F., & Demaria, S. SnapShot: CGAS-STING Signaling. *Cell* 22;173(1), 276–276. <https://doi.org/10.1016/j.cell.2018.03.015>
- Gao, P., Ascano, M., Zillinger, T., Wang, W., Dai, P., Serganov, A. A., Gaffney, B. L., Shuman, S., Jones, R. A., Deng, L., Hartmann, G., Barchet, W., Tuschl, T., & Patel, D. J. (2013).

- Structure-function analysis of STING activation by c[G(2',5')pA(3',5')p] and targeting by *antiviral* DMXAA. *Cell*, 154(4), 748–762. <https://doi.org/10.1016/j.cell.2013.07.023>
- García-Muse, T., & Aguilera, A. (2016). Transcription-replication conflicts: how they occur and how they are resolved. *Nature reviews. Molecular cell biology*, 17(9), 553–563. <https://doi.org/10.1038/nrm.2016.88>
- Gazdar, A. F., Bunn, P. A., & Minna, J. D. (2017). Small-cell lung cancer: what we know, what we need to know and the path forward. *Nature reviews. Cancer*, 17(12), 725–737. <https://doi.org/10.1038/nrc.2017.87>
- Gellert, M., Lipsett, M. N., & Davies, D. R. (1962). Helix formation by guanylic acid. *Proc Natl Acad Sci USA*. 1962 Dec 15;48(12):2013-8. <https://doi.org/10.1073/pnas.48.12.2013>
- Gessner, R. V., Frederick, C. A., Quigley, G. J., Rich, A., & Wang, A. H. (1989). The molecular structure of the left-handed Z-DNA double helix at 1.0-Å atomic resolution. Geometry, conformation, and ionic interactions of d(CGCGCG). *The Journal of biological chemistry*, 264(14), 7921–7935. <https://doi.org/10.2210/pdb1dcg/pdb>
- Ginno, P. A., Lott, P. L., Christensen, H. C., Korf, I., & Chédin, F. (2012). R-loop formation is a distinctive characteristic of unmethylated human CpG island promoters. *Molecular cell*, 45(6), 814–825. <https://doi.org/10.1016/j.molcel.2012.01.017>
- Gómez-González, B., & Aguilera, A. (2007). Activation-induced cytidine deaminase action is strongly stimulated by mutations of the THO complex. *Proceedings of the National Academy of Sciences of the United States of America*, 104(20), 8409–8414. <https://doi.org/10.1073/pnas.0702836104>
- Gonugunta, V.K., Sakai, T., Pokatayev, V., Yang, K., Wu, J., Dobbs, N., & Yan, N. (2017). Trafficking-Mediated STING Degradation Requires Sorting to Acidified Endolysosomes and Can Be Targeted to Enhance Anti-tumor Response. *Cell Rep*. 12;21(11), 3234–3242. <https://doi.org/10.1016/j.celrep.2017.11.061>
- Gorgoulis, V. G., Vassiliou, L. V., Karakaidos, P., Zacharatos, P., Kotsinas, A., Liloglou, T., Venere, M., Ditullio, R. A., Jr, Kastrinakis, N. G., Levy, B., Kletsas, D., Yoneta, A., Herlyn, M., Kittas, C., & Halazonetis, T. D. (2005). Activation of the DNA damage checkpoint and genomic instability in human precancerous lesions. *Nature*, 434(7035), 907–913. <https://doi.org/10.1038/nature03485>
- Gowan, S. M., Harrison, J. R., Patterson, L., Valenti, M., Read, M. A., Neidle, S., & Kelland, L. R. (2002). A G-quadruplex-interactive potent small-molecule inhibitor of telomerase exhibiting in vitro and in vivo antitumor activity. *Molecular pharmacology*, 61(5), 1154–1162. <https://doi.org/10.1124/mol.61.5.1154>
- Gratia, M., Rodero, M. P., Conrad, C., Bou Samra, E., Maurin, M., Rice, G. I., Duffy, D., Revy, P., Petit, F., Dale, R. C., Crow, Y. J., Amor-Gueret, M., & Manel, N. (2019). Bloom syndrome protein restrains innate immune sensing of micronuclei by

- cGAS. *The Journal of experimental medicine*, 216(5), 1199–1213. <https://doi.org/10.1084/jem.20181329>
- Grogan, D.W. (1998), Hyperthermophiles and the problem of DNA instability. *Molecular Microbiology*, 28: 1043-1049. <https://doi.org/10.1046/j.1365-2958.1998.00853.x>
- Gui, X., Yang, H., Li, T., Tan, X., Shi, P., Li, M., Du, F., & Chen, Z. J. (2019). Autophagy induction via STING trafficking is a primordial function of the cGAS pathway. *Nature*, 567(7747), 262–266. <https://doi.org/10.1038/s41586-019-1006-9>
- Haag, S. M., Gulen, M. F., Reymond, L., Gibelin, A., Abrami, L., Decout, A., Heymann, M., van der Goot, F. G., Turcatti, G., Behrendt, R., & Ablasser, A. (2018). Targeting STING with covalent small-molecule inhibitors. *Nature*, 559(7713), 269–273. <https://doi.org/10.1038/s41586-018-0287-8>
- Haider, S.M., Neidle, S., & Parkinson, G.N. (2011). A structural analysis of G-quadruplex/ligand interactions. *Biochimie* 93(8), 1239–51. <https://doi.org/10.1016/j.biochi.2011.05.012>
- Hamperl, S., & Cimprich, K.A. (2014). The contribution of co-transcriptional RNA:DNA hybrid structures to DNA damage and genome instability. *DNA Repair* 19, 84–94. <https://doi.org/10.1016/j.dnarep.2014.03.023>
- Hamperl, S., Bocek, M. J., Saldivar, J. C., Swigut, T., & Cimprich, K. A. (2017). Transcription-Replication Conflict Orientation Modulates R-Loop Levels and Activates Distinct DNA Damage Responses. *Cell*, 170(4), 774–786.e19. <https://doi.org/10.1016/j.cell.2017.07.043>.
- Hänsel-Hertsch, R., Beraldi, D., Lensing, S. V., Marsico, G., Zyner, K., Parry, A., Di Antonio, M., Pike, J., Kimura, H., Narita, M., Tannahill, D., & Balasubramanian, S. (2016). G-quadruplex structures mark human regulatory chromatin. *Nature genetics*, 48(10), 1267–1272. <https://doi.org/10.1038/ng.3662>
- Harding, S. M., Benci, J. L., Irianto, J., Discher, D. E., Minn, A. J., & Greenberg, R. A. (2017). Mitotic progression following DNA damage enables pattern recognition within micronuclei. *Nature*, 548(7668), 466–470. <https://doi.org/10.1038/nature23470>
- Hartwell, D., Jones, J., Loveman, E., Harris, P., Clegg, A., & Bird, A. (2011). Topotecan for relapsed small cell lung cancer: a systematic review and economic evaluation. *Cancer treatment reviews*, 37(3), 242–249. <https://doi.org/10.1016/j.ctrv.2010.07.005>
- Hatch E.M., Fischer, A.H., Deerinck, T.J., Hetzer, M.W. Catastrophic nuclear envelope collapse in cancer cell micronuclei. *Cell*. 2013 Jul 3;154(1):47-60. <https://doi.org/10.1016/j.cell.2013.06.007>
- Heijink, A. M., Talens, F., Jae, L. T., van Gijn, S. E., Fehrmann, R., Brummelkamp, T. R., & van Vugt, M. (2019). BRCA2 deficiency instigates cGAS-mediated inflammatory

- signaling and confers sensitivity to tumor necrosis factor-alpha-mediated cytotoxicity. *Nature communications*, 10(1), 100. <https://doi.org/10.1038/s41467-018-07927-y>
- Holmström, M., & Winters, V. (1992). Micronucleus induction by camptothecin and amsacrine in bone marrow of male and female CD-1 mice. *Mutagenesis*, 7(3), 189–193. <https://doi.org/10.1093/mutage/7.3.189>
- Hoogsteen, K. (1962). The crystal and molecular structure of a hydrogen-bonded complex between 1-methylthymine and 9-methyladenine. *Acta Crystal.*, 16, 907-916. <https://doi.org/10.1107/S0365110X63002437>
- Hopfner, K. P., & Hornung, V. (2020). Molecular mechanisms and cellular functions of cGAS-STING signalling. *Nature reviews. Molecular cell biology*, 21(9), 501–521. <https://doi.org/10.1038/s41580-020-0244-x>
- Hou, Y., Gan, T., Fang, T., Zhao, Y., Luo, Q., Liu, X., Qi, L., Zhang, Y., Jia, F., Han, J., Li, S., Wang, S., & Wang, F. (2022). G-quadruplex inducer/stabilizer pyridostatin targets SUB1 to promote cytotoxicity of a transplatinum complex. *Nucleic acids research*, 50(6), 3070–3082. <https://doi.org/10.1093/nar/gkac151>
- Huertas, P., & Aguilera, A. (2003). Cotranscriptionally formed DNA:RNA hybrids mediate transcription elongation impairment and transcription-associated recombination. *Molecular cell*, 12(3), 711–721. <https://doi.org/10.1016/j.molcel.2003.08.010>
- Ishikawa, H., Ma, Z., & Barber, G. N. (2009). STING regulates intracellular DNA-mediated, type I interferon-dependent innate immunity. *Nature*, 461(7265), 788–792. <https://doi.org/10.1038/nature08476>
- Jahchan, N. S., Lim, J. S., Bola, B., Morris, K., Seitz, G., Tran, K. Q., Xu, L., Trapani, F., Morrow, C. J., Cristea, S., Coles, G. L., Yang, D., Vaka, D., Kareta, M. S., George, J., Mazur, P. K., Nguyen, T., Anderson, W. C., Dylla, S. J., Blackhall, F., ... Sage, J. (2016). Identification and Targeting of Long-Term Tumor-Propagating Cells in Small Cell Lung Cancer. *Cell reports*, 16(3), 644–656. <https://doi.org/10.1016/j.celrep.2016.06.021>
- Jakobsen, A. K., Yuusufi, S., Madsen, L. B., Meldgaard, P., Knudsen, B. R., & Stougaard, M. (2022). TDP1 and TOP1 as targets in anticancer treatment of NSCLC: Activity and protein level in normal and tumor tissue from 150 NSCLC patients correlated to clinical data. *Lung cancer*, 164, 23–32. <https://doi.org/10.1016/j.lungcan.2021.12.010>
- Khoo, L. T., & Chen, L. Y. (2018). Role of the cGAS-STING pathway in cancer development and oncotherapeutic approaches. *EMBO reports*, 19(12), e46935. <https://doi.org/10.15252/embr.201846935>

- Kim, H. G., Reddoch, J. F., Mayfield, C., Ebbinghaus, S., Vigneswaran, N., Thomas, S., Jones, D. E., Jr, & Miller, D. M. (1998). Inhibition of transcription of the human c-myc protooncogene by intermolecular triplex. *Biochemistry*, 37(8), 2299–2304. <https://doi.org/10.1021/bi9718191>
- Kim, N. (2019). The Interplay between G-quadruplex and Transcription. *Curr Med Chem* 26(16), 2898-2917. <https://doi.org/10.2174/0929867325666171229132619>
- Kitai, Y., Kawasaki, T., Sueyoshi, T., Kobiyama, K., Ishii, K. J., Zou, J., Akira, S., Matsuda, T., & Kawai, T. (2017). DNA-Containing Exosomes Derived from Cancer Cells Treated with Topotecan Activate a STING-Dependent Pathway and Reinforce Antitumor Immunity. *Journal of immunology*, 198(4), 1649–1659. <https://doi.org/10.4049/jimmunol.1601694>
- Koster, D. A., Croquette, V., Dekker, C., Shuman, S., & Dekker, N. H. (2005). Friction and torque govern the relaxation of DNA supercoils by eukaryotic topoisomerase IB. *Nature*, 434(7033), 671–674. <https://doi.org/10.1038/nature03395>
- Lee, H.T., Bose, A., Lee, C.Y., Opresko, P.L., & Myong, S. (2017). Molecular mechanisms by which oxidative DNA damage promotes telomerase activity. *Nucleic Acids Res* 45(20), 11752–11765. <https://doi.org/10.1093/nar/gkx789>
- Lerner, L.K., & Sale, J.E. (2019). Replication of G Quadruplex DNA. *Genes* 10(2), 95. <https://doi.org/10.3390/genes10020095>
- Li, X., Shu, C., Yi, G., Chaton, C. T., Shelton, C. L., Diao, J., Zuo, X., Kao, C. C., Herr, A. B., & Li, P. (2013). Cyclic GMP-AMP synthase is activated by double-stranded DNA-induced oligomerization. *Immunity*, 39(6), 1019–1031. <https://doi.org/10.1016/j.immuni.2013.10.019>
- Liu, C., Zhou, S., Begum, S., Sidransky, D., Westra, W. H., Brock, M., & Califano, J. A. (2007). Increased expression and activity of repair genes TDP1 and XPF in non-small cell lung cancer. *Lung cancer*, 55(3), 303–311. <https://doi.org/10.1016/j.lungcan.2006.10.019>
- Liu, H.Y., Zhao, Q., Zhang, T.P., Wu, Y., Xiong, Y.X., Wang, S.K., Ge, Y.L., He, J.H., Lv, P., Ou, T.M., Tan, J.H., Li, D., Gu, L.Q., Ren, J., Zhao, Y., & Huang, Z.S. (2016). Conformation Selective Antibody Enables Genome Profiling and Leads to Discovery of Parallel G-Quadruplex in Human Telomeres. *Cell Chem Biol* 23(10), 1261-1270. <https://doi.org/10.1016/j.chembiol.2016.08.013>
- Liu, L.F., & Wang, J.C. (1987). Supercoiling of the DNA template during transcription. *Proc Natl Acad Sci USA* 84(20), 7024–7027. <https://doi.org/10.1073/pnas.84.20.7024>
- Liu, S., Cai, X., Wu, J., Cong, Q., Chen, X., Li, T., Du, F., Ren, J., Wu, Y. T., Grishin, N. V., & Chen, Z. J. (2015). Phosphorylation of innate immune adaptor proteins MAVS, STING, and TRIF induces IRF3 activation. *Science* 347(6227). <https://doi.org/10.1126/science.aaa2630>

- Liu, Y., Nielsen, C. F., Yao, Q., & Hickson, I. D. (2014). The origins and processing of ultra fine anaphase DNA bridges. *Current opinion in genetics & development*, *26*, 1–5. <https://doi.org/10.1016/j.gde.2014.03.003>
- Mackenzie, K. J., Carroll, P., Martin, C. A., Murina, O., Fluteau, A., Simpson, D. J., Olova, N., Sutcliffe, H., Rainger, J. K., Leitch, A., Osborn, R. T., Wheeler, A. P., Nowotny, M., Gilbert, N., Chandra, T., Reijns, M., & Jackson, A. P. (2017). cGAS surveillance of micronuclei links genome instability to innate immunity. *Nature*, *548*(7668), 461–465. <https://doi.org/10.1038/nature23449>
- Maffia, A., Ranise, C., & Sabbioneda, S. (2020). From R-Loops to G-Quadruplexes: Emerging New Threats for the Replication Fork. *International journal of molecular sciences*, *21*(4), 1506. <https://doi.org/10.3390/ijms21041506>
- Manzo, S. G., Hartono, S. R., Sanz, L. A., Marinello, J., De Biasi, S., Cossarizza, A., Capranico, G., & Chedin, F. (2018). DNA Topoisomerase I differentially modulates R-loops across the human genome. *Genome biology*, *19*(1), 100. <https://doi.org/10.1186/s13059-018-1478-1>
- Marinello, J., Arleo, A., Russo, M., Delcuratolo, M., Ciccarelli, F., Pommier, Y., & Capranico, G. (2022). Topoisomerase I poison-triggered immune gene activation is markedly reduced in human small-cell lung cancers by impairment of the cGAS/STING pathway. *British journal of cancer*, *127*(7), 1214–1225. <https://doi.org/10.1038/s41416-022-01894-4>
- Marinello, J., Chillemi, G., Bueno, S., Manzo, S. G., & Capranico, G. (2013). Antisense transcripts enhanced by camptothecin at divergent CpG-island promoters associated with bursts of topoisomerase I-DNA cleavage complex and R-loop formation. *Nucleic acids research*, *41*(22), 10110–10123. <https://doi.org/10.1093/nar/gkt778>
- Marsico, G., Chambers, V.S., Sahakyan, A.B., McCauley, P., Boutell, J.M., Antonio, M.D., & Balasubramanian, S. (2019). Whole genome experimental maps of DNA G-quadruplexes in multiple species. *Nucleic Acids Res* *47*(8), 3862–3874. <https://doi.org/10.1093/nar/gkz179>
- Martino, E., Della Volpe, S., Terribile, E., Benetti, E., Sakaj, M., Centamore, A., Sala, A., & Collina, S. (2017). The long story of camptothecin: From traditional medicine to drugs. *Bioorganic & medicinal chemistry letters*, *27*(4), 701–707. <https://doi.org/10.1016/j.bmcl.2016.12.085>
- Marzano, S., Miglietta, G., Morigi, R., Marinello, J., Arleo, A., Procacci, M., Locatelli, A., Leoni, A., Pagano, B., Randazzo, A., Amato, J., & Capranico, G. (2022). Balancing Affinity, Selectivity, and Cytotoxicity of Hydrazone-Based G-Quadruplex Ligands for Activation of Interferon β Genes in Cancer Cells. *Journal of medicinal chemistry*, *65*(18), 12055–12067. <https://doi.org/10.1021/acs.jmedchem.2c00772>

- Massé, E., Phoenix, P., & Drolet, M. (1997). DNA topoisomerases regulate R-loop formation during transcription of the *rrnB* operon in *Escherichia coli*. *The Journal of biological chemistry*, 272(19), 12816–12823. <https://doi.org/10.1074/jbc.272.19.12816>
- Masukata, H., & Tomizawa, J. (1984). Effects of point mutations on formation and structure of the RNA primer for ColE1 DNA replication. *Cell*, 36(2), 513–522. [https://doi.org/10.1016/0092-8674\(84\)90244-7](https://doi.org/10.1016/0092-8674(84)90244-7)
- McLuckie, K.I., Di Antonio, M., Zecchini, H., Xian, J., Caldas, C., Krippendorff, B.F., Tannahill, D., Lowe, C., & Balasubramanian, S. (2013). G-quadruplex DNA as a molecular target for induced synthetic lethality in cancer cells. *J Am Chem Soc* 135(26), 9640–3. <https://doi.org/10.1021/ja404868t>
- Miao, Z. H., Agama, K., Sordet, O., Povirk, L., Kohn, K. W., & Pommier, Y. (2006). Hereditary ataxia SCAN1 cells are defective for the repair of transcription-dependent topoisomerase I cleavage complexes. *DNA repair*, 5(12), 1489–1494. <https://doi.org/10.1016/j.dnarep.2006.07.004>
- Miao, Z. H., Player, A., Shankavaram, U., Wang, Y. H., Zimonjic, D. B., Lorenzi, P. L., Liao, Z. Y., Liu, H., Shimura, T., Zhang, H. L., Meng, L. H., Zhang, Y. W., Kawasaki, E. S., Popescu, N. C., Aladjem, M. I., Goldstein, D. J., Weinstein, J. N., & Pommier, Y. (2007). Nonclassic functions of human topoisomerase I: genome-wide and pharmacologic analyses. *Cancer research*, 67(18), 8752–8761. <https://doi.org/10.1158/0008-5472.CAN-06-4554>
- Miglietta, G., Marinello, J., Russo, M., & Capranico, G. (2022). Ligands stimulating antitumour immunity as the next G-quadruplex challenge. *Mol Cancer* 21(1), 180. <https://doi.org/10.1186/s12943-022-01649-y>
- Miglietta, G., Russo, M., & Capranico, G. (2020). G-quadruplex-R-loop interactions and the mechanism of anticancer G-quadruplex binders. *Nucleic acids research*, 48(21), 11942–11957. <https://doi.org/10.1093/nar/gkaa944>
- Miglietta, G., Russo, M., Duardo, R. C., & Capranico, G. (2021). G-quadruplex binders as cytostatic modulators of innate immune genes in cancer cells. *Nucleic acids research*, 49(12), 6673–6686. <https://doi.org/10.1093/nar/gkab500>
- Mordes, D. A., Glick, G. G., Zhao, R., and Cortez, D. (2008). TopBP1 activates ATR through ATRIP and a PIKK regulatory domain. *Genes Dev.* 22, 1478–1489. <https://doi.org/10.1101/gad.1666208>
- Moye, A.L., Porter, K.C., Cohen, S.B., Phan, T., Zyner, K.G., Sasaki, N., Lovrecz, G.O., Beck, J.L., Bryan, T.M. (2015). Telomeric G-quadruplexes are a substrate and site of localization for human telomerase. *Nat Commun* 9(6), 7643. <https://doi.org/10.1038/ncomms8643>

- Muers M. (2011). Mutation: the perils of transcription. *Nature reviews. Genetics*, 12(3), 156. <https://doi.org/10.1038/nrg2960>
- Murphy, S.L., Kochanek, K.D., Xu, J., & Arias, E. (2021). Mortality in the United States, 2020. *NCHS Data Brief* 427, 1–8.
- Naumann, R. W., & Coleman, R. L. (2011). Management strategies for recurrent platinum-resistant ovarian cancer. *Drugs*, 71(11), 1397–1412. <https://doi.org/10.2165/11591720-000000000-00000>
- Ohle, C., Tesorero, R., Schermann, G., Dobrev, N., Sinning, I., & Fischer, T. (2016). Transient RNA-DNA Hybrids Are Required for Efficient Double-Strand Break Repair. *Cell*, 167(4), 1001–1013.e7. <https://doi.org/10.1016/j.cell.2016.10.001>
- Olmos, Y., Perdrix-Rosell, A., & Carlton, J. G. (2016). Membrane Binding by CHMP7 Coordinates ESCRT-III-Dependent Nuclear Envelope Reformation. *Current biology: CB*, 26(19), 2635–2641. <https://doi.org/10.1016/j.cub.2016.07.039>
- Paeschke, K., Juranek, S., Simonsson, T., Hempel, A., Rhodes, D., & Lipps, H.J. (2008). Telomerase recruitment by the telomere end binding protein-beta facilitates G-quadruplex DNA unfolding in ciliates. *Nat Struct Mol Biol*. 15(6), 598–604. <https://doi.org/10.1038/nsmb.1422>
- Palecek E. (1991). Local supercoil-stabilized DNA structures. *Critical reviews in biochemistry and molecular biology*, 26(2), 151–226. <https://doi.org/10.3109/10409239109081126>
- Phoenix, P., Raymond, M. A., Massé, E., & Drolet, M. (1997). Roles of DNA topoisomerases in the regulation of R-loop formation in vitro. *The Journal of biological chemistry*, 272(3), 1473–1479. <https://doi.org/10.1074/jbc.272.3.1473>
- Pilger, D., Seymour, L. W., & Jackson, S. P. (2021). Interfaces between cellular responses to DNA damage and cancer immunotherapy. *Genes & development*, 35(9-10), 602–618. <https://doi.org/10.1101/gad.348314.121>
- Pladevall-Morera, D., Munk, S., Ingham, A., Garribba, L., Albers, E., Liu, Y., Olsen, J. V., & Lopez-Contreras, A. J. (2019). Proteomic characterization of chromosomal common fragile site (CFS)-associated proteins uncovers ATRX as a regulator of CFS stability. *Nucleic acids research*, 47(15), 8004–8018. <https://doi.org/10.1093/nar/gkz510>
- Poirier, J. T., Gardner, E. E., Connis, N., Moreira, A. L., de Stanchina, E., Hann, C. L., & Rudin, C. M. (2015). DNA methylation in small cell lung cancer defines distinct disease subtypes and correlates with high expression of EZH2. *Oncogene*, 34(48), 5869–5878. <https://doi.org/10.1038/onc.2015.38>
- Pommier, Y. (2006). Topoisomerase I inhibitors: camptothecins and beyond. *Nature reviews. Cancer*, 6(10), 789–802. <https://doi.org/10.1038/nrc1977>

- Pommier, Y. (2013). Drugging topoisomerases: lessons and challenges. *ACS chemical biology* 8(1), 82-95. <https://doi.org/10.1021/cb300648v>
- Pommier, Y., & Cushman, M. (2009). The indenoisoquinoline noncamptothecin topoisomerase I inhibitors: update and perspectives. *Molecular cancer therapeutics*, 8(5), 1008–1014. <https://doi.org/10.1158/1535-7163.MCT-08-0706>
- Pommier, Y., Leo, E., Zhang, H., & Marchand, C. (2010). DNA topoisomerases and their poisoning by anticancer and antibacterial drugs. *Chemistry & biology*, 17(5), 421–433. <https://doi.org/10.1016/j.chembiol.2010.04.012>
- Pommier, Y., Sun, Y., Huang, S. N., & Nitiss, J. L. (2016). Roles of eukaryotic topoisomerases in transcription, replication and genomic stability. *Nature reviews. Molecular cell biology*, 17(11), 703–721. <https://doi.org/10.1038/nrm.2016.111>
- Raab, M., Gentili, M., de Belly, H., Thiam, H.R., Vargas, P., Jimenez, A.J., Lautenschlaeger, F., Voituriez, R., Lennon-Duménil, A.M., Manel, N., Piel, M. ESCRT III repairs nuclear envelope ruptures during cell migration to limit DNA damage and cell death. *Science*. 2016 Apr 15;352(6283):359-62. <https://doi.org/10.1126/science.aad7611>
- Ratmeyer, L., Vinayak, R., Zhong, Y. Y., Zon, G., & Wilson, W. D. (1994). Sequence specific thermodynamic and structural properties for DNA.RNA duplexes. *Biochemistry*, 33(17), 5298–5304. <https://doi.org/10.1021/bi00183a037>
- Reaban, M. E., Lebowitz, J., & Griffin, J. A. (1994). Transcription induces the formation of a stable RNA.DNA hybrid in the immunoglobulin alpha switch region. *The Journal of biological chemistry*, 269(34), 21850–21857.
- Richardson J. P. (1975). Attachment of nascent RNA molecules to superhelical DNA. *Journal of molecular biology*, 98(3), 565–579. [https://doi.org/10.1016/s0022-2836\(75\)80087-8](https://doi.org/10.1016/s0022-2836(75)80087-8)
- Roberts R. W., and Crothers D. M., (1992). Stability and properties of double and triple helices: dramatic effects of RNA or DNA backbone composition. *Science*, 258 (5087), 1463-1466. <https://doi:10.1126/science.1279808>
- Robijns, J., Molenberghs, F., Sieprath, T., Corne, T. D., Verschuuren, M., & De Vos, W. H. (2016). In silico synchronization reveals regulators of nuclear ruptures in lamin A/C deficient model cells. *Scientific reports*, 6, 30325. <https://doi.org/10.1038/srep30325>
- Roca, J. (2009). Topoisomerase II: a fitted mechanism for the chromatin landscape, *Nucleic Acids Research* 37(3), 721–730. <https://doi.org/10.1093/nar/gkn994>
- Rodgers, K. & McVey, M. (2016). Error-Prone Repair of DNA Double-Strand Breaks. *J Cell Physiol*. 231(1), 15-24. <https://doi.org/10.1002/jcp.25053>
- Rodriguez, R., Miller, K. M., Forment, J. V., Bradshaw, C. R., Nikan, M., Britton, S., Oelschlaegel, T., Xhemalce, B., Balasubramanian, S., & Jackson, S. P. (2012). Small-

- molecule-induced DNA damage identifies alternative DNA structures in human genes. *Nature chemical biology*, 8(3), 301–310. <https://doi.org/10.1038/nchembio.780>
- Rodriguez, R., Müller, S., Yeoman, J. A., Trentesaux, C., Riou, J. F., & Balasubramanian, S. (2008). A novel small molecule that alters shelterin integrity and triggers a DNA-damage response at telomeres. *Journal of the American Chemical Society*, 130(47), 15758–15759. <https://doi.org/10.1021/ja805615w>
- Rodriguez-Nieto, S., & Sanchez-Cespedes, M. (2009). BRG1 and LKB1: tales of two tumor suppressor genes on chromosome 19p and lung cancer. *Carcinogenesis*, 30(4), 547–554. <https://doi.org/10.1093/carcin/bgp035>
- Rogakou, E. P., Nieves-Neira, W., Boon, C., Pommier, Y., & Bonner, W. M. (2000). Initiation of DNA fragmentation during apoptosis induces phosphorylation of H2AX histone at serine 139. *The Journal of biological chemistry*, 275(13), 9390–9395. <https://doi.org/10.1074/jbc.275.13.9390>
- Rohs, R., Jin, X., West, S. M., Joshi, R., Honig, B., & Mann, R. S. (2010). Origins of specificity in protein-DNA recognition. *Annual review of biochemistry*, 79, 233–269. <https://doi.org/10.1146/annurev-biochem-060408-091030>
- Roy, D., & Lieber, M. R. (2009). G clustering is important for the initiation of transcription-induced R-loops in vitro, whereas high G density without clustering is sufficient thereafter. *Molecular and cellular biology*, 29(11), 3124–3133. <https://doi.org/10.1128/MCB.00139-09>
- Rudin, C. M. & Poirier, J. T. (2017). Small-cell lung cancer in 2016: shining light on novel targets and therapies. *Nat. Rev. Clin. Oncol.* 14, 75–76. <https://doi.org/10.1038/nrclinonc.2016.203>
- Rudin, C. M., Durinck, S., Stawiski, E. W., Poirier, J. T., Modrusan, Z., Shames, D. S., Bergbower, E. A., Guan, Y., Shin, J., Guillory, J., Rivers, C. S., Foo, C. K., Bhatt, D., Stinson, J., Gnad, F., Haverty, P. M., Gentleman, R., Chaudhuri, S., Janakiraman, V., Jaiswal, B. S., ... Seshagiri, S. (2012). Comprehensive genomic analysis identifies SOX2 as a frequently amplified gene in small-cell lung cancer. *Nature genetics*, 44(10), 1111–1116. <https://doi.org/10.1038/ng.2405>
- Ruggiero, E., & Richter, S.N. (2018). G-quadruplexes and G-quadruplex ligands: targets and tools in antiviral therapy. *Nucleic Acids Res* 46(7), 3270–3283. <https://doi.org/10.1093/nar/gky187>
- Salvati, E., Scarsella, M., Porru, M., Rizzo, A., Iachettini, S., Tentori, L., Graziani, G., D'Incalci, M., Stevens, M.F., Orlandi, A., Passeri, D., Gilson, E., Zupi, G., Leonetti, C., & Biroccio, A. (2010). PARP1 is activated at telomeres upon G4 stabilization: possible

- target for telomere-based therapy. *Oncogene* 29(47), 6280–93. <https://doi.org/10.1038/onc.2010.344>
- Santos-Pereira, J. M., & Aguilera, A. (2015). R loops: new modulators of genome dynamics and function. *Nature reviews. Genetics*, 16(10), 583–597. <https://doi.org/10.1038/nrg3961>
- Sanz, L.A., & Chédin, F. (2019). High-resolution, strand-specific R-loop mapping via S9.6-based DNA-RNA immunoprecipitation and high-throughput sequencing. *Nat Protoc*. 14(6), 1734-1755. <https://doi.org/10.1038/s41596-019-0159-1>
- Schneider, W. M., Chevillotte, M. D., & Rice, C. M. (2014). Interferon-stimulated genes: a complex web of host defenses. *Annual review of immunology*, 32, 513–545. <https://doi.org/10.1146/annurev-immunol-032713-120231>
- Semenova, E. A., Nagel, R., & Berns, A. (2015). Origins, genetic landscape, and emerging therapies of small cell lung cancer. *Genes & development*, 29(14), 1447–1462. <https://doi.org/10.1101/gad.263145.115>
- Sen, T., Rodriguez, B. L., Chen, L., Corte, C. M. D., Morikawa, N., Fujimoto, J., Cristea, S., Nguyen, T., Diao, L., Li, L., Fan, Y., Yang, Y., Wang, J., Glisson, B. S., Wistuba, I. I., Sage, J., Heymach, J. V., Gibbons, D. L., & Byers, L. A. (2019). Targeting DNA Damage Response Promotes Antitumor Immunity through STING-Mediated T-cell Activation in Small Cell Lung Cancer. *Cancer discovery*, 9(5), 646–661. <https://doi.org/10.1158/2159-8290.CD-18-1020>
- Shao, R. G., Cao, C. X., Zhang, H., Kohn, K. W., Wold, M. S., & Pommier, Y. (1999). Replication-mediated DNA damage by camptothecin induces phosphorylation of RPA by DNA-dependent protein kinase and dissociates RPA:DNA-PK complexes. *The EMBO journal*, 18(5), 1397–1406. <https://doi.org/10.1093/emboj/18.5.1397>
- Shelby M. D. (1988). The genetic toxicity of human carcinogens and its implications. *Mutation research*, 204(1), 3–15. [https://doi.org/10.1016/0165-1218\(88\)90113-9](https://doi.org/10.1016/0165-1218(88)90113-9)
- Shivapurkar, N., Reddy, J., Matta, H., Sathyanarayana, U. G., Huang, C. X., Toyooka, S., Minna, J. D., Chaudhary, P. M., & Gazdar, A. F. (2002). Loss of expression of death-inducing signaling complex (DISC) components in lung cancer cell lines and the influence of MYC amplification. *Oncogene*, 21(55), 8510–8514. <https://doi.org/10.1038/sj.onc.1205941>
- Siddiqui-Jain, A., Grand, C. L., Bearss, D. J., & Hurley, L. H. (2002). Direct evidence for a G-quadruplex in a promoter region and its targeting with a small molecule to repress c-MYC transcription. *Proceedings of the National Academy of Sciences of the United States of America*, 99(18), 11593–11598. <https://doi.org/10.1073/pnas.182256799>

- Skourti-Stathaki, K., Proudfoot, N. J., & Gromak, N. (2011). Human senataxin resolves RNA/DNA hybrids formed at transcriptional pause sites to promote Xrn2-dependent termination. *Molecular cell*, 42(6), 794–805. <https://doi.org/10.1016/j.molcel.2011.04.026>
- Sollier, J., & Cimprich, K. A. (2015). Breaking bad: R-loops and genome integrity. *Trends in cell biology*, 25(9), 514–522. <https://doi.org/10.1016/j.tcb.2015.05.003>
- Sollier, J., Stork, C. T., García-Rubio, M. L., Paulsen, R. D., Aguilera, A., & Cimprich, K. A. (2014). Transcription-coupled nucleotide excision repair factors promote R-loop-induced genome instability. *Molecular cell*, 56(6), 777–785. <https://doi.org/10.1016/j.molcel.2014.10.020>
- Sordet, O., Redon, C.E., Guirouilh-Barbat, J., Smith, S., Solier, S., Douarre, C., Conti, C., Nakamura, A.J., Das, B.B., Nicolas, E., Kohn, K.W., Bonner, W.M., & Pommier, Y. (2009). Ataxia telangiectasia mutated activation by transcription- and topoisomerase I-induced DNA double-strand breaks. *EMBO Rep* 10(8), 887–93. <https://doi.org/10.1038/embor.2009.97>
- Soret, J., Gabut, M., Dupon, C., Kohlhagen, G., Stévenin, J., Pommier, Y., & Tazi, J. (2003). Altered serine/arginine-rich protein phosphorylation and exonic enhancer-dependent splicing in Mammalian cells lacking topoisomerase I. *Cancer research*, 63(23), 8203–8211.
- Sparapani, S., Bellini, S., Gunaratnam, M., Haider, S. M., Andreani, A., Rambaldi, M., Locatelli, A., Morigi, R., Granaiola, M., Varoli, L., Burnelli, S., Leoni, A., & Neidle, S. (2010). Bis-guanylhydrazone diimidazo[1,2-a:1,2-c]pyrimidine as a novel and specific G-quadruplex binding motif. *Chemical communications (Cambridge, England)*, 46(31), 5680–5682. <https://doi.org/10.1039/c0cc00020e>
- Stewart, A. C., Tong, P., Cardnell, R. J., Sen, T., Li, L., Gay, C. M., Masrourpour, F., Fan, Y., Bara, R. O., Feng, Y., Ru, Y., Fujimoto, J., Kundu, S. T., Post, L. E., Yu, K., Shen, Y., Glisson, B. S., Wistuba, I., Heymach, J. V., Gibbons, D. L., ... Byers, L. A. (2017). Dynamic variations in epithelial-to-mesenchymal transition (EMT), ATM, and SLFN11 govern response to PARP inhibitors and cisplatin in small cell lung cancer. *Oncotarget*, 8(17), 28575–28587. <https://doi.org/10.18632/oncotarget.15338>
- Stewart, L., Redinbo, M. R., Qiu, X., Hol, W. G., & Champoux, J. J. (1998). A model for the mechanism of human topoisomerase I. *Science (New York, N.Y.)*, 279(5356), 1534–1541. <https://doi.org/10.1126/science.279.5356.1534>
- Su, T., Zhang, Y., Valerie, K., Wang, X. Y., Lin, S., & Zhu, G. (2019). STING activation in cancer immunotherapy. *Theranostics*, 9(25), 7759–7771. <https://doi.org/10.7150/thno.37574>

- Sun, D., Thompson, B., Cathers, B. E., Salazar, M., Kerwin, S. M., Trent, J. O., Jenkins, T. C., Neidle, S., & Hurley, L. H. (1997). Inhibition of human telomerase by a G-quadruplex-interactive compound. *Journal of medicinal chemistry*, *40*(14), 2113–2116. <https://doi.org/10.1021/jm970199z>
- Sun, S., Schiller, J. H., & Gazdar, A. F. (2007). Lung cancer in never smokers--a different disease. *Nature reviews. Cancer*, *7*(10), 778–790. <https://doi.org/10.1038/nrc2190>
- Sung, P., & Klein, H. (2006). Mechanism of homologous recombination: mediators and helicases take on regulatory functions. *Nature reviews. Molecular cell biology*, *7*(10), 739–750. <https://doi.org/10.1038/nrm2008>
- Takebayashi, Y., Pourquier, P., Zimonjic, D. B., Nakayama, K., Emmert, S., Ueda, T., Urasaki, Y., Kanzaki, A., Akiyama, S. I., Popescu, N., Kraemer, K. H., & Pommier, Y. (2001). Antiproliferative activity of ecteinascidin 743 is dependent upon transcription-coupled nucleotide-excision repair. *Nature medicine*, *7*(8), 961–966. <https://doi.org/10.1038/91008>
- Takemura, H., Rao, V. A., Sordet, O., Furuta, T., Miao, Z. H., Meng, L., Zhang, H., & Pommier, Y. (2006). Defective Mre11-dependent activation of Chk2 by ataxia telangiectasia mutated in colorectal carcinoma cells in response to replication-dependent DNA double strand breaks. *The Journal of biological chemistry*, *281*(41), 30814–30823. <https://doi.org/10.1074/jbc.M603747200>
- Takeuchi, O., & Akira, S. (2010). Pattern recognition receptors and inflammation. *Cell*, *140*(6), 805–820. <https://doi.org/10.1016/j.cell.2010.01.022>
- Tan, J. & Lan, L. (2020). The DNA secondary structures at telomeres and genome instability. *Cell Biosci* *10*, 47. <https://doi.org/10.1186/s13578-020-00409-z>
- Thomas, A., & Pommier, Y. (2016). Small cell lung cancer: Time to revisit DNA-damaging chemotherapy. *Science translational medicine*, *8*(346), 346fs12. <https://doi.org/10.1126/scitranslmed.aaf6282>
- Todd, A. K., Johnston, M., & Neidle, S. (2005). Highly prevalent putative quadruplex sequence motifs in human DNA. *Nucleic acids research*, *33*(9), 2901–2907. <https://doi.org/10.1093/nar/gki553>
- Tu, J., Duan, M., Liu, W., Lu, N., Zhou, Y., Sun, X., & Lu, Z. (2021). Direct genome-wide identification of G-quadruplex structures by whole-genome resequencing. *Nature communications*, *12*(1), 6014. <https://doi.org/10.1038/s41467-021-26312-w>
- Tuduri, S., Crabbé, L., Conti, C., Tourrière, H., Holtgreve-Grez, H., Jauch, A., Pantesco, V., De Vos, J., Thomas, A., Theillet, C., Pommier, Y., Tazi, J., Coquelle, A., & Pasero, P. (2009). Topoisomerase I suppresses genomic instability by preventing interference between replication and transcription. *Nature cell biology*, *11*(11), 1315–1324. <https://doi.org/10.1038/ncb1984>

- Van Cutsem, E., Verslype, C., & Demedts, I. (2002). The treatment of advanced colorectal cancer: where are we now and where do we go?. Best practice & research. *Clinical gastroenterology*, 16(2), 319–330. <https://doi.org/10.1053/bega.2002.0288>
- Van Wietmarschen, N., Merzouk, S., Halsema, N., Spierings, D. C. J., Guryev, V., & Lansdorp, P. M. (2018). BLM helicase suppresses recombination at G-quadruplex motifs in transcribed genes. *Nature communications*, 9(1), 271. <https://doi.org/10.1038/s41467-017-02760-1>
- Varshney, D., Spiegel, J., Zyner, K., Tannahill, D., & Balasubramanian, S. (2020). The regulation and functions of DNA and RNA G-quadruplexes. *Nature reviews. Molecular cell biology*, 21(8), 459–474. <https://doi.org/10.1038/s41580-020-0236-x>
- Vashi, N., & Bakhoun, S. F. (2021). The Evolution of STING Signaling and Its Involvement in Cancer. *Trends in biochemical sciences*, 46(6), 446–460. <https://doi.org/10.1016/j.tibs.2020.12.010>
- Venepureddy, A., Atallah, J. P., & Terjanian, T. (2015). Role of Topotecan in Non-Small Cell Lung Cancer: A Review of Literature. *World journal of oncology*, 6(5), 429–436. <https://doi.org/10.14740/wjon950e>
- Vietri, M., Stenmark, H., & Campsteijn, C. (2016). Closing a gap in the nuclear envelope. *Current opinion in cell biology*, 40, 90–97. <https://doi.org/10.1016/j.ceb.2016.03.001>.
- Wahba, L., Amon, J. D., Koshland, D., & Vuica-Ross, M. (2011). RNase H and multiple RNA biogenesis factors cooperate to prevent RNA:DNA hybrids from generating genome instability. *Molecular cell*, 44(6), 978–988. <https://doi.org/10.1016/j.molcel.2011.10.017>
- Wall, M. E., & Wani, M. C. (1995). Camptothecin and taxol: discovery to clinic--thirteenth Bruce F. Cain Memorial Award Lecture. *Cancer research*, 55(4), 753–760.
- Wan, S., Pestka, S., Jubin, R. G., Lyu, Y. L., Tsai, Y. C., & Liu, L. F. (2012). Chemotherapeutics and radiation stimulate MHC class I expression through elevated interferon-beta signaling in breast cancer cells. *PloS one*, 7(3), e32542. <https://doi.org/10.1371/journal.pone.0032542>
- Watson, J. D., Crick, F. H. C., (1953). Molecular structures of Nucleic acids. *Nature* 171, 737-738. <https://doi.org/10.1038/171737a0>
- Weterings, E., & Chen, D. J. (2008). The endless tale of non-homologous end-joining. *Cell research*, 18(1), 114–124. <https://doi.org/10.1038/cr.2008.3>
- Willan, J., Cleasby, A.J., Flores-Rodriguez, N. et al. ESCRT-III is necessary for the integrity of the nuclear envelope in micronuclei but is aberrant at ruptured micronuclear envelopes generating damage. *Oncogenesis* 8, 29 (2019). <https://doi.org/10.1038/s41389-019-0136-0>

- Wongsurawat, T., Gupta, A., Jenjaroenpun, P., Owens, S., Forrest, J. C., & Nookaew, I. (2020). R-loop-forming Sequences Analysis in Thousands of Viral Genomes Identify A New Common Element in Herpesviruses. *Scientific reports*, *10*(1), 6389. <https://doi.org/10.1038/s41598-020-63101-9>
- Wright, W. D., Shah, S. S., & Heyer, W. D. (2018). Homologous recombination and the repair of DNA double-strand breaks. *The Journal of biological chemistry*, *293*(27), 10524–10535. <https://doi.org/10.1074/jbc.TM118.000372>
- Xiao, S., Zhang, J. Y., Zheng, K. W., Hao, Y. H., & Tan, Z. (2013). Bioinformatic analysis reveals an evolutionary selection for DNA:RNA hybrid G-quadruplex structures as putative transcription regulatory elements in warm-blooded animals. *Nucleic acids research*, *41*(22), 10379–10390. <https://doi.org/10.1093/nar/gkt781>
- Xu, B., & Clayton, D. A. (1996). RNA-DNA hybrid formation at the human mitochondrial heavy-strand origin ceases at replication start sites: an implication for RNA-DNA hybrids serving as primers. *The EMBO journal*, *15*(12), 3135–3143.
- Xu, H., Di Antonio, M., McKinney, S., Mathew, V., Ho, B., O'Neil, N. J., Santos, N. D., Silvester, J., Wei, V., Garcia, J., Kabeer, F., Lai, D., Soriano, P., Banáth, J., Chiu, D. S., Yap, D., Le, D. D., Ye, F. B., Zhang, A., Thu, K., ... Aparicio, S. (2017). CX-5461 is a DNA G-quadruplex stabilizer with selective lethality in BRCA1/2 deficient tumours. *Nature communications*, *8*, 14432. <https://doi.org/10.1038/ncomms14432>
- Yang, X. Q., Li, C. Y., Xu, M. F., Zhao, H., & Wang, D. (2015). Comparison of first-line chemotherapy based on irinotecan or other drugs to treat non-small cell lung cancer in stage IIIB/IV: a systematic review and meta-analysis. *BMC cancer*, *15*, 949. <https://doi.org/10.1186/s12885-015-1978-2>
- Zahler, A.M., Williamson, J.R., Cech, T.R., & Prescott, D.M. (1991). Inhibition of telomerase by G-quartet DNA structures. *Nature* *350*(6320), 718–20. <https://doi.org/10.1038/350718a0>
- Zhang, C. Z., Spektor, A., Cornils, H., Francis, J. M., Jackson, E. K., Liu, S., Meyerson, M., & Pellman, D. (2015). Chromothripsis from DNA damage in micronuclei. *Nature*, *522*(7555), 179–184. <https://doi.org/10.1038/nature14493>
- Zhang, D., Liu, Y., Zhu, Y., Zhang, Q., Guan, H., Liu, S., Chen, S., Mei, C., Chen, C., Liao, Z., Xi, Y., Ouyang, S., Feng, X. H., Liang, T., Shen, L., & Xu, P. (2022). A non-canonical cGAS-STING-PERK pathway facilitates the translational program critical for senescence and organ fibrosis. *Nature cell biology*, *24*(5), 766–782. <https://doi.org/10.1038/s41556-022-00894-z>
- Zhang, X., Wu, J., Du, F., Xu, H., Sun, L., Chen, Z., Brautigam, C. A., Zhang, X., & Chen, Z. J. (2014). The cytosolic DNA sensor cGAS forms an oligomeric complex with DNA and

- undergoes switch-like conformational changes in the activation loop. *Cell reports*, 6(3), 421–430. <https://doi.org/10.1016/j.celrep.2014.01.003>
- Zou, L., & Elledge, S. J. (2013). Sensing DNA damage through ATRIP recognition of RPA-ssDNA complexes. *Science* 300, 1542–1548. <https://doi.org/10.1126/science.1083430>
- Zou, M., Li, J. Y., Zhang, M. J., Li, J. H., Huang, J. T., You, P. D., Liu, S. W., & Zhou, C. Q. (2021). G-quadruplex binder pyridostatin as an effective multi-target ZIKV inhibitor. *International journal of biological macromolecules*, 190, 178–188. <https://doi.org/10.1016/j.ijbiomac.2021.08.121>

Publications

- Marzano, S., Miglietta, G., Morigi, R., Marinello, J., **Arleo, A.**, Procacci, M., Locatelli, A., Leoni, A., Pagano, B., Randazzo, A., Amato, J., & Capranico, G. (2022). Balancing Affinity, Selectivity, and Cytotoxicity of Hydrazone-Based G-Quadruplex Ligands for Activation of Interferon β Genes in Cancer Cells. *Journal of medicinal chemistry*, 65(18), 12055–12067. <https://doi.org/10.1021/acs.jmedchem.2c00772>
- Marinello, J., **Arleo, A.**, Russo, M., Delcuratolo, M., Ciccarelli, F., Pommier, Y., & Capranico, G. (2022). Topoisomerase I poison-triggered immune gene activation is markedly reduced in human small-cell lung cancers by impairment of the cGAS/STING pathway. *British journal of cancer*, 127(7), 1214–1225. <https://doi.org/10.1038/s41416-022-01894-4>